THESIS FOR THE DEGREE OF DOCTOR OF PHILOSOPHY

Hydrodeoxygenation (HDO) catalysts

Characterization, reaction and deactivation studies

HOUMAN OJAGH

Department of Chemistry and Chemical Engineering

CHALMERS UNIVERSITY OF TECHNOLOGY

Gothenburg, Sweden 2018

Hydrodeoxygenation (HDO) catalysts

Characterization, reaction and deactivation studies

Houman Ojagh

ISBN: 978-91-7597-704-1

Doktorsavhandlingar vid Chalmers tekniska högskola

Ny serie Nr. 4385

ISSN: 0346-718X

Department of Chemistry and Chemical Engineering

Chalmers University of Technology

SE-41296 Gothenburg, Sweden

Telephone +46(0)31-7721000

Printed by:

Chalmers Reproservice

Gothenburg, Sweden (2018)

Hydrodeoxygenation (HDO) catalysts

Characterization, reaction and deactivation studies

Houman Ojagh
Department of Chemistry and Chemical Engineering
Chalmers University of Technology

Abstract

Production of biomass derived fuels such as renewable diesel, are primarily intended to reduce the reliance of the conventional engines on petroleum fuels as well as the emission of CO_2 from fossil hydrocarbons. Hydrodeoxygenation (HDO) is a powerful technique that has been regularly used in the fuel upgrading processes. Sulfided molybdenum catalysts, supported on alumina and promoted by cobalt or nickel, are frequently used in the HDO processes. Despite the high efficiency of the HDO, catalyst activity and selectivity have raised major concerns from the economic and technological perspectives. The aim of this study was to gain a better understanding of the HDO catalyst structure, and then to assess the effect of different pretreatment and operational conditions on the catalyst activity and selectivity.

The effect of preparation and pretreatment conditions on hydrogen uptake capacity and dispersion of the prepared Ni, Co and Mo containing catalysts was evaluated by using several characterization techniques such as BET, ICP-SFMS, SEM, TEM, TPO, ethylamine-TPD, XPS and H_2-chemisorption. The H_2-chemisorption, XPS and SEM results confirmed the detrimental effect of calcination on hydrogen uptake capacity of catalysts. The effect of pH of the impregnating solutions on the dispersion of the metal phases was also assessed from the TEM experiments. Moreover, HDO reactions of oleic acid and abietic acid over a prepared sulfided NiMo catalyst were studied. The results show that addition of DMDS to an oleic acid feed clearly promoted maintenance of the active sulfided phases on the NiMo catalysts. Higher concentration of DMDS also promoted the decarbonylation/decarboxylation (DCO_x) route, and more importantly, decreased the amount of carbon deposition on the NiMo catalyst. On the other hand, addition of abietic acid to an oleic acid feed, is shown to decrease the deoxygenation rate of the oleic acid and increase the amount of carbon deposition on the catalyst. The inhibition effect of abietic acid on the HDO of oleic acid was related to stronger adsorption of the bulkier abietic acid molecules on the active sites compared to oleic acid that may have sterically hindered adsorption of oleic acid on neighboring sites.

Furthermore, the poisoning effect of iron on the HDO of oleic acid over sulfided NiMo and Mo catalysts was investigated. It is shown that addition of iron to an oleic acid feed decreased the oxygenate conversion activity of both catalysts and changed their selectivities towards the final products. TEM results of the poisoned spent NiMo catalyst revealed that iron was mainly deposited on and in the vicinity of the Ni particles. This may also indicate that iron has reacted with Ni phase and as a result modified the catalyst activity. Finally, hydroconversion of rosin acids over supported NiMoS catalysts on alumina, USY-zeolite and mixed alumina/USY-zeolite was investigated. Various catalyst properties such as dispersion of the NiMo phases and Brønsted acidity affected the selectivity for the products. The results also indicate that the Brønsted acidity of the support could be optimized by the USY-zeolite content of the catalyst to achieve a satisfactory level of deoxygenation, ring opening and cracking of the rosin acid while avoiding excessive coke formation.

Keywords: *Renewable diesel, Hydrodeoxygenation (HDO), Hydroconversion, Ring opening, Carbon deposition, Sulfided phase, Deactivation, Poisoning, Brønsted acid sites*

Publications

This thesis is based on the studies presented in the following papers:

I. Effect of thermal treatment on hydrogen uptake and characteristics of Ni-, Co-, and Mo-containing catalysts

Houman Ojagh, Derek Creaser, Stefanie Tamm, Chaoquan Hu, Louise Olsson.

Ind. Eng. Chem. Res. 2015. 54 (46), 11511-11524.

DOI:10.1021/acs.iecr.5b02510

II. Effect of dimethyl disulfide on activity of NiMo catalysts used in hydrodeoxygenation of oleic acid

Houman Ojagh, Derek Creaser, Stefanie Tamm, Prakhar Arora, Stefan Nyström, Eva Lind Grennfelt, Louise Olsson.

Ind. Eng. Chem. Res. 2017. 56 (19), 5547-5557.

DOI:10.1021/acs.iecr.6b04703

III. The effect of rosin acid on hydrodeoxygenation of fatty acid

Houman Ojagh, Derek Creaser, Muhammad Abdus Salam, Eva Lind Grennfelt, Louise Olsson.

J. Energy. Chem. 2018. In press.

DIO: https://doi.org/10.1016/j.jechem.2018.01.023

IV. Investigating the effect of Fe as a poison for catalytic HDO over sulfided NiMo alumina catalysts

Prakhar Arora, Houman Ojagh, Jungwon Woo, Louise Olsson, Stefan Nyström, Eva Lind Grennfelt, Derek Creaser

Appl. Catal., B. 2018. 227, 240-251.

DOI: https://doi.org/10.1016/j.apcatb.2018.01.027

V. Hydroconversion of rosin acids into value-added fuel components over NiMo catalysts with varying support acidity

Houman Ojagh, Derek Creaser, Muhammad Abdus Salam, Eva Lind Grennfelt, Louise Olsson.

Submitted manuscript.

Other publications that are not included in this thesis:

I. Catalytic hydrogenation of C=C and C=O in unsaturated fatty acid methyl esters

Chaoquan Hu, Derek Creaser, Samira Siahrostami, Henrik Grönbeck, Houman Ojagh, Magnus Skoglundh

Catal. Sci. Technol. 2014. 4 (8). DOI: 10.1039/c4cy00267a

II. Selectivity and kinetics of methyl crotonate hydrogenation over Pt/Al_2O_3

Chaoquan Hu, Derek Creaser, Henrik Grönbeck, Houman Ojagh, Magnus Skoglundh

Catal. Sci. Technol. 2015. 5 (3). 1716-1730. DOI: 10.1039/c4cy01470g

III. Modelling of particulate matter transformations and capture efficiency

Jonas Sjöblom, Ananda Subramani Kannan, Houman Ojagh, Henrik Ström

Can. J. Chem. Eng. 2014. 92 (9). 1542-1551. DOI: 10.1002/cjce.22004

IV. Experimental validation of particulate matter (PM) capture in open substrate

Jonas Sjöblom, Henrik Ström, Ananda Subramani Kannan, Houman Ojagh

Ind. Eng. Chem. Res. 2014. 53 (9), 3749-3759. DOI: 10.1021/ie404046y

V. Near-wall dispersion, deposition and transformation of particles in automotive exhaust gas aftertreatment systems

Henrik Ström, Jonas Sjöblom, Ananda Subramani Kannan, Houman Ojagh, Oskar Sundborg, Jan Koegler

Int. J. Heat. Fluid. Flow. 2018. Accepted manuscript.

Contribution to the papers:

Paper I:

The author planned the experiments, prepared the catalysts and performed the characterization methods, except SEM and TEM techniques. The author also analyzed and interpreted the results with the co-authors. The author was responsible for writing the manuscript.

Paper II:

The author planned the experiments, prepared the catalysts and performed the characterization methods, except TEM. The author also performed the hydrodeoxygenation reactions, analyzed the results with the co-authors and wrote the manuscript.

Paper III:

The author planned the experiments, prepared the catalysts and performed the characterization methods as well as hydrodeoxygenation reactions. Analyzed the results with the co-authors. The author also wrote the manuscript.

Paper IV:

The author performed some experiments with Prakhar Arora and also analyzed the results with co-authors.

Paper V:

The author planned the experiments, prepared the catalysts and performed the characterization methods, except SEM and TEM techniques. The author preformed the hydrodeoxygenation reactions and analyzed the results with the co-authors. The author also wrote the manuscript.

List of abbreviations

AC	Active carbon
BET	Brunauer Emmett Teller
BJH	Barret Joyner Halenda
BSTFA	Bis trimethylsilyl trifluoroacetamide
CN	Cetane number
CTO	Crude tall oil
CUS	Coordinatively unsaturated sites
DFT	Density functional theory
DMDS	Dimethyl disulfide
DSC	Differential Scanning Calorimeter
DTO	Distilled tall oil
DCO_x	Decarbonylation/Decarboxylation
DO	Deoxygenation
EELS	Electron energy loss spectroscopy
EDX	Energy dispersive x-ray
FAME	Fatty acid methyl ester
FA	Fatty acid
FFA	Free fatty acid
GC	Gas chromatograph
HEFA	Hydroprocessed esters and fatty acids
HAADF	High angle annular dark field
HDO	Hydrodeoxygenation
HDM	Hydrodemetalation
HDN	Hydrodenitrogenation
HDS	Hydrodesulfurization
H_2-TPR	Hydrogen temperature programmed reduction
HYD	Hydrogenation

IC	Internal combustion
ICP-SFMS	Inductively coupled plasma and sector field mass spectroscopy
IFFT	Inverse fast Fourier transform
LGO	Light gas oil
LCO	Light cycle oil
MFC	Mass flow controller
MS	Mass spectrometer
RME	Rapeseed methyl ester
SEM	Scanning electron microscopy
SE	Secondary electron
STEM	Scanning transmission electron microscopy
STM	Scanning tunneling microscopy
TG	Triglyceride
TEM	Transmission electron microscopy
TOFA	Tall oil fatty acid
TOR	Tall oil rosin acid
TPO	Temperature programmed oxidation
XPS	X-ray photoelectron spectroscopy
XEDS	X-ray energy dispersive spectrometry

Contents

1 Introduction

1.1 The development in sustainable biofuel production

The exploitation of cheaply available fossil based fuels, used in the production of fuel and energy, started in twentieth century [1]. Ever since, the fossil fuel demand of combustion engines, which are the most important sources of mobility in the world, is rapidly rising as a result of population and economic growth [2]. The world consumption of non-renewable petroleum fuels is estimated to grow from 80 million barrels per day in 2015 to 90 million barrels per day in 2040 by the U.S. Energy Information Administration's (EIA's) International Energy Outlook 2017 [3]. Moreover, fossil fuel usage is the primary source of the world carbon dioxide (CO_2) emission which is a greenhouse gas [4]. There are serious concerns over long term climate change and global warming due to increasing consumption of fossil fuels. Moreover, considering ecological and environmental aspects, burning fossil fuels are not a sustainable way of producing energy [5]. Thus, producing renewable fuels compatible with the existing petrochemical infrastructure has been the prime interest of many academic and industrial studies.

It is generally accepted that producing biofuel from renewable sources such as biomass can reduce the reliance on fossil fuels as well as the emission of CO_2. The produced CO_2 from biofuels is recycled in the earth's biosphere therefore biofuels emissions are considered carbon neutral [1, 6, 7]. Biomass is becoming increasingly important globally as a clean alternative source of energy to fossil resources [1]. Biomass is a concept used for all organic matter derived from living or recently living organisms such as plants and animals. Biomass resources include wood and wood wastes, agricultural crops and their waste by-products, animal wastes, wastes from food processing, aquatic plants and algae [8, 9].

The first generation biofuels that have been used as transportation fuels are bioethanol and fatty acid methyl ester (FAME) diesel. Bioethanol and bioethanol/gasoline blends have a long history as alternative transportation fuels. They have been used in Germany and France as early as 1894 due to the emerging use of internal combustion (IC) engines [10]. Bioethanol can literally be produced from any organic matter which contains high sugar and starch contents such as sugarcane and corn [11, 12]. However, the sustainability of long term production of first generation biofuels is under serious reviews due to their direct competition with land and water used in food production [1].

FAME diesel is a mixture of saturated and unsaturated mono-alkyl esters of long chain fatty acids which is predominantly produced via transesterification of triglyceride, as the main component in vegetable oils and animal fats, by methanol [13-15]. Rapeseed methyl ester (RME) is one of the most common FAMEs [16, 17]. However, compared to conventional petroleum diesel, FAME diesel is very unstable due to its high oxygen content, and thus, it is only blended with conventional petroleum diesel in an attempt to produce a partly sustainable fuel [18-20]. For example, a fuel coded as B20 which is a blend of 20% FAME diesel with conventional diesel has been introduced in the US. A major disadvantage with FAME however is that it may precipitate at low temperatures (in colder climates) if over 2-5% of it is blended with conventional petroleum diesel [21, 22]. Moreover, European fuel regulation (EN 590) only allows 7% FAME blended in diesel [23]. Thus, attention has shifted towards the second and third generation biofuels that are produced from non-edible agricultural, forest and lignocellulosic feedstocks and Algae.

Tall oil is a by-product from the Kraft cooking process in the pulp and paper industry which is used as a feedstock for the production of second generation biofuels [24]. Tall oil is a nonedible bio-oil source, derived from renewable woody biomass that is typically cultivated on non-arable land. Moreover, in countries with a high capacity for Kraft pulping such as Sweden, Finland, United States, Canada, Russia and China, tall oil can be produced on a cost competitive basis compared to other bio-oil sources like vegetable oil [25, 26]. Crude tall oil (CTO) is a mixture of free fatty acids (FFA, 38-55 wt%), rosin acids (RA, 35-53 wt%) and unsaponified compounds (neutrals, 7-18 wt%) and is produced via acidification of tall oil soap by sulfuric acid [27-29].

FFAs and FAME can be hydroprocessed by hydrogen via catalytic hydrodeoxygenation (HDO) to produce highly paraffinic diesel like hydrocarbons [20, 30, 31]. Recently, a lot of attention has been paid to a new type of renewable liquid fuel called hydroprocessed esters and fatty acids (HEFA). HEFA fuels are produced from renewable feedstocks such as vegetable or animal waste oils and tall oil, and they are also known as drop-in fuels due to their similarity to fossil derived fuels. HEFA biofuels have been recognized as the most common biofuels produced with a capacity of more than one billion gallons in 2014 [32]. During an HDO process, the oxygen in the triglycerides, FFAs and esters of biofeeds is removed by hydrogen in the form of CO, CO_2 and water [33]. NEXBTL™, UOP/Eni Ecofining™, Vegan™ and Hydroflex™ are examples of commercial HDO processes that produce HEFA fuels.

The conventional metal sulfide (NiMo and CoMo) catalysts supported on alumina are the most common catalysts used in industrial HDO processes [34]. But, noble metals such as platinum (Pt), palladium (Pd), rhodium (Rh), ruthenium (Ru) or base metals nickel (Ni), cobalt (Co), molybdenum (Mo) and tungsten (W), supported on alumina, silica, zeolites and activated carbons have also been demonstrated as HDO catalysts in research and laboratory studies [31, 35-37].

There has been growing interest in HDO process optimization to justify the economic and technical aspects of using tall oil as the feedstock for production of biofuels and other chemicals. Catalytic HDO process is a relatively new and complex process. Many

different reactions such as hydrodecarboxylation, hydrodecarbonylation, hydrogenation, hydrodeoxygenation, isomerization and cracking are involved in the HDO process which can affect the properties of the produced biofuels. These reactions and their mechanisms are critical and must be well understood. Moreover, the activity of HDO catalysts can be affected by many critical factors such as the catalyst support, chemical composition, catalyst preparation, catalyst pretreatment steps, hydrogen uptake capacity and deactivation mechanisms.

1.2 Objectives

The main objective of this thesis is to deepen the understanding of catalyst deactivation due to loss of sulfidity, iron poisoning and coke formation during HDO of tall oil. To realize this, alumina and zeolite supported Ni, Co and Mo containing catalysts were prepared and the effect of the preparation conditions such as calcination on the hydrogen uptake capacity and textural properties of these catalysts has been studied. Then, the activity of an alumina supported metal sulfide (NiMo) catalyst towards production of the final deoxygenated products in an HDO reaction of tall oil fatty acid was investigated.

The goal was to study the effects of several process parameters such as temperature, pressure, feed concentration, iron (Fe) as a poison and dimethyl disulfide (DMDS) on fatty acid HDO activity. Additionally, the objective was to investigate the effect of rosin acid on hydrodeoxygenation of fatty acid. Oleic acid and abietic acid were used as model compounds for fatty acid and rosin acid respectively in tall oil. Several characterization techniques such as SEM, TEM, XPS, TPO, TPD, TPR, elemental microanalysis and hydrogen chemisorption were used.

Finally, the possibility of converting rosin acid into fuel components and other valuable products via a hydroconversion reaction over supported NiMoS catalysts was investigated.

2 Background

2.1 Catalytic hydrotreating process

The first catalytic hydroprocessing, known as the Sabatier process, was performed by the French chemist Paul Sabatier in 1897 [38]. He discovered that the introduction of a trace of nickel catalyst facilitated the reaction of hydrogen with gaseous hydrocarbons. Catalytic hydrotreating processes have long been used as a powerful technique in many fuel production industries such as petroleum refining and coal liquefaction processes [34, 39-41].

The conventional hydrotreating process consists of several reactions such as hydrodesulfurization (HDS), hydrodenitrogenation (HDN), hydrodemetalation (HDM) and hydrodeoxygenation (HDO). During these reactions, the heteroatom species such as sulfur, nitrogen, metal and oxygen (from coal derived liquid feedstocks) are removed via hydrogenolysis of the reactants C-heteroatom bands by hydrogen [42, 43]. Examples of typical reactants found in petroleum are presented in Figure 1.

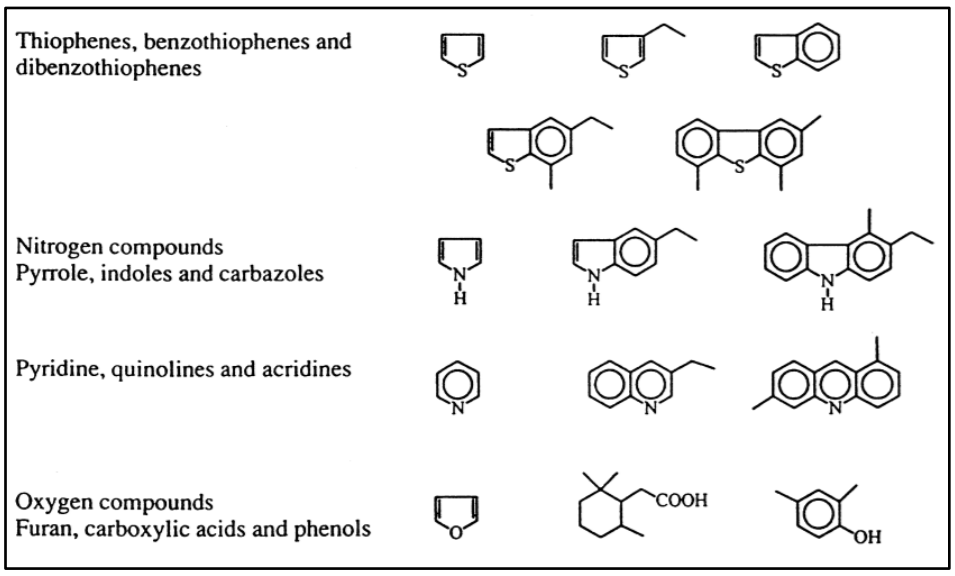

Figure 1. Typical petroleum reactants containing sulfur, nitrogen and oxygen heteroatoms [43]. Reprinted permission from reference [43].

Industrial hydrotreating processes have been performed as three phase reactions (hydrogen gas, liquid feedstock and solid catalysts), in various multiphase catalytic packed-bed reactors such as trickle-bed or in ebullating-bed reactors, at elevated

temperature and pressure [43]. In a multiphase catalytic reaction system where gas, liquid and solid co-exist, physical transport processes such as external and internal diffusions are often more responsible for limiting the rate of the reaction [44, 45]. A simplified schematic of the packed bed reactors for three phase (gas-liquid-solid) reactions is shown in Figure 2.

In such systems, hydrogen gas must first diffuse through the gas-liquid interface, dissolve in the liquid feedstock bulk, and then alongside the liquid reactant diffuse though pores of the catalyst and finally react on the active sites. Thus, a high pressure of hydrogen is always required to facilitate the diffusion of hydrogen through the gas-liquid interface and to increases the solubility of hydrogen in the liquid reactant. Also, HDO reactions are performed at high temperatures since high temperature facilitates an adequate rate of conversion per mass of catalyst or reactor volume.

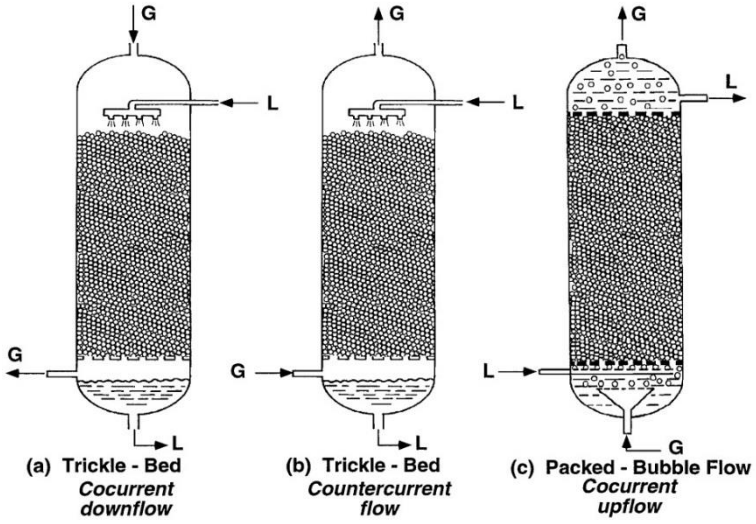

Figure 2. Schematic diagrams of three phase reactor systems. (a) Trickle-bed in co-current mode (b) Trickle-bed in counter-current mode (c) Packed bed with bubble flow [46]. Reprinted permission from reference [46].

2.1.1 Hydrodeoxygenation (HDO) process in renewable fuel production

The HDO process is an important refinery and upgrading treatment that is used to reduce the oxygen contents of both fossil based and bio-based feedstocks [47, 48]. For instance, pyrolysis derived bio oils generally have low energy density and low chemical stability in contrast to fossil derived oils due to their high oxygenate contents (ketones, aldehydes, esters, carboxylic acid and aromatic alcohols), thus, they need to be upgraded via an HDO process [48-50]. Similarly, FAME diesels (Biodiesel) derived from vegetable oils or animal fats have significantly lower stability compared to petroleum diesel so, they also need to be upgraded via an HDO process [17, 51]. HDO processes of feedstocks such as animal fats, tall oil and vegetable oils have been developed to produce highly paraffinic hydrocarbons in the same boiling temperature range of petroleum diesel [52-54]. HEFA fuels derived from triglyceride and fatty acid based bio-oils are considered the most common commercial biofuels which are produced via an HDO process.

An HDO process with renewable feedstocks is generally considered to involve a very complex network of different reactions including: cracking, decarbonylation/decarboxylation (DCO_x), hydrocracking, hydrogenation (HYD) and

deoxygenation (DO) [55, 56]. Examples of these reactions are presented in Figure 3. Amongst these reactions, HDO mainly proceeds through DCO_x and DO in which CO and CO_2 are formed during decarbonylation and decarboxylation routes, respectively, and water is formed during DO [33, 51, 57, 58]. Thus, the produced diesel is a mixture of alkanes with an odd and even number of carbon atoms.

In principle, HDO and conventional HDS processes are closely related as hydrogen is used in both HDO and HDS processes to remove oxygen and sulfur respectively. Therefore, HDO can be performed in co-hydrotreatment units where biodiesel and petroleum derived diesel are mixed and co-processed [54, 59-62]. Moreover, the hydrodeoxygenation route is an exothermic reaction (due to high oxygen content of bio feedstocks) and one practical way to control the exotherm is to co-process bio feedstocks with petroleum derived feedstocks such as light gas oil (LGO) with negligible oxygen content (O/C ≤ 0.03) [63]. Nonetheless, many studies have indicated that the HDO process could be performed in dedicated stand-alone units when operating with 100% renewable feeds [64-68].

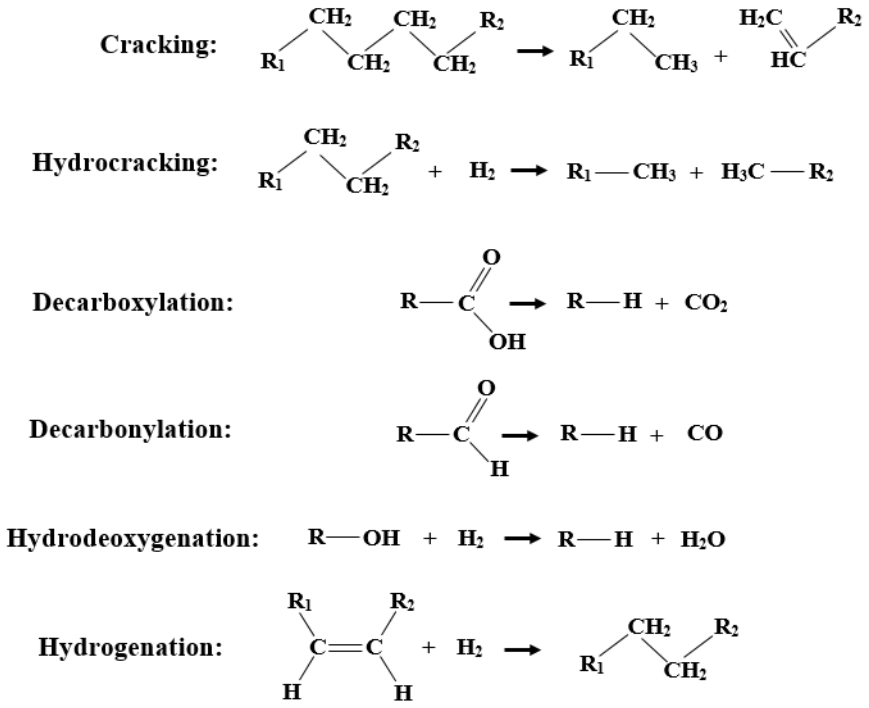

Figure 3. Reactions associated with catalytic HDO process [47].

Many operating factors such as pressure, temperature, catalyst, type of feedstock, feed velocity and the ratio of hydrogen to oil (H/O) can affect the HDO reaction rate. For instance, in continuous operations, depending on the liquid velocity, the reaction rate can be limited by the mass transfer and the reaction kinetics. At lower velocities, when the thickness of the hydrodynamic boundary layer around the catalysts particles are larger, the rate is limited by the transport and at higher velocities, when the thickness of the boundary layer is decreased, the rate is limited by the reaction kinetics [47]. Also, in patent and open literature a high pressure ranging from 10 to 300 bar has been reported to facilitate the solubility of hydrogen in the liquid feeds [47, 67, 69-71]. Furthermore, due to the exothermic

nature of HDO reactions, it has been proposed that the operating temperature should be decided based on the kinetic characteristics [47]. Still, a temperature range from 250 to 450 °C has been reported to be carried out as operating conditions in HDO processes [47, 72].

Tall oil, in contrast to other bio feed stocks like vegetable oils, is considered as one of the most cost competitive commercial feedstock for biodiesel production [26, 73]. Tall oil is an American phrase adapted from the Swedish word "tallolja" (pine oil) which is a by-product from the alkaline pulping process (Kraft pulping). In a Kraft process, fatty acids and rosin acids in wood are converted to their sodium salts and then separated from the black liquor (spent cooking liquor) in form of a soapy material [74, 75]. The extracted tall oil soap, however, is reported to have low calorific value (half of fuel oil), therefore, it needs to be upgraded [76]. The upgrading is done via acidification (by sulfuric acid) and crude tall oil (CTO) is produced [73, 75, 76]. CTO is a mixture of free fatty acids (FFA), resin acids (RA) and unsaponifiables compounds (neutrals) [27, 29]. Current global production of CTO is estimated at 2 million metric tons annually [25, 77]. Nevertheless, the exact composition of a CTO is subject to the wood species and pulping process from which it is derived. Regional composition of CTO is exemplified in Table 1.

Table 1. Regional composition of CTO [75].

Composition (wt%)	South-eastern USA	Northern USA and Canada	Scandinavia
Rosin Acids	35-45	25-35	20-30
Fatty acids	45-55	50-60	50-60
Unsaponifiables	7-10	12-18	18-24

The FFA portion of tall oil are long chain monocarboxylic acids, mainly C_{18}, with saturated or unsaturated aliphatic chains such as oleic acid, stearic acid, linoleic acid and palmitic acid [73]. On the contrary, rosin acids have very different molecular structures containing a tri-ring structure, conjugated double bounds and a carboxylic group with a general formula $C_{20}H_{30}O_2$ [75, 78]. Abietic acid and dehydroabietic acid are the main components of tall oil rosin acids. Phytosterols, containing both sterol and stanol molecules, fatty and wax alcohols (long chain alcohols (C_{22} and C_{24})) and terpenes are the major components of CTO unsaponifiables (neutrals) compounds [73, 75]. Figure 4 presents the major FFAs, RAs and neutral compounds in CTO.

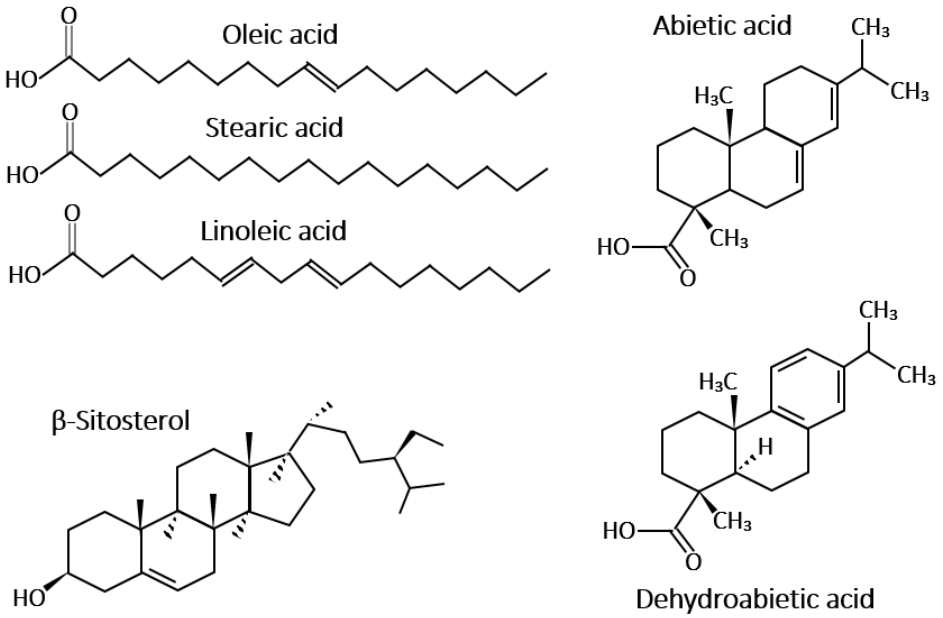

Figure 4. Major FFA, RA and unsaponifiables compounds in crude tall oil (CTO).

CTO is often vacuum distilled and depending on the distillation process, a head fraction, tall oil fatty acid (TOFA), distilled tall oil (DTO) and tall oil rosin acid (TOR), and a pitch fraction are produced and commercially available [76, 79-81]. Amongst the CTO upgraded fractions, the TOFA and DTO, containing high portions of FFAs (≥ 70 wt%), are generally considered as the most desirable fractions for biodiesel production [28, 82, 83].

2.2 HDO catalysts

HDO catalysts are reported to be mostly heterogeneous catalysts containing noble and base metal nanoparticles such as platinum (Pt), palladium (Pd), ruthenium (Ru), rhodium (Rh), nickel (Ni), cobalt (Co), molybdenum (Mo) and tungsten (W), dispersed onto acidic and basic supports such as alumina (Al_2O_3), active carbon (AC), magnesium oxide (MgO), silica (SiO_2), zirconia (ZrO_2), titania (TiO_2) and zeolite [36, 56, 84-93]. Noble metals such as Pt and Pd have generally shown to have high activity for HDO of fatty acids and their esters, but their high cost has restricted their industrial HDO uses and they are limited to laboratory evaluations only [94]. Compared to noble metals, the low cost base metals such as Ni are considered as good alternatives. Though, the supported Ni catalysts are reactive for other undesirable reactions such as hydrogenolysis of C-C and methanation that decrease the product yields [95]. It has however been suggested that the structure of Ni can be modified by addition of a second metal with lower reactivity such as Mo and Fe and those undesirable reactions can be avoided to a great extent [96]. So far, the conventional bimetallic HDS sulfided catalysts such as $NiMo/Al_2O_3$ and $CoMo/Al_2O_3$ have been the most commonly used catalysts for the commercial HDO processes [61, 97].

Catalyst supports can have major impact on the activity and selectivity of the catalysts by varying the dispersion of the active phase and imposing metal-support interactions [98-100]. Gamma alumina (γ-Al_2O_3) has been exclusively used as a support for the

commercial HDO catalysts due its excellent properties such as strong textural and mechanical properties, high surface area, high packing density and its low cost [98, 101, 102]. However, alumina is not inert and it reacts with the supported active metals, to change their chemical structures and hampers their activities [98, 103, 104]. Alumina is also reported to become unstable in the presence of large amount of water that can be formed during a large scale HDO of highly oxygenated feeds (pyrolysis oils) [72, 105]. Also, when operating at higher temperatures which e.g. is the case for deoxygenation of phenolic type molecules in pyrolysis oils, alumina is susceptible to be clogged by carbonaceous compounds (coking) that are mainly adsorbed on the existing acid sites on the alumina surface (The concept of coking will be fully described in section (2.3)) [34, 43, 62, 105, 106]. Moreover, to meet the new fuel specifications to comply with the tougher upcoming environmental regulations, the activity, selectivity and stability of the commercial hydrotreatment catalysts must be improved.

Compared to alumina, high surface area carbon materials (~ 1000 m^2/g) are inert and they are more water tolerant [91, 98, 106]. The carbon supported hydrotreating catalysts are also reported to be more active and stable compared to those supported on alumina [107]. Nevertheless, for HDO of larger molecules (e.g. polyaromatics), extensive micro porosity of microporous carbons may have a negative impact on the number of available active metal sites since some of the metal particles will be deposited inside the inaccessible small pores, and thus, they will effectively be inactive. To rectify this shortcoming, utilizing the mesoporous carbons with larger pores seems to be a better option.

Similar to carbon supports, zirconia (ZrO_2) and titania (TiO_2) supports are reported to be more water resistant, more active at lower temperatures, less acidic and also have minimal interactions with the active metal phases [91, 106, 108]. Still, the main drawbacks for using zirconia and titania are their low surface area (typically ~ 30-120 m^2/g), which is approximately half that of alumina, and their low porosity for hydrotreating processes [92, 106]. The emerging new preparation methods such as digestion method are able to improve the surface area of zirconia supports (350 m^2/g) but these methods are very complex and difficult to execute [92, 109].

Basic supports such as MgO have shown to improve the dispersion of the acidic molybdenum oxide phase, decrease the rate of coking due to the basic character of the supports and to have higher HDO/HDS activities compared to the corresponding alumina supported molybdenum based catalysts [93, 110, 111]. Amongst hydrotreating acidic supports, zeolite (crystalline aluminosilicates) supports have gained considerable attention. Zeolite materials can offer manageable and well-ordered pore structures, on the molecular level, as well as providing a sufficient number of Brønsted acid sites that are needed to convert the low value multi-ring aromatic and heavy molecules present in residual oils into value-added products [112-114].

Modification of the alumina supports has also been shown to improve the catalysts activity. For instance, covering the surface of alumina by a thin layer of carbon, before impregnation of metals, was shown to reduce the metal-support interactions and improve the activity and stability [115]. Also, addition of phosphorous to alumina supports has been reported to improve the activity of hydrotreating catalysts [116, 117]. It has also been proposed that unsupported transient metal sulfides can effectively be used as hydroprocessing catalysts in order reduce the interference effect of the supports [118].

2.2.1 $NiMo/Al_2O_3$ and $CoMo/Al_2O_3$ catalyst preparation method

$NiMo/Al_2O_3$ and $CoMo/Al_2O_3$ catalysts are often prepared via impregnation and co-precipitation methods [119-121]. The simplicity of the impregnation method has made it the method of choice in industrial practice [122]. A typical weight concentration of these metals are reported as (1-5) wt% for Ni/ Co and (8-16) wt% for Mo in which nickel and cobalt are regarded as promoters and molybdenum as the main catalyst [123]. The first step in an impregnation method starts by making an aqueous solution of the metal salts (metal oxide precursor). Nitrate salts such as $Ni(NO_3)_2 \cdot 6H_2O$, $Co(NO_3)_2 \cdot 6H_2O$ and ammonium salt as $(NH_4)_6Mo_7O_{24} \cdot 4H_2O$ are very often preferred over chloride salts due to the environmental restrictions on chloride containing materials. Then, the prepared aqueous solution is mixed alumina.

During a contact time of typically an hour, the cationic complexes of metals such as $Ni(NH_3)_x^{2+}$ in the aqueous solution adsorbs on the surface of support and then, the prepared mixture is dried [124, 125]. After drying, the impregnated metal salts are decomposed into metal oxides via thermal treatment that is known as calcination at a temperature range between 400-600 °C [126, 127]. Depending on the reaction mode (batch or continuous), solid catalysts can be configured in different shapes such as powder or pellets.

Figure 5 shows a photograph of calcined $NiMo/Al_2O_3$ catalyst prepared via an impregnation method as an example. Many different parameters such as pH of the impregnating solution and calcination operating conditions, are involved in such catalyst preparation procedures that can significantly affect the performance of supported catalysts [104, 128]. The number of available active sites and the state of dispersion (surface to volume ratio) is generally accepted as very critical properties that can significantly affect activity of a catalyst.

It has been reported that three important parameters such as: isoelectric point of the support, pH of the impregnating solution and the nature of the metallic complex precursors must be carefully regulated in order to prepare supported catalysts with high dispersion. For example, a pH range of 9 to 11 has been reported to be an optimum range for producing highly dispersed alumina supported catalysts containing metals situated in groups 8 and 1b such as Co, Ni, Cu, Ru, Rh, Pd, Ag, Ir and Pt in the periodic table [125].

Figure 5. Calcined non-sulfided $NiMo/Al_2O_3$ powder catalyst.

2.2.2 $NiMo/Al_2O_3$ and $CoMo/Al_2O_3$ catalysts activation process

After calcination treatment, the metal phases in $NiMo/Al_2O_3$ and $CoMo/Al_2O_3$ catalysts are in many different oxide forms such as single phase metal oxides NiO, Ni_2O_3, CoO, Co_2O_3 and MoO_3 or spinels $NiAl_2O_4$ and $CoAl_2O_4$, and mixed phase oxides such as $NiMoO_4$ and $CoMoO_4$ [104, 129-133]. These oxide phases are stable with minimal reactivity, therefore, they need to be activated. Activation is achieved by either reducing the inactive metal oxide phases to their active metallic states or converting them to sulfide forms in a sulfidation process [134-136]. The reduction process is generally performed in a hydrogen atmosphere (often pure) at elevated temperatures (300-600 °C).

It has been suggested that long term use of the sulfided catalysts can affect the quality of fuel products due to possible sulfur contamination leaching from the sulfided catalysts [137]. However, the sulfided forms of $NiMo/Al_2O_3$ and $CoMo/Al_2O_3$ catalysts are reported to be more active for HDO processes, also more tolerant against sulfur contaminants in feedstocks [34, 134]. Sulfidation is performed by using a sulfiding agent such as hydrogen sulfide (H_2S), carbon disulfide (CS_2), elemental sulfur and dimethyl disulfide (DMDS) in a hydrogen containing atmosphere at elevated temperatures in a temperature range of 300 to 400 °C [67, 70, 138, 139]. These sulfiding agents have also been used to maintain the sulfidity of the catalysts used for renewable fuel productions as a necessary procedure to reduce the possible modification effects of oxygen containing compounds in renewable feedstocks [34, 66, 140].

During the sulfidation processes, the metal oxide phases are converted into more active metal sulfides such as Ni_xS_y, Co_xS_y, MoS_2, NiMoS and CoMoS phases [141-143]. Literature studies have indicated that different sites are responsible for different reactions occurring during an HDO process. But, a complication comes in the fact that the precise mechanistic role of the catalyst is still a subject of debate. TEM images of freshly sulfided $NiMo/Al_2O_3$ and $CoMo/Al_2O_3$ catalysts are shown in Figure 6. The black thread-shape fringes represents the MoS_2 phase that is dispersed on the surface of alumina.

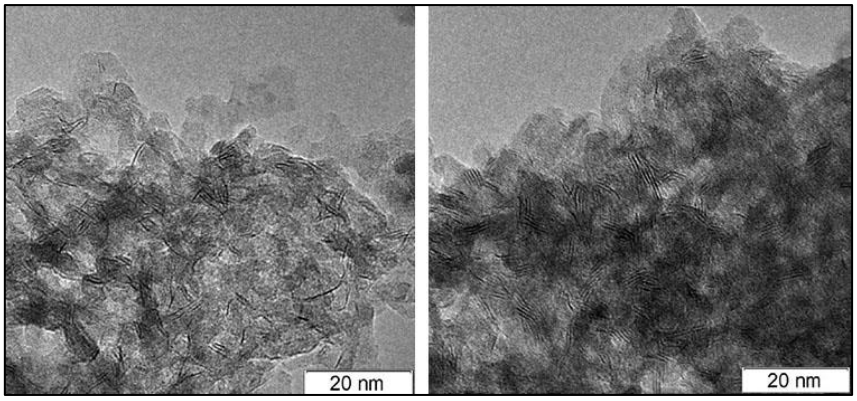

Figure 6. TEM micrographs of freshly sulfided $NiMo/Al_2O_3$ (left) and freshly sulfided $CoMo/Al_2O_3$ (right) [67].

A model that is still widely accepted, was proposed by Topsøe et al. more than three decades ago based on the structure of Ni-Mo-S and Co-Mo-S phases [144]. In this model, the active phases of the $NiMo/Al_2O_3$ and $CoMo/Al_2O_3$ catalysts were attributed to the Ni-Mo-S and Co-Mo-S phases in form of type (I) and type (II). Type (I) consists of the MoS_2 monolayer slabs and type (II) consists of multilayer slabs of MoS_2 which are decorated by the promoter metals Ni or Co on their edges [61, 144-147]. The type (I) is reported to be less active due to the higher interaction between the MoS_2 monolayer and alumina support through the electronic transfer Mo-O-Al linkages [43].

It was further reported that the active sites in unpromoted alumina supported molybdenum sulfide catalysts are coordinatively unsaturated sites (CUS) i.e. sulfur vacancies with Lewis acid characters and the Brønsted acid sites that are associated to the S-H groups [148, 149]. The presence of hydrogen results in formation of H_2S which creates the sulfur vacancies on the metallic edge of MoS_2 phase. Also, the hydrolytic dissociation of hydrogen on the edges of MoS_2 slabs leads to formations of one S-H group and one Mo-H group (Figure 7) [150]. The adsorption and dissociation of H_2S can also change a Lewis acid character site (sulfur vacancy) to a Brønsted acid site (S-H) [151].

Addition of promotors such as Ni and Co to the sulfided Mo/Al_2O_3 increases the number of sulfur vacancies which results in more activity of the promoted catalysts [149, 152-154]. According to these studies, new sulfur vacancies are created when the Mo-S bonds become weaker due to donation of electrons from the promoters such as Ni and Co. However, the increase in the concentration of promoters (Ni and Co) does not increase the number of vacancies significantly, but it may create vacancies with higher activities compared to vacancies present on the unprompted molybdenum sulfide catalysts [34]. The HDY activity of these catalysts is related to the CUS (sulfur vacancies) on the metallic edge of MoS_2 slabs, where two or more neighboring vacancies are present and the hydrogenolysis (C-O cleavage) activity is linked to the Brønsted acid sites (S-H groups) located on the sulfur edges [149, 153, 154].

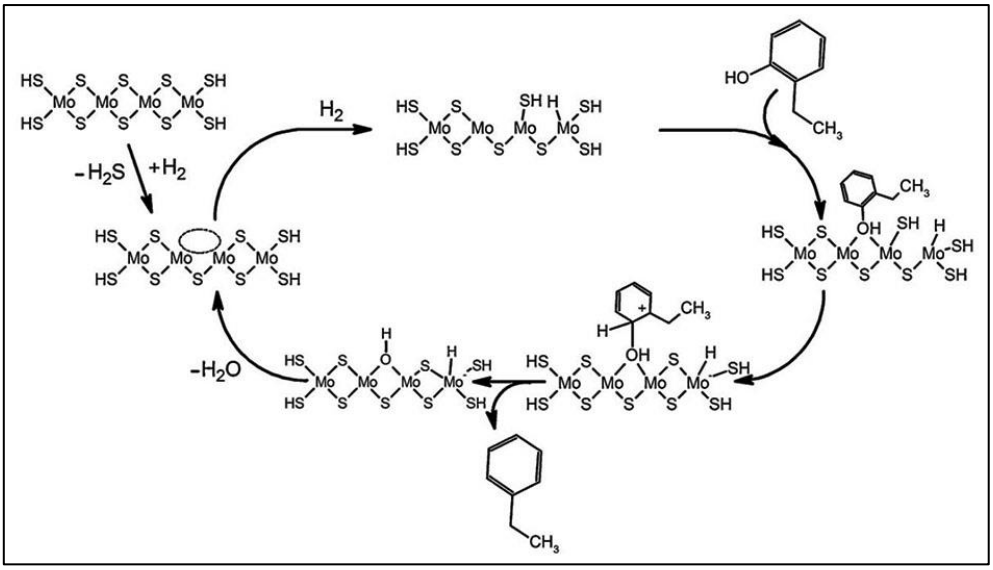

Figure 7. Suggested mechanism of HDO of 2-ethylphenol by a sulfided CoMoS catalyst. The circle indicates the catalytically active vacancy site [149]. Reprinted permission from reference [47].

The concentration of S-H groups and vacancy sites are closely related to the sulfided structure of the catalysts (Ni-Mo-S and Co-Mo-S phases), the concentration of H_2S that is needed to create the S-H groups and negate the oxidizing nature of the oxygenate feedstock and reaction intermediates [43, 155-158]. The alumina support itself may also show some catalytic activity. Alumina contains acid sites that can interact with oxygenate feeds (dehydration of alcohols) [149].

The combination of density functional theory (DFT) and scanning tunneling microscopy (STM) studies have also proposed a model that attribute the active sites in both promoted and unpromoted sulfided Mo/Al_2O_3 catalysts to the so called brim sites [159]. These sites are reported to be specific sites located on the metallic edges of MoS_2 clusters that can simply be identified during STM as bright brims. These brim sites may be responsible for both HYD and hydrogenolysis reactions.

2.3 Catalyst deactivation

Major concerns, from economic and technological perspectives, have raised regarding loss in activity with time on stream or catalyst deactivation [43]. In the literature the key reason for the loss in activity of HDO catalysts is commonly shown to be due to four major mechanisms such as: poisoning, coking, support pore blockage and thermal degradation [160 161-163]. Loss of sulfidity or gradual sulfur removal from the catalysts are also reported to be another main reason for the deactivation of sulfided HDO catalysts [140, 158, 164].

Poisoning is generally defined as strong chemisorption of a poison, which can be the reactant, products or impurities, on the active sites [43, 160]. Poisons can either occupy the active sites or compete with other reactant for the active sites. In either case, the main reaction rate will decrease. Depending on the strength of chemisorption, poisoning can be either a reversible or an irreversible mechanism. In the reversible case, poisons can be removed and the catalyst activity can be restored. Since the catalyst activity is only

temporarily diminished during the reversible poisoning, the reversible poisons are often described as inhibitors for the main reaction [43, 162]. On the other hand, an irreversible poison can permanently occupy an active site, maintain a depressed catalyst activity, change the catalyst structure and contribute to the overall deactivation. However, an irreversible poison at low temperature can become reversible at higher temperatures [162]. Thus, sometimes it can be difficult to make clear distinctions. The main poisons in HDO of renewable feedstocks are reported to be the naturally occurring impurities such as phosphorous and alkaline earth metals such as Na, Ca and Mg [66, 165].

As mentioned earlier (section (2.1)), metal impurities are separated from the oil in a hydrodemetalation (HDM) process. Since achieving a 100% HDM is often difficult, it has been reported that even a very low concentration ($\leq$ 1 ppm) metal impurities such as vanadium can be deposited on hydrotreating catalysts ($NiMo/Al_2O_3$ and $CoMo/ Al_2O_3$) with a moderate rate of nearly 1 $mgh^{-1}kg^{-1}$ [166]. The same study has also reported that vanadium can compete with Ni and Co, interfere with their promoting effects on MoS_2 edges and form the topotatic structures such as V_5S_8 and VMo_4S_8 that also can block the support. Iron impurities also can exist in renewable feedstocks either because they are naturally occurring and/or their accumulation during storage and transportation due to the reaction between iron vessels and the feedstocks (e.g. fatty acids) because of their high total acid number (TAN) [47]. It is thermodynamically possible that iron react with hydrotreating catalysts to form species such as $FeMoO_4$, $CoFe_2O_4$, $NiFe_2O_4$ and $FeAl_2O_4$ [43, 167]. However, only two patented reports suggested that iron may deactivate hydroprocessing catalysts [168, 169].

Coking is known to be an ever-present deactivation mode for all hydroprocessing catalysts [43]. Deactivation by coking is defined as the coverage or blockage of both active sites and micro pores due to strong chemisorption of carbonaceous material on the active sites as a monolayer as well as physical adsorption of carbon as multilayers [160]. Coke build-up can significantly reduce the surface area and pore volume of catalysts and with extreme accumulation, can also cause disintegration of catalysts and complete blockage of void space in a catalyst bed [162]. Figure 8 presents an inverse fast Fourier transform (IFFT) pattern of the pore structure of a spent NiMo catalyst with a high carbon content (~ 22 wt%). It can clearly be observed, the majority of the pores are blocked by carbon deposition. Coke deactivation is a relatively fast reaction and several studies have shown that up to 30% of the catalysts pores can be blocked in the initial stage of an HDO reaction [170, 171]. Coke can literally be formed from all HDO feedstocks but olefins and aromatics are reported to be the main coke precursors [172, 173]. The amount of coke deposition is however related to many factors such as feed composition, HDO operating conditions and the structure of HDO catalyst [174, 175]. For example, a high level of impurities in the feed and high reaction temperature may stimulate the coke deposition while high partial pressure of hydrogen can reduce the coke deposition [176].

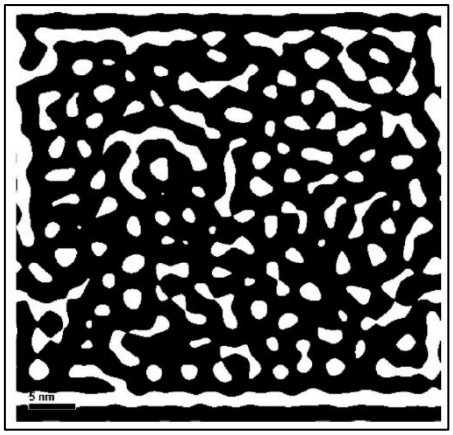

Figure 8. IFFT pattern of a spent $NiMo/Al_2O_3$ catalyst used in an HDO reaction for 24 h [70] .

A general mechanism for the coke formation that has been proposed in literature, includes a reaction path which contains several steps such as adsorption, dehydrogenation, condensation/polymerization and cyclization of hydrogen deficient fragments that form polynuclear deposits [43, 160, 162].

Loss of sulfidity is another main reason for the deactivation of sulfided HDO/HDS catalysts. Long-term presence of the chemisorbed oxygenate compounds on the metallic edges of the MoS_2 slabs can convert them into less active oxide and sulfate phases [34, 140, 164, 177]. Also, gradual preferential sulfur leaching from the more active multilayer MoS_2 phases (Type I), can convert them into less active MoS_2 monolayers [147]. The active sulfided structures of the molybdenum based catalysts and their active sites can be preserved if during a hydrotreatment, certain amount of a sulfiding agent such as H_2S is used. The promotional effect of H_2S on the overall HDO activity of NiMo and CoMo catalysts for conversion of aliphatic acids and esters is reported [140, 177, 178]. However, using an excess amount of H_2S may have an adverse effect on the activity of hydrotreating catalysts for other feeds.

High temperature can affect the supported metal catalysts and deactivate them via three main processes. First, growth of active metal phases which results in loss in the catalytic surface area or reduction of dispersion. Second, reducing the accessibility of active phases due to support pore collapse. And third, transformation of active metal phase into inactive phases due to solid phase chemical reactions. The first and second processes are referred to as deactivation by sintering [160]. A low rate of sintering has been reported at low temperatures, but the sintering rate considerably increases at temperatures around one third of the melting temperature of the metals and in the presence of water [176]. Moreover, the thermally induced degradation can happen during different stages of the life process of a catalyst such as during the catalyst preparation due to calcination and reduction, during the reaction due to presence of hot spots, or during the catalyst regeneration (burning coke) [162]. Sintering is known as an irreversible process so measures should be focused on prevention [160].

3 Experimental

3.1 Catalysts preparation

Two sets of alumina supported base metal catalysts were prepared via impregnation methods. The first set of samples, contained alumina supported monometallic and bimetallic catalysts such as Ni, Co, Mo, NiMo and CoMo, and the second set only contained a bimetallic alumina supported NiMo catalyst. Detailed preparation methods for both sets are described in Paper I and Paper II.

After the preparation, the catalysts in the first set were further treated via calcination and reduction processes. The calcination processes were performed in atmospheric air at two different temperatures 400°C for 1.5 h as a mild condition and 550°C for 2 h as a harsher condition. Based on the calcination treatments, they were divided into different groups. Calcination was followed by the reduction treatments which were performed at 450°C, with different concentrations of hydrogen (5%, 10% and 15% H_2 in Ar) and different durations of 3, 6 and 12 h. It has to be mentioned that some samples in the first set were kept uncalcined but reduced in the same reduction procedures as described above. The prepared NiMo catalysts in the second set was first calcined at 400°C for 1.5 h, not reduced, but instead it was sulfided in a sulfidation process which is fully described in Paper II.

Additionally, a series of NiMo catalysts supported on mixed alumina/ ultrastable Y-type (USY)-zeolite were synthesized via a sequential impregnation method that is further described in Paper V. The metal contents of all catalysts were the same (4 wt% Ni and 12 wt% Mo), but their alumina/USY-zeolite ratios were varied.

3.2 Catalyst characterization

Catalyst samples were characterized by inductively coupled plasma and sector field mass spectroscopy (ICP-SFMS), nitrogen physisorption, elemental microanalysis, hydrogen chemisorption, temperature programmed oxidation (TPO), temperature programmed reaction (H_2-TPR), ethylamine-temperature programmed desorption (ethylamine-TPD), scanning electron microscopy (SEM), transmission electron microscopy (TEM) and X-ray photoelectron spectroscopy (XPS).

3.2.1 Nitrogen physisorption

The textural properties of the samples such as specific surface area, pore size and pore volume were evaluated by nitrogen physisorption using a TriStar 3000 gas

adsorption analyzer (Paper I and Paper IV). Before nitrogen physisorption analysis, approximately 300 mg of each sample was thermally dried (degassed) at 200°C for 3 h under vacuum. The specific surface area was calculated by using the Brunauer-Emmett-Teller equation (BET).

After drying, samples were cooled under vacuum to -195°C (78 K) and subsequently dosed with a small amount of nitrogen. After each dosing, the partial pressure of N_2, when it reached an equilibrium state, was recorded and then the volume of the adsorbed of N_2 was calculated via the ideal gas law. First a monolayer of N_2 is formed which gradually becomes a multilayer. By assuming no interaction between layers, the volume of the monolayer is calculated by using the BET equation.

$$\frac{P}{V(P_0-P)} = \frac{1}{V_m C} + \frac{C-1}{V_m C}\frac{P}{P_0} \quad ; \; C = EXP(\frac{H_1-H_L}{RT})$$

Where P is the partial pressure of nitrogen at equilibrium, P_0 is the saturation pressure of nitrogen, V is the calculated volume of adsorbed nitrogen, V_m is volume of the nitrogen monolayer, C is the BET coefficient, H_1 and H_L are the heat of adsorption of the first and succeeding monolayers, R is the gas constant and T is the adsorption temperature. V_m is calculated via plotting $\left(\frac{P}{V(P_0-P)}\right)$ against $(\frac{P}{P_0})$ and calculating the slope when linear ($0.05 < (P/P_0) < 0.3$).

It is assumed that the surface of a solid catalyst contains equivalent sites and each site adsorbs only one molecule of nitrogen gas in which the adsorbate nitrogen molecules do not interact with each other. Based on this assumption, it has been shown that one molecule of N_2 occupies 0.16 nm^2 [179]. Thus, the BET surface area can be calculated as: (V_mN/VM). M is the mass of solid and N is Avogadro's number. The pore size was calculated by using the Barret-Joyner-Halenda equation (BJH) from the desorption isotherm. The pore volume was assessed from a single point adsorption of N_2 at the P/P_0 = 0.99.

3.2.2 Hydrogen chemisorption and temperature programmed oxidation and desorption

Hydrogen chemisorption studies were conducted to assess the effect of calcination and reduction treatments on the hydrogen uptake capacity of non-sulfided catalysts (Paper I). Temperature programmed oxidation (TPO) studies were performed to measure the carbon content of spent sulfided catalyst (Paper II, Paper III and Paper V). Ethylamine temperature programmed desorption (ethylamine-TPD) were done to measure the acidity of the non-sulfided catalysts (Paper V).

The experimental set up for H_2-chemisorption, TPO and ethylamine-TPD consisted of a manifold of gas mass flow controllers (MFC, Bronkhorst), a Differential Scanning Calorimeter (DSC, Setaram Sensys) and a mass spectrometer (MS, Hiden Analytical HPR 20). An illustration of this setup is presented in Figure 9. The desired inlet gas flow and composition was obtained from the gas manifold prior to the DSC. In the DSC, the heat released due to H_2 chemisorption was detected. The DSC consisted of two vertical quartz tubes used for reference and sampling, respectively. The reference tube was

kept empty but the sampling tube contained sample which was placed on a sintered quartz bed located in the middle of the tube. Subsequently, the outlet gas compositions were analyzed by the MS. Briefly, in H_2- chemisorption experiments samples were first degassed by a flow of 8% H_2 in Ar at 500°C for 15 min. Following the degassing treatment, samples were reduced with different flows of H_2 and different durations. Then, samples were cooled in Ar to 80°C. Finally, the samples were exposed to 100 ppm of H_2 in Ar at 80°C for 1 h. The DSC heat signals and the MS concentration signals were both monitored and the amount of adsorbed hydrogen was calculated. Detailed experimental procedures of H_2-chemisorption are described in Paper I.

In TPO experiments, samples were first pre-treated in a flow of Ar at 110 °C for 1h and at 250 °C for 3h to remove adsorbed water and loosely bound stearic acid and then, the samples were cooled to 50 °C. Following the pretreatment steps, samples were oxidized in a flow of 21% O_2/Ar and 9% O_2/Ar with the heating rate of 2 °C/min to 800 °C. The carbon contents of the spent samples were measured by monitoring the evolved CO, CO_2 concentrations from MS analysis during the oxidation treatment. (Paper II, III and V).In ethylamine-TPD, samples were first pre-treated in a flow of Ar at 110 °C for 1 h and at 250 °C for 3 h to remove adsorbed water, and then reduced by a flow of 13% H_2 in Ar at 600 °C for 2 h. Then, the temperature was decreased to 100 °C and the sample was stabilized in a flow of Ar for 1 h. After stabilization, the sample was exposed to a flow of 543 ppm ethylamine ($C_2H_5NH_2$) in Ar at 100 °C for 3 h (adsorption). Following the adsorption, sample was flushed with Ar for 2 h at 100 °C. Finally, desorption was performed by exposing the sample to a flow of Ar while the temperature was linearly increased at a rate of 5 °C/min to 600 °C.

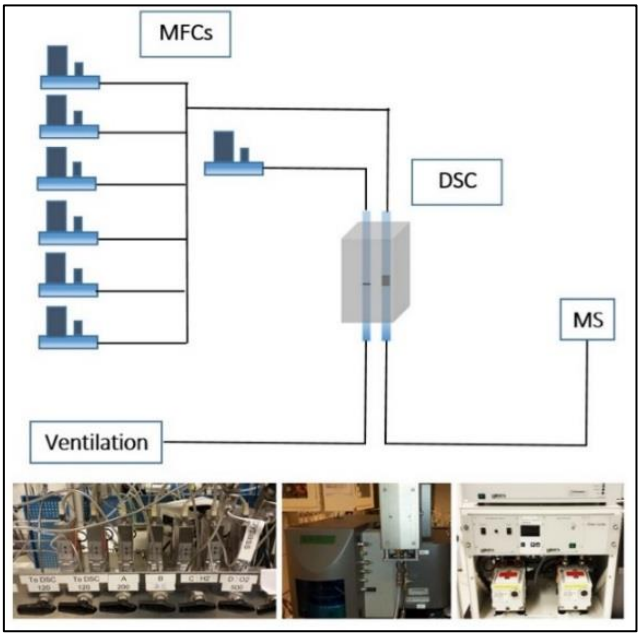

Figure 9. Hydrogen chemisorption, TPO and ethylamine-TPD experimental setup. MFCs = mass flow controllers, DSC = differential scanning calorimeter oven, MS = mass spectrometer.

3.2.3 Scanning electron microscopy (SEM) and transmission electron microscopy (TEM)

Scanning electron microscopy (SEM) was used to observe the surface structure of non-sulfided samples by using a Zeiss Ultra 55 FEG SEM microscope combined with an energy dispersive x-ray spectrometry (EDS) system. The images were formed by secondary electrons (SEs) for all measurements. The transmission electron microscopy (TEM) studies were performed to obtain quantitative overviews on size and shape of metal species on the samples. The TEM investigation was done using an FEI Titan 80-300 microscope equipped with a field emission gun (FEG), a probe C_s corrector and a Gatan image filter (GIF) Tridium. This instrument operated at an acceleration voltage of 300 kV. The microscope was set in scanning TEM (STEM) mode and a high angle annular dark field (HAADF) detector was used. Further description of TEM experiment setups are presented in Papers I, II, IV and V.

3.2.4 X-ray photoelectron spectroscopy (XPS)

The basis of X-ray photoelectron spectroscopy (XPS) is to detect and count the ejected electrons from the surface of a sample when exposed to an X-ray source. In an XPS system, X-rays are produced by exposing aluminum (Al) or magnesium (Mg) with an electron beam resulting in emission photons at energy levels of *hν=1486.6* (Al $K\alpha_{1,2}$) and *hν=1253.6* (Mg $K\alpha_{1,2}$) [180]. Then, a sample is exposed to the x-ray source, which results in emission of photoelectrons with characteristic kinetic energies. The ejected photoelectrons are detected in an electron energy analyzer to form spectrum with intensities at electron energy levels which can provide both quantitative and qualitative information such as the composition and electronic state of the surface region of a sample.

XPS measurements were done to investigate the oxidation states and the chemical compositions of the non-sulfided catalysts as well as the sulfidation sates of the sulfided catalysts by using a Perkin Elmer PHI 5000C ESCA system. The reduced non-sulfided samples were degreened in a flow of 8% H_2 in Ar at 500°C for 15 min to remove hydrocarbon contaminations, but, the sulfided samples were not degreened. The samples were placed on carbon rubber pads which were situated on a sample holder. When the pressure of the main chamber was dropped to $1.2 \cdot 10^{-8}$, the sample holder was shifted to the ultrahigh vacuum chamber. The XPS spectra were collected using a monochromatic Al Kα source with a binding energy of 1486.6 eV. A 90° angle between the x-ray source and the detected photoelectrons was used for all measurements. Sample charge neutralization was done on all samples. The O 1s peak from the alumina with a binding energy of 531.0 eV was taken as reference for all obtained spectra for the non-sulfided samples whereas, the C 1s peak with a binding energy of 284.6 eV was taken as reference for all obtained spectra for the sulfided samples.

3.3 Hydrodeoxygenation and hydroconversion experiments

3.3.1 Materials

Oleic acid (≥ 90%, Sigma Aldrich and 90%, Fluka) and abietic acid (≥ 85%, Sigma Aldrich) were chosen as model compounds for the fatty acid and rosin acid in tall oil, respectively. According to GC-MS analysis, the oleic acid contained oleic acid (90

wt%), myristic acid (5 wt%), pentadecanoic acid (3 wt%) and tridecane (2 wt%). The GC-MS analysis also showed that abietic acid contained abietic acid (85 wt. %), dehydroabietic acid (9 wt%), pimaric acid (4 wt%) and dihydroabietic acid (2 wt%). Dodecane (grade ≥ 99%, Sigma Aldrich) was used as solvent, mainly to minimize possible temperature peaks due to exothermic HDO reactions. Dimethyl disulfide (DMDS, grade ≥ 99%, Sigma Aldrich) was used as a sulfiding agent. The purity of hydrogen feed used in all experiments was over 99.9%. A complex called iron oleate was synthesized as a poison according to a synthesis method described elsewhere [181].

3.3.2 Hydrodeoxygenation and hydroconversion reactor setup

The hydrodeoxygenation (HDO) and hydroconversion reactions were carried out in a 300 mL stainless steel autoclave (Parr instrument). A simplified schematic and a picture of the reactor setup is shown in Figure 10.

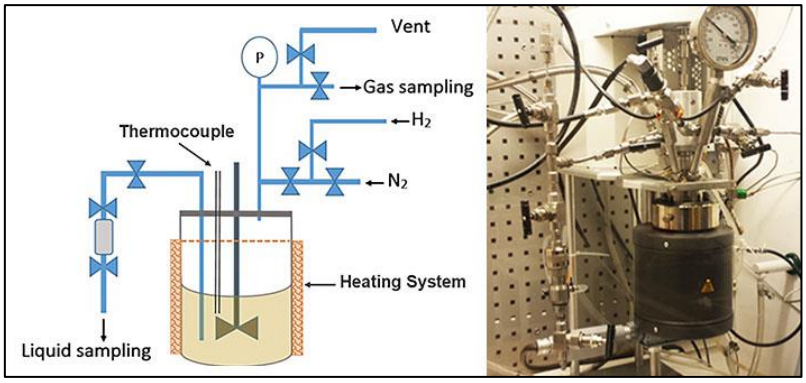

Figure 10. Schematic presentation of the reactor setup used in HDO and hydroconversion reactions.

The catalyst activation process for all HDO experiments was performed via a sulfidation treatment. In brief, 500 mg of the prepared $NiMo/Al_2O_3$ catalyst was activated by 0.5 mL of DMDS with 20 bar of H_2 at 350°C for 4h. The catalyst activation process for all hydroconversion experiments was done via a reduction-sulfidation treatment. In short, 1 g of each catalyst was loaded in the reactor, then first reduced with H_2 (20 bar) at 350 °C for 3 h. Following the reduction treatment, the reduced catalyst was sulfided using 0.1 mL DMDS with H_2 (20 bar) at 350°C for 3 h. After activation, the catalysts were mixed with a feed containing oxygenates (oleic acid and abietic acid), dodecane (solvent) and DMDS, and based on the objective of the study, the concentration of the feeds were varied. However, the total volumes of the feeds were maintained at 150 mL in all experiments.

Then, the system was purged three times with N_2 and H_2, and after that, the temperature was elevated and stabilized at desired reaction temperature. When the temperature was stabilized, stirring was adjusted to 1000 rpm and the reactor was pressurized with hydrogen. The pressure of hydrogen was calculated based on the stoichiometric moles of hydrogen needed for a complete reaction with oleic acid, abietic acid and DMDS. During the experiment, liquid samples were taken at certain time intervals to assess the catalyst activities. The pressure drop after each sampling was compensated by adding more H_2 immediately following each withdrawal of liquid sample. Finally, after

completing each experiment, a portion of the gas was transferred from the reactor to a cylinder that was pressurized to 10 bar with product gas samples at room temperature.

3.3.3 Effect of temperature and pressure on the activity of a HDO catalyst

Five HDO experiments were performed with varying starting temperature from 300°C to 340 °C and the effect of temperature on the activity of a sulfided $NiMo/Al_2O_3$ was studied. In these set of HDO experiments, 500 mg of sulfided catalyst was mixed with 150 mL of a feed containing 10 wt% oleic acid, 90 wt% dodecane and 0.03 mL DMDS. These reactions were all started with the same quantity of hydrogen (0.165 mole) and run for 6h. Also, during each HDO experiment, the temperature, stirring rate and total pressure were all kept constant. Then, after completion of each HDO run, the catalysts were recovered from the reaction mixture and further characterized. In the next set of experiments, three HDO experiments were performed to assess the effect of pressure on the activity of a sulfided $NiMo/Al_2O_3$. In this set of experiments, three HDO experiments were done with three hydrogen partial pressures (60 bar, 65 bar and 70 bar), at 310 °C for 6h. Also, the concentrations of the oleic acid and dodecane were still kept constant at 10 wt% and 90 wt%, respectively, and the total volume of the feed, containing 0.03 mL DMDS, was maintained at 150 mL.

3.3.4 Effect of DMDS concentration on the activity of a $NiMo/Al_2O_3$ catalyst

The effect of the DMDS concentration on the activity of a sulfided $NiMo/Al_2O_3$ catalyst was investigated in two sets of experiments and each set contained three HDO experiments. In the first set of experiments, three different quantities of DMDS (0.015 mL, 0.03 mL and 0.3 mL) were added to 150 mL of reaction mixture containing 10 wt% oleic acid in dodecane. Then, depending on the quantity of added DMDS, HDO reactions were started with 49.3 bar, 49.6 bar and 53 bar of H_2, respectively, and they were run for 4h. It should be noted that H_2 is consumed during the decomposition of DMDS during heating to 320°C. Thus, at higher DMDS concentrations, a larger amount of H_2 was required to produce H_2S. The pressure of H_2 was therefore varied to maintain a constant partial pressure of H_2 after the decomposition of the DMDS. In the second set, three HDO experiments were run under a constant concentration of DMDS, but different pressure of hydrogen. In these experiments, 0.03 mL DMDS was added to a 150 mL of reaction mixture containing 10 wt% oleic acid in dodecane and the reactions were started with three different total pressures of 50, 60 and 70 bar. The second set of HDO experiments were run for 4h.

3.3.5 Effect of rosin acid concentration on the HDO activity of fatty acid

The effect of the abietic acid concentration on the deoxygenation rate of oleic acid was investigated with a set of HDO experiments that were performed with a sulfided $NiMo/Al_2O_3$ catalyst. The HDO experiments were performed with 10 wt% oxygenates, including varying ratios of abietic acid and oleic acid, in 90 wt% dodecane (solvent), at 320 °C, with 500 mg of catalyst and 0.1 mL of DMDS. For complete stoichiometric HDO of each mole of oleic acid and abietic acid, 4 moles and 5 moles of H_2 were required, respectively. Thus, the start pressure of hydrogen was adjusted based on the compositions

of oxygenates in the feed. During each HDO experiment, the temperature, stirring rate and total pressure were all kept constant.

3.3.6 Effect of iron poison on the activity of HDO catalysts

The poisoning effect of iron on the activity of sulfided Mo/Al_2O_3 and $NiMo/Al_2O_3$ used in HDO of oleic acid was studied. In these studies, different quantities of an iron containing compound (iron oleate), used as poison, was added to a 150 mL feed containing 15 wt% oleic acid mixed in dodecane, 0.1 mL of DMDS and 1g of sulfided catalyst. All experiments were carried out at 60 bar H_2, at 325 °C and with a stirring rate of 1000 rpm for 330 minutes.

3.3.7 Activity changes of the spent catalyst

A number of HDO reactions were repeated with the recovered catalysts from their corresponding previous HDO reactions. In short, after each HDO experiment, the catalysts were recovered from the reaction mixtures by filtration, washed with warm ethanol and acetone, and dried overnight. It was expected that the catalyst sulfidity would be fairly maintained during the HDO runs due to the presence of DMDS, thus the recovered catalysts were used in the subsequent HDO reactions without additional sulfidation. The liquid sampling procedure was also the same as that performed in the previous HDO experiments with fresh catalysts. The spent catalysts from the repeated experiments were also recovered and further characterized.

3.3.8 Hydroconversion of rosin acids into fuel components

Hydroconversion reactions of abietic acid were performed using alumina, USY-zeolite and mixed alumina/USY-zeolite supported NiMoS catalysts. In each experiment, 1 g of the activated catalyst was mixed with a feed (150 mL), containing 5 wt% of abietic acid and 95 wt% dodecane. Also, 0.1 mL DMDS was added to maintain the sulfidity of the catalysts during the course of reactions. Then, the system was purged three times with first N_2 and then H_2, before the temperature was elevated to 380 °C and stirring was adjusted to 1000 rpm. Afterward, the reactor was pressurized with 75 bar of hydrogen (99.9%) to start the hydroconversion reactions.

3.3.9 Liquid and gas sample analysis

The liquid samples were analyzed by GC/MS technique. The reaction products were identified by a mass selective detector system (Agilent 5977) and quantified by a gas chromatograph system (Agilent 7890B). Before the GC/MS analysis, liquid samples that were partially solidified due to their stearic acid content, were first liquefied in a warm water bath at 70°C. Then, 1 mL of the liquefied samples were mixed with 200 µl pyridine (grade ≥ 99%, Sigma Aldrich) to obtain a single liquid phase.

The liquid samples were subsequently centrifuged (WIFUG Lab centrifuges, 500 E) at 1500 rpm for 2 min, and 200 µl of the clear solution were mixed with 30 µl *N*,*O*-Bis(trimethylsilyl)trifluoroacetamide (BSTFA). After this, the mixtures were kept for 17h at room temperature to achieve complete silylation of the compounds. Finally, 1 µl of the filtrate was analyzed by GC/MS. The oven ramp settings for the GC were as follows: 100°C for 1min, ramp 10 °C/min to 190 °C, and continued to ramp at 30°C/min to 300°C and

retained for 5 min. The GC was equipped with an HP-5 column, and an FID detector (maintained at 335°C). The injector temperature was maintained at 325°C.

The gas samples were analyzed by a calibrated GC (Scion 456 GC, Bruker) that was equipped with a FID detector for organic components and a TCD detector for H_2, CO and CO_2. The initial oven temperature in the GC was 40 °C and increased at 5 °C min^{-1} to 80 °C and then increased at 30 °C min^{-1} to 150 °C where it was held constant for 1 min.

4 Results and Discussion

This study was performed to investigate the activity of alumina and USY-zeolite supported Ni, Co and Mo containing catalysts used for HDO and hydroconversion of tall oil fatty acid and tall oil rosin acid. In the first part, the effect of different pretreatment steps on the resulting properties such as the hydrogen uptake capacity of non-sulfided alumina supported Ni, Co and Mo containing catalysts were investigated (Paper I). Next, HDO of a tall oil fatty acid (oleic acid) over a prepared sulfided $NiMo/Al_2O_3$ was studied and effects of temperature, hydrogen pressure and concentration of DMDS on the catalyst activity was analyzed (Paper II). In the second part of this study, HDO of a tall oil rosin acid (abietic acid) over a prepared sulfided $NiMo/Al_2O_3$ was studied. Also, the inhibition of oleic acid HDO activity due to addition of abietic acid was investigated (Paper III). Moreover, the poisoning effect of iron on the activity of sulfided Mo/Al_2O_3 and $NiMo/Al_2O_3$ catalysts used in HDO of oleic acid was studied (Paper IV). Finally, the activity of alumina, USY-zeolite and mixed alumina/USY-zeolite supported NiMo sulfide catalysts used for hydroconversion of abietic-type rosin acids was examined (Paper V).

4.1 Effect of pre-treatments on hydrogen uptake capacity

In industrial hydrotreating processes, hydrogen gas is chemisorbed on the surface of the catalysts. Therefore, hydrogen uptake capacity is an imperative property that affects the performance of all hydrotreating catalysts. The hydrogen uptake capacity can be influenced by several physical and chemical properties of a catalyst such as textural, surface structure, state of dispersion and oxidation of metal phases [104, 125]. The physical and chemical properties of a catalyst can also be affected due to variations in their preparations and different treatments throughout their use. The textural properties of the catalysts studied are shown in Paper I. The reported metal contents of these samples were measured by inductively coupled plasma and sector field mass spectroscopy (ICP-SFMS). The increase in calcination temperature from 400 °C to 550 °C did not have any significant effect on the physical properties such as the BET surface area, pore size and volume of the non-sulfided samples (see Paper I).

The effect of calcination on the surface structure of the non-sulfided catalysts was studied by SEM measurements. A selection of SEM results including micrographs of the alumina supported Ni sample calcined at 550 °C (a), alumina supported Co sample, calcined at 400 °C (b) and alumina supported CoMo sample, calcined at 550 °C (c) are

shown in Figure 11. A distribution of small and irregular shaped particles (≤ 10 μm), dispersed among larger particles (~ 140 μm) were observed in all the calcined samples.

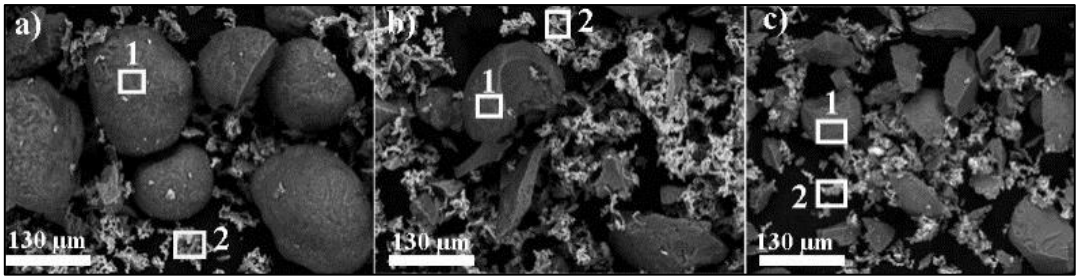

Figure 11. SEM micrograph of Ni/Al_2O_3 calcined at 550 °C (a), Co/Al_2O_3 calcined at 400 °C (b) and $CoMo/Al_2O_3$ calcined at 550 °C (c).

The chemical composition of the small and large particles were analyzed using X-ray energy dispersive spectrometry (XEDS) elemental mapping on different locations of the calcined samples. The analyzed areas are marked as box 2 for the smaller and inhomogeneously shaped particles, and box 1 for the larger and more homogeneously shaped particles in Figure 11. The XEDS results showed large variations in the metal concentrations between large and small (fractured) particles. For instance, the metal/alumina ratio of smaller particles were 10 times higher than the metal/alumina of larger particles in the calcined Co sample (Paper I, Table 2).

The chemical composition of the small particles also indicated that the metal oxides formed new phases that are known as heteropolymetal compounds which are composed of alumina as their central heteroatom [182]. These heteropolymetal compounds could have been formed during two different processes: either during the impregnation of the alumina with the metal precursors or during the calcination of the samples. The second possibility would imply that, the metal oxide precursors have interacted with the alumina support to form a new phase as heteropolymetal compounds. To validate the possibility of calcination, two additional SEM measurements on two uncalcined samples (Co and NiMo) were performed (Figure 12).

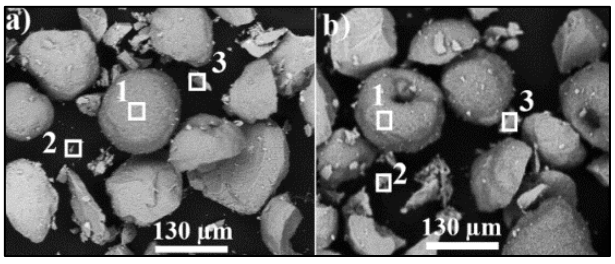

Figure 12. SEM micrograph of uncalcined Co/Al_2O_3 (a), and uncalcined $NiMo/Al_2O_3$ (b).

The XEDS analyzed areas are marked as box 2 for the very small particles (~ 10 μm), box 1 and box 3 for the larger particles (20- 150 μm) in Figure 12. From the SEM micrograph shown in Figure 12, it can be observed that the distribution of the small particles (≤ 10 μm), are still present in both uncalcined Co/Al_2O_3 and $NiMo/ Al_2O_3$ samples. However, the detected concentrations of alumina for the area 2 were very small (1.4% and 1.1%). Moreover, the distribution of the small particles (≤ 10 μm), in both uncalcined

samples, are reduced in comparison to the calcined samples (Figure 11). Therefore, we propose that the small particles (~ 10 µm, heteropolymetal compounds) are predominately formed during the calcination of dried salt precursors. The formation of the heteropolymetal phase would reduce the catalyst activity due to reducing the surface area of the metal particles on the support.

The dispersion (surface to volume ratio) of the active metal is a decisive property that steers many catalytic reactions. The dispersion of a catalyst can be affected by many parameters such as pH of the impregnating solutions during the catalyst preparations. Scanning transmission electron microscopy (STEM) analysis was used to assess the dispersion of the prepared catalysts. Figure 13 presents the STEM micrographs of two $NiMo/Al_2O_3$ samples that were prepared via two different impregnation methods, under different pH values. Detailed preparation procedures are described in Paper I and Paper II.

Briefly, the first $NiMo/Al_2O_3$ sample (Figure 13a) was prepared by a co-impregnation method in which both solutions of nickel and molybdenum precursors were added to a prepared alumna slurry, which its pH was maintained at 10.5. The second $NiMo/Al_2O_3$ sample (Figure 13b) was prepared by a sequential impregnation method in which the molybdenum precursor solution was first added to a prepared alumna slurry, maintained with a pH of 4, and then the mixture of alumina and molybdenum precursor was freeze-dried and calcined. Afterwards, the nickel precursor solution was added to a slurry of the prepared Mo/Al_2O_3 sample and its pH was increased and stabilized at 9, and then the final solution was freeze-dried and calcined. The freeze drying and calcination conditions for both $NiMo/Al_2O_3$ sample were the same. Also, in both preparations, the concentrations of Ni and Mo in the aqueous solutions were adjusted to result in a targeted metal loading on the sample of 5 wt% and 15 wt%, respectively. The metallic nanoparticles were analyzed using XEDS and electron energy loss spectroscopy (EELS) analysis.

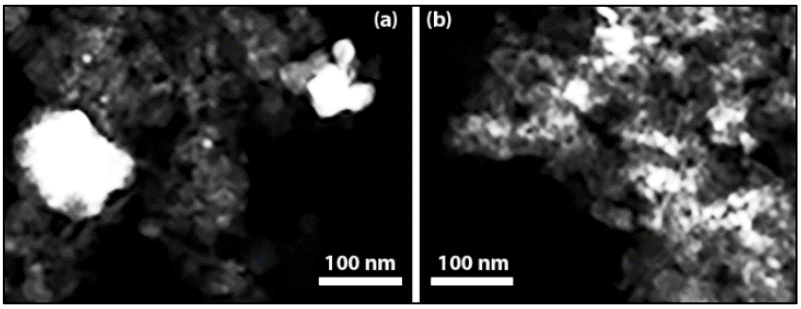

Figure 13. STEM micrographs of a $NiMo/Al_2O_3$ sample prepared by co-impregnation under pH of 10.5 (a) , and a $NiMo/Al_2O_3$ sample prepared by sequential impregnation under pH of 4 and 9.

The averaged nanoparticle sizes on the first $NiMo/Al_2O_3$ (Figure 13, a) were calculated to be 125 nm (28 particles counted). Whereas, the averaged nanoparticle sizes on the second $NiMo/Al_2O_3$ sample (Figure 13, b) were calculated to be 28 nm (45 particles counted). The NiMo nanoparticles in the sample which was prepared by co-impregnation under alkaline condition (pH of 10.5) seemed to be agglomerated to form larger NiMo nanoparticles which resulted in a lower NiMo dispersion.

The effect of calcination treatment on the hydrogen uptake capacity of non-sulfided catalysts was studied by performing H_2-chemisorption experiments. In the H_2-chemisorption experiments, samples were first calcined in different calcination conditions and then they were reduced in the same reduction conditions. Detailed experimental procedures are described in Paper I. Figure 14 presents the hydrogen chemisorption measurements from three Ni/Al_2O_3 samples, with the same Ni loadings but different calcination conditions. The hydrogen chemisorption results evidently show that the hydrogen uptake of the sample precalcined at 400 °C was considerably higher compared to the sample precalcined at 550 °C. Also, the highest hydrogen uptake occurred on the Ni sample which was not previously calcined (fresh sample) but instead the precursor was decomposed during the reduction treatment in a flow of hydrogen.

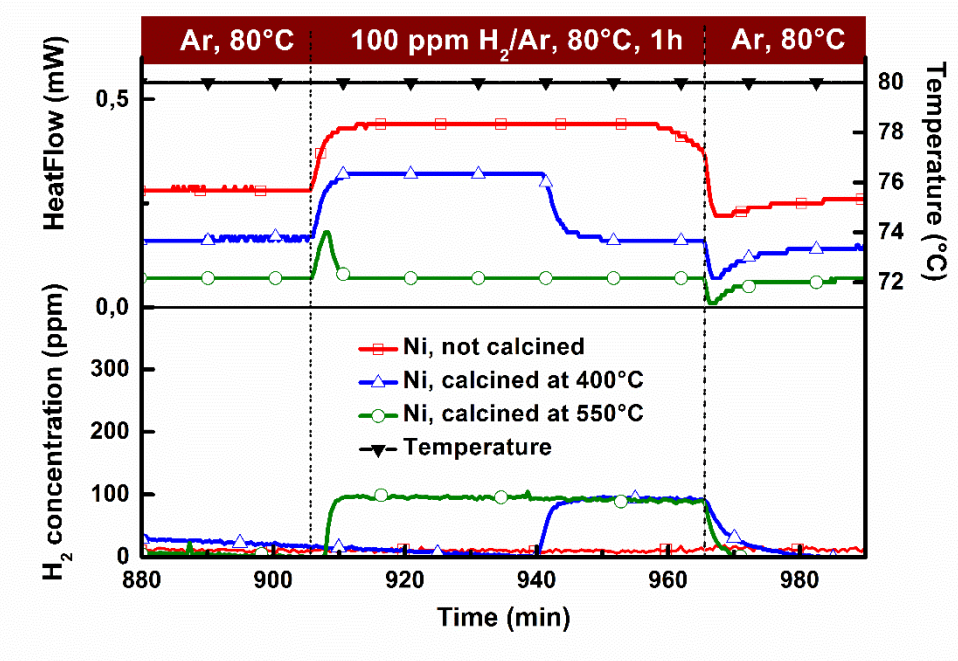

Figure 14. The effect of calcination on the reducibility of Ni/Al_2O_3 (10 wt%) samples. The top panel shows the heat signal from the DSC and the sample temperature during the adsorption. The bottom panel presents the corresponding hydrogen concentration signal measured by MS.

The difference in the hydrogen uptake may be explained by the oxidation states of the Ni sites. The X-ray photoelectron spectroscopy (XPS) measurements were performed to investigate the changes in oxidation state of Ni sites caused by the initial calcination of the samples. The XPS spectra for all three samples are shown in Figure 15. The left panel presents the Ni 2p core level spectrums including clear peaks of Ni $2p_{1/2}$, Ni $2p_{3/2}$ and their shake-ups satellites. The Ni $2p_{3/2}$ peaks of all three samples were further investigated and deconvoluted by fitting a Gaussian–Lorentzian function (Figure 15, right panel). The center of the Ni $2p_{3/2}$ peaks are positioned in a region of 853.4-855.2 eV with apparent satellite features with approximately 6 eV higher than the main photoemissions. This would clearly indicate the presence of Ni^{2+} in all samples. The deconvolution of the Ni $2p_{3/2}$ peak of the uncalcined Ni sample revealed three peaks with binding energies of 852.7 eV, 853.8 eV and 854.3 eV, respectively. These binding energies can be attributed to Ni° and Ni^{2+} sites [183]. It can clearly be observed that the uncalcined Ni sample mainly

contained the metallic form of Ni (Ni°) and a very small fraction of the oxide form (Ni^{+2}). The deconvoluted Ni $2p_{3/2}$ peak of the sample calcined at 400 °C contained four peaks with binding energies of 852.7 eV, 853.4 eV, 854.1 eV and 855.6 eV. These peaks can be attributed to Ni°, Ni^{2+} and $Ni^{3+}/NiAl_2O_4$ sites respectively. The fraction of Ni° sites gradually decreased while the fraction of Ni^{2+} and particularly $Ni^{3+}/NiAl_2O_4$ increased due to the pre-calcination treatment. The deconvolution results of the Ni $2p_{3/2}$ peak of the sample calcined at 550°C showed that this sample mainly contained the oxide forms of Ni, including Ni^{2+} and $Ni^{3+}/NiAl_2O_4$. These results are indicative of a detrimental effect of a pre-calcination treatment on the reducibility of Ni samples. However, the $NiMo/Al_2O_3$ samples that were calcined and reduced with similar conditions as those for Ni/Al_2O_3 samples, showed small hydrogen adsorption and the following XPS measurements confirmed that their Ni and Mo phases were mainly in forms of metal oxides and spinels such as Ni^{2+}, $NiMoO_4$, MoO_3 and $Al_2(MoO_4)_3$. The calcined CoMo samples also did not show any hydrogen uptakes since the metal phases where in the form of oxides and spinels. Further results are reported in Paper I.

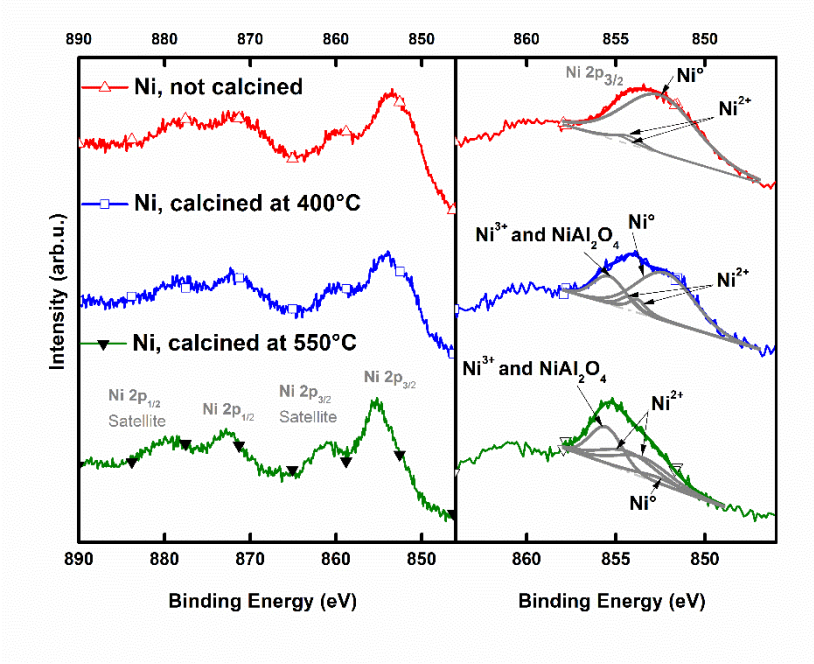

Figure 15. The left panel shows the XPS spectra of three Ni/Al_2O_3 samples for binding energies between 890 and 840 eV, which contain the Ni $2p_{1/2}$ and Ni $2p_{3/2}$ and their satellite peak positions. The right panel shows the deconvolution of the Ni $2p_{3/2}$ peaks.

To summarize, higher calcination temperature (550 °C versus 400 °C) caused lower dispersions of metal phases on the surface of catalysts and at the same time, it stimulated the metal-support interactions by increasing the formation of spinels. Moreover, the detrimental effect of using an inappropriate pH of the impregnating solutions on the dispersion of the metal phases was also found.

4.2 Characterization of alumina supported MoS and NiMoS catalysts

Alumina supported Mo and NiMo catalysts were prepared via an impregnation method and thereafter they were sulfided. The preparation and sulfidation

procedures are described in Papers II, III and IV. After sulfidation, the sulfur, metal and carbon contents of the catalysts were characterized by inductively coupled plasma and sector field mass spectroscopy (ICP-SFMS) and elemental microanalysis. Afterwards, the catalysts were further characterized by XPS, TEM, SEM, temperature programme oxidation (TPO) and hydrogen temperature programmed reaction (H_2-TPR). The ICP and elemental microanalysis results are presented in Table 2.

Table 2. The chemical composition of sulfided $NiMo/Al_2O_3$ sample following sulfidation treatment.

Methods	Ni (wt%)	Mo (wt%)	S (wt%)	C (wt%)
ICP-SFMS [a]	4.6	13.8	10.2	-
Elemental Microanalysis [b]	-	-	9.7	0

[a] Inductively coupled plasma and sector field mass spectroscopy (ALS Scandinavia AB). [b] Elemental Microanalysis Ltd. UK.

The sulfidation state of the sulfided catalysts was analyzed by XPS measurements. The Ni 2p core level spectrum includes Ni $2p_{1/2}$, Ni $2p_{3/2}$, and shake-up satellites, and the Mo 3d/S 2s core level spectrum includes Mo $3d_{3/2}$, Mo$3d_{5/2}$, S 2s and shake-up satellites were deconvoluted by fitting a Gaussian-Lorentzian function. The peak positions and areas were optimized until the standard deviation (χ^2) stabilized to a minimum at 0.5. The deconvolution of the Ni $2p_{3/2}$ peak of all samples revealed four peaks with binding energies of 852.7 eV, 853.8 eV, 854.4 eV and 855.9 eV. These binding energies can be attributed to NiS, NiMoS, Ni^{+2} and $NiMoO_4$, respectively [129, 142, 183]. The deconvolution of the Mo $3d_{5/2}$ peak revealed two peaks with binding energies of 229.1 eV and 229.8 eV which can be attributed to MoS_2 and Mo^{+6}, respectively [129, 142]. Also, the broadened low intensity S 2s peak with the binding energy of 226.4 eV can be attributed to elemental sulfur (S). The XPS results of the deconvoluted Ni 2p and Mo 3d core level spectra for a freshly sulfided catalyst before being used in the reaction are presented in Figure 16.

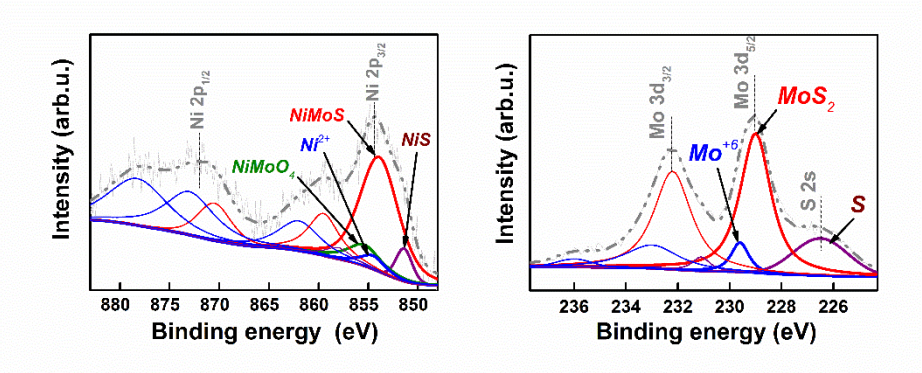

Figure 16. XPS spectra of the Ni 2p, Mo 3d and S 2s core level spectrum for a freshly sulfided sample.

The composition of the nickel and molybdenum phases were also estimated based on the area of different deconvoluted peaks. The results indicate that the activated (sulfided) catalysts mainly contained the mixed phase NiMoS (79% of total nickel content) and MoS_2 (87% of total molybdenum content). Still, small portions of NiS (6% of total

nickel content) and metal oxides such as Ni^{+2} (8% of total nickel content), $NiMoO_4$ (7% of total nickel content) and Mo^{+6} (13% of total molybdenum content) were detected.

The detected metal oxides may be a result of either incomplete sulfidation or superficial oxidation of the catalyst, when exposed to air during its transfer from reactor to XPS instrument. The presence of a strong peak for the elemental sulfur may indicate that an excess amount of DMDS was used during the sulfidation process. However, the amount of the detected elemental sulfur, which is often added to the total sulfur contented of a catalyst (Table 2) from a bulk elemental sulfur analysis, should not be considered as an assessment of the catalyst sulfidity.

The NiMoS and MoS_2 phases in the sulfided catalyst were also identified by using transmission electron microscopy (TEM) analysis. A TEM micrograph showing typical structures of the NiMoS and MoS_2 phases in the sulfided catalyst is presented in Figure 17. The black thread-shape fringes represents the MoS_2 slabs that are dispersed on the surface of the alumina. The presence of a single NiS phase was not observed in the TEM analysis. An average slab length for this sample was calculated to be 4.3 nm, based on measuring 150 slabs.

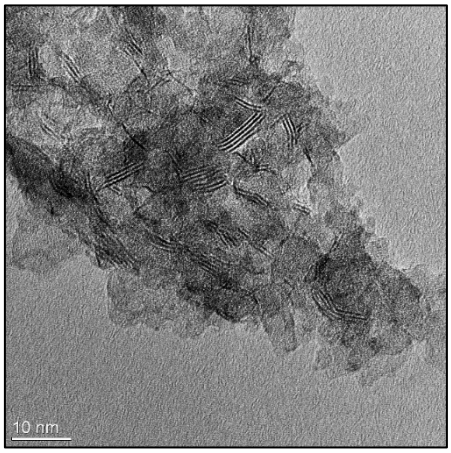

Figure 17. TEM micrograph of freshly sulfided $NiMo/Al_2O_3$.

4.3 Hydrodeoxygenation (HDO) reaction of oleic acid

During HDO of oleic acid, the activity and selectivity of a prepared sulfided $NiMo/Al_2O_3$ catalyst were measured. Figure 18 shows the distribution of yields of the liquid products, including error bars, as a function of time and the gas phase composition of the HDO experiments. The reproducibility of the experiments were confirmed from the repeated experiments and the molar balances of liquid products were 94% on average. The baseline experiment was performed at 320 °C, with 500 mg of the sulfided catalyst, under 49 bar H_2 for 4h (without $DMDS/H_2S$). The volume of the feed mixture, including oleic acid (reactant) and dodecane (solvent), was 150 mL and a reactant/catalyst mass ratio of 25.4 was used in this experiment.

The concentration of oleic acid dropped sharply (during the first two hours of the reaction) and then reached a very small concentration of 0.15% after 4h. Thus, an almost complete conversion of oleic acid was observed in the end of experiment (Figure 18A).

Also, at the beginning of the reaction (during the first 60 min), a sharp increase in concentration of stearic acid was observed.

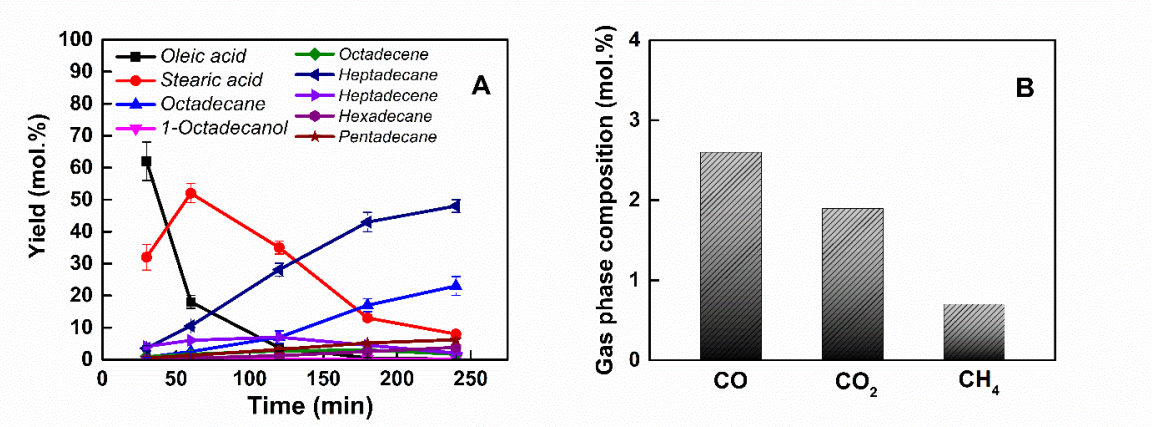

Figure 18. Distribution of the detected reactant and products (A), and final gas phase composition (B) of a baseline HDO reaction of oleic acid. The reported yields are calculated as the ratio of the number of moles of product to the initial number of moles of the oleic acid, excluding the solvent (dodecane).

The quick formation of the stearic acid can be explained by the fast HYD reaction of the unsaturated carbon double bond (C=C) of oleic acid by H_2 which is in good agreement with previous studies [20, 184]. Then, the concentration of stearic acid, however, gradually decreased while the concentrations of the heptadecane (C_{17}) and octadecane (C_{18}), increased with time towards the end of the reaction. Unsaturated hydrocarbons such as heptadecene and octadecene, and other oxygen containing compounds such as 1-octadecanol were also detected in the liquid samples and their concentration profiles are shown in Figure 18A. Other identified oxygenates such as heptadecanal and octadecanal were detected but they are not shown here because their detected yields were very small (less than 1%).

According to many studies, C_{17} and C_{18} hydrocarbons are formed via three reaction routs: decarbonylation/decarboxylation (DCO_x) and deoxygenation (DO) [17, 185-187]. In a recent HDO study, Coumans et al. [187] proposed that fatty acids are first deoxygenated to aldehydes and alcohols intermediates by releasing water. Then, these intermediates undergo further deoxygenation and decarbonylation to produce olefin intermediates with even and odd numbers of carbon (octadecene and heptadecene). These olefins intermediates are finally hydrogenated to produce alkanes (C_{18} and C_{17}) [187].

From the concentration profiles (Figure 18), it may be suggested that C_{17} is produced via DCO_x of stearic acid and/or HDY of unsaturated heptadecene, which may have been formed by DCO_x of oleic acid and/or DO of stearic acid. The presence of CO and CO_2 in the gas phase composition (Figure 18B) is an indication of the occurrence of decarboxylation and decarbonylation routes, respectively. Higher concentrations of heptadecane and CO can also indicate that the decarbonylation route was favored. The small detected concentration of hexadecane (C_{16}) and pentadecane (C_{15}) can indicate a minor hydrogenolysis reactions of C_{18} and C_{17} occurred on the acid sites of the weakly acidic gamma alumina catalyst support. The presence of CH_4, in the gas phase composition

(Figure 18B), partially indicates the occurrence of methanation of CO and CO_2 and partially hydrogenolysis of C_{18} and C_{17}.

4.4 Effect of temperature and pressure on the activity of $NiMo/Al_2O_3$ catalyst

The effect of temperature and pressure on activity and selectivity of the $NiMo/Al_2O_3$ catalyst used in HDO of oleic acid was investigated. To assess the effect of temperature, five HDO experiments were performed, with varying starting temperature from 300 °C to 340 °C, under hydrogen partial pressures from 53 bar to 57 bar for 6h and 1000 rpm stirring rate (Figure 19). In all experiments, 500 mg of sulfided catalyst was mixed with 150 mL of a feed containing 10 wt% oleic acid, 90 wt% dodecane and 0.03 mL DMDS.

The strong temperature dependence of the conversion indicates that the HDO of oleic acid is likely to be a kinetically limited process. The results in Figure 19 (A and B) also show that the yields of the main products, heptadecane (C_{17}) and octadecane (C_{18}), increased when temperature increased. Also, under all the studied temperatures, C_{17} was the main product. However, the selectivity towards C_{17} increased by 6% when temperature increased from 300 °C to 310 °C and then slightly decreased at higher temperatures up to 340 °C (Figure 19D). On the other hand, the selectivity towards C_{18} was near constant for lower temperatures (300 °C to 310 °C) and then slightly increased for higher temperatures (310 °C to 340 °C).

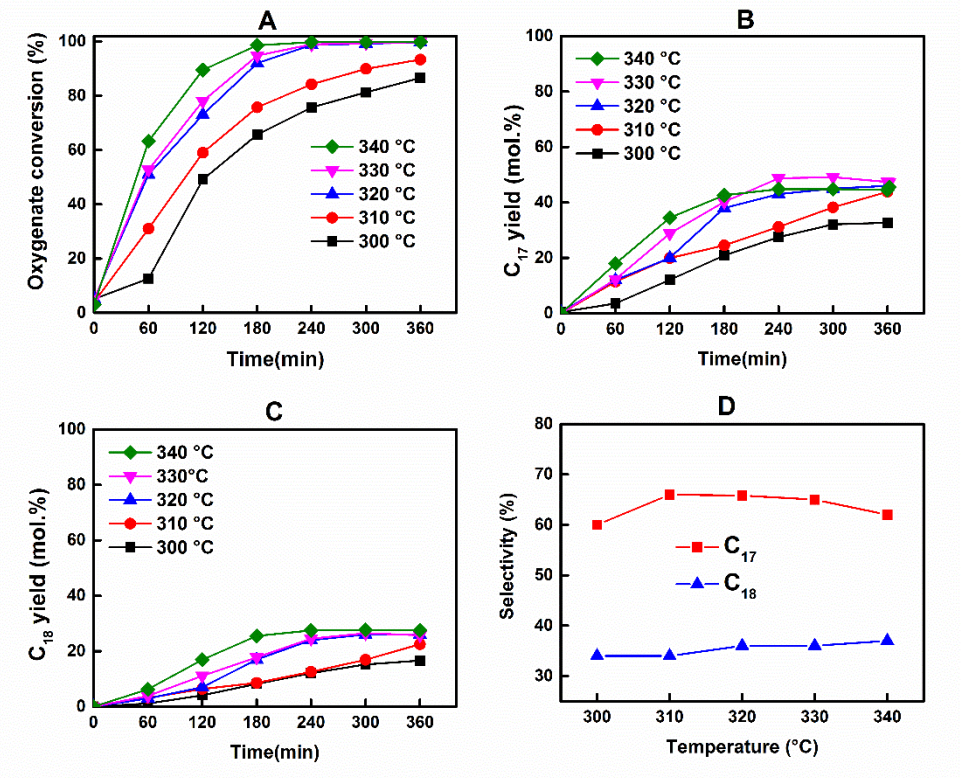

Figure 19. Effect of temperature on: (A) oxygenate conversion (B) yields of heptadecane (C_{17}), (C) yields of octadecane (C_{18}) and (D) selectivity.

Figure 20 presents the activity and selectivity changes of sulfided $NiMo/Al_2O_3$ catalyst due to the change in HDO pressure. These experiments were started at 310 °C, with 500 mg of sulfided catalyst mixed with 150 mL of a feed (10 wt% oleic

acid and 90 wt% dodecane) and 0.03 mL DMDS with varying total pressure from 50 bar to 70 bar. In all experiments, the oxygenate conversion rate was generally unaffected when pressure increased from 50 bar to 70 bar and stayed nearly constant with an overall rate of ~ 22 $mmolg^{-1}h^{-1}$ (Figure 20A). If the reaction is first order with respect to hydrogen concentration (partial pressure), then the rate of increase of conversion would be independent of the starting partial pressure of hydrogen. However, for a reaction order greater than one, a lower start partial pressure would also reduce the rate of increase of conversion and if reaction order is lesser than one then the opposite effect would be expected. Thus, according to results in Figure 20, the rate of conversion of oleic acids is nearly first order reaction with respect to hydrogen partial pressure. Also, for lower pressures (50 bar and 60 bar), the selectivity towards both products C_{17} and C_{18} was constant (Figure 20B). However, at higher pressure of 70 bar, the selectivity towards C_{17} decreased slightly by 6% while it increased by the same percentage of 6% for C_{18}.

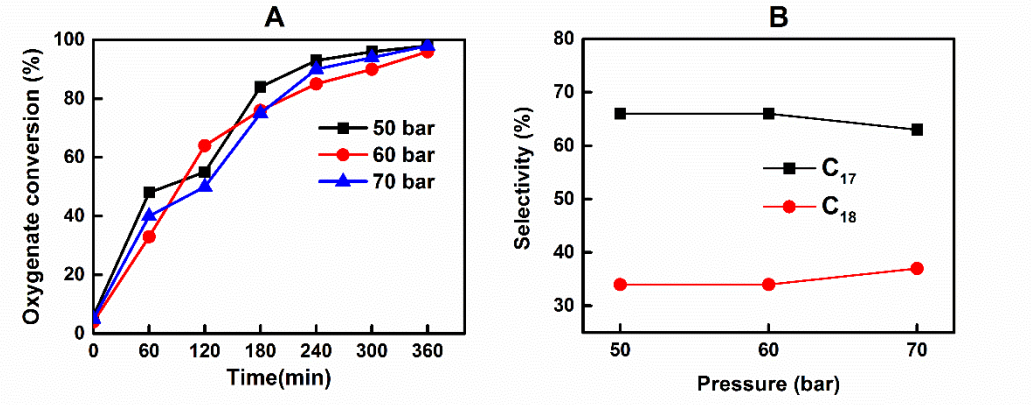

Figure 20. Effect of pressure on: (A) oxygenate conversion (B) C_{17} and C_{18} selectivity.

4.5 Effect of DMDS concentration on the activity of $NiMo/Al_2O_3$ catalyst

The effect of DMDS concentration on the activity of the $NiMo/Al_2O_3$ catalyst, used for HDO of oleic acid, was evaluated in two sets of experiments. DMDS is added to the feed to maintain the sulfided state of the catalyst. In the first set, three HDO experiments were done at 320 °C, with 500 mg of the freshly sulfided catalyst (1^{st} runs) and with varying quantities of added DMDS (0.015 mL, 0.03 mL and 0.3 mL) to the initial feed. In order to use the same hydrogen partial pressure in the HDO experiments, depending on the quantity of added DMDS (0.015 mL, 0.03 mL and 0.3 mL), reactions were started with pressures of 49.3 bar, 49.6 bar and 53 bar of H_2, respectively. After 4 h reaction, the catalysts were recovered and analyzed. In the second set, three HDO experiments were done by using the recovered catalysts (2^{nd} runs) from the first run experiments, under the same conditions as the corresponding first HDO experiments.

4.5.1 Activity and selectivity changes in 1^{st} run and 2^{nd} run $NiMo/Al_2O_3$ catalysts

Figure 21 and 22 present the activity and selectivity results from the HDO reactions that were performed by the 1^{st} (freshly sulfided) and 2^{nd} run (recovered from the 1^{st} runs) catalysts, respectively. Initial and average rates of conversion were calculated based on the slope of the conversion curves (Figure 21) for the first 60 min reaction time and over the entire reaction period, respectively.

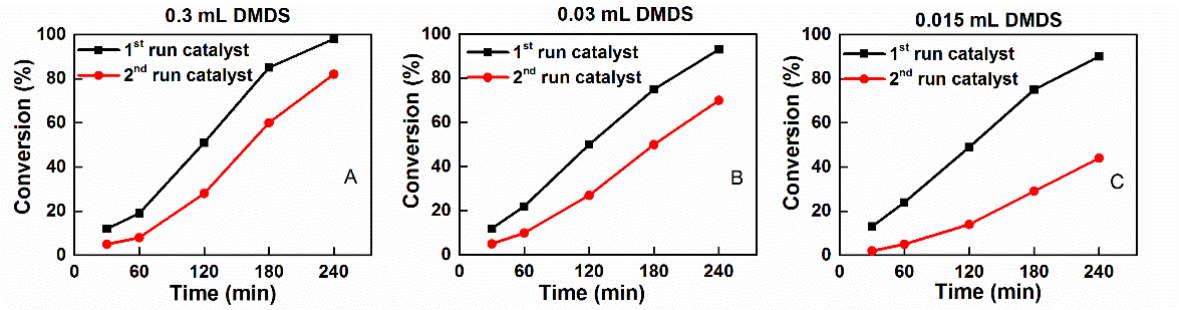

Figure 21. Conversion during the first run and second runs of HDO experiments. Reactions were performed with (A) 0.3 mL DMDS, (B) 0.03 mL DMDS and (C) 0.015 mL DMDS.

For short reaction times (less than 60 min), the initial rate of conversion with both catalysts (1st and 2nd runs) slightly deceased, when the concentration of DMDS increased. In other words, the initial rate of conversion was somewhat inhibited when higher concentration of DMDS was used. However, the overall rate of conversion for all catalysts was promoted when a higher concentration of DMDS was used.

The selectivity results (Figure 22) also show that higher concentration of DMDS promoted the selectivity towards C_{17} and suppress the selectivity of C_{18}. In other words, DMDS clearly promoted DCO_x routes and suppressed the DO route. Our results are in line with the work done by Coumans et al [187] and Senol et al [188]. Also, for all DMDS concentrations, the overall rate of conversion for 1st run catalysts was more than the 2nd runs. Results from the characterization of used catalysts will be shown in sections 4.5.2 and 4.5.3.

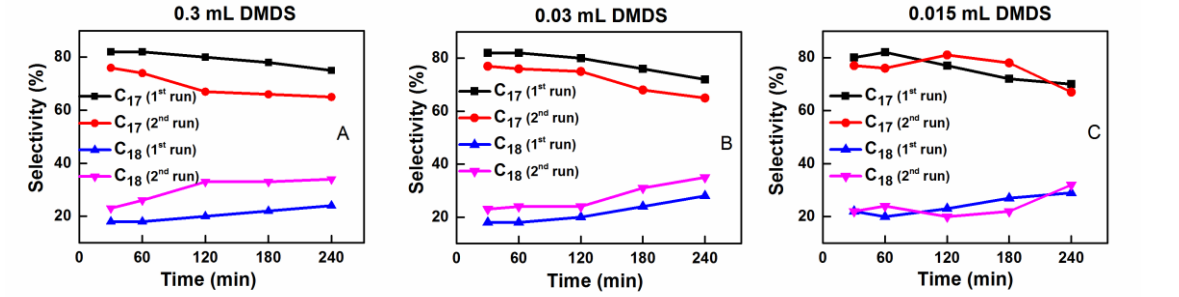

Figure 22. Selectivities of heptadecane and octadecane formed during the first run and second runs of HDO experiments. Reactions were performed with (A) 0.3 mL DMDS, (B) 0.03 mL DMDS and (C) 0.015 mL DMDS.

4.5.2 Sulfidation state of 1st run and 2nd run $NiMo/Al_2O_3$ catalysts

As previously stated, loss of sulfidity is considered as one of the main contributing factor to a drop in activity of sulfided catalysts. During an HDO reaction, the coexistence of sulfided catalysts with oxygenate reactants and products such as oxygenate feeds, CO, CO_2 and water, would result in oxidation of active metal sulfide phases NiMoS and MoS_2) to their less active oxide forms. Therefore, a sulfiding agent such as DMDS, H_2S and CS_2 must be added to the feed to maintain the sulfided state of the catalyst. Rapid deactivation of a sulfided $NiMo/Al_2O_3$ catalyst during HDO of oleic acid, which was performed without a sulfiding agent, is reported elsewhere [187].

Figures 23 present the XPS results of recovered catalysts from the 1st HDO run and Figure 24 present the XPS results of recovered catalysts from both 1st and 2nd HDO runs.

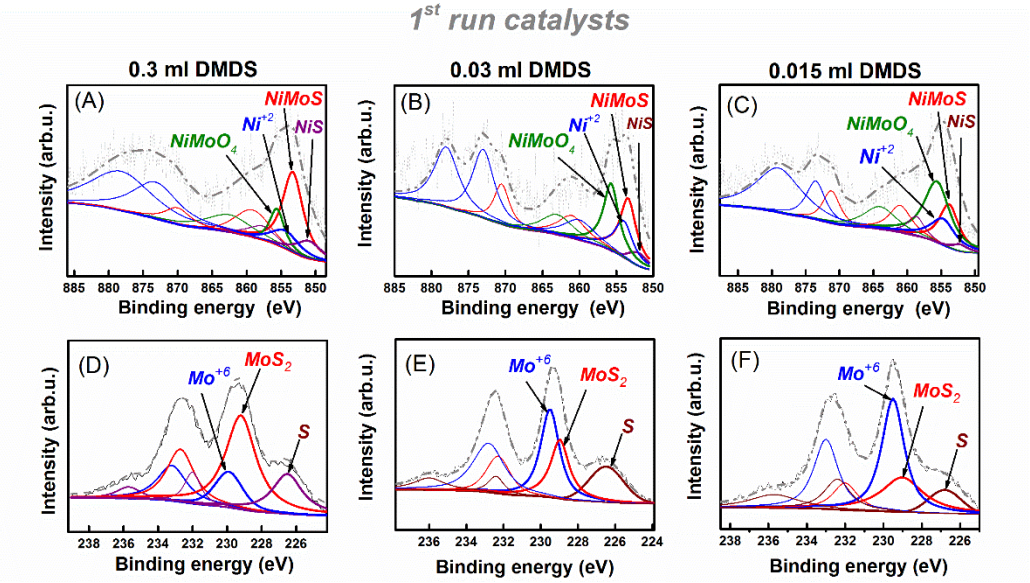

Figure 23. XPS deconvolution of the Ni 2p, Mo 3d and S 2s for the 1st run catalysts; (A) Ni , 0.3 mL DMDS (B) Ni , 0.03 mL DMDS (C) Ni , 0.015 mL DMDS (D) Mo , 0.3 mL DMDS (E) Mo , 0.03 mL DMDS (F) Mo , 0.015 mL DMDS.

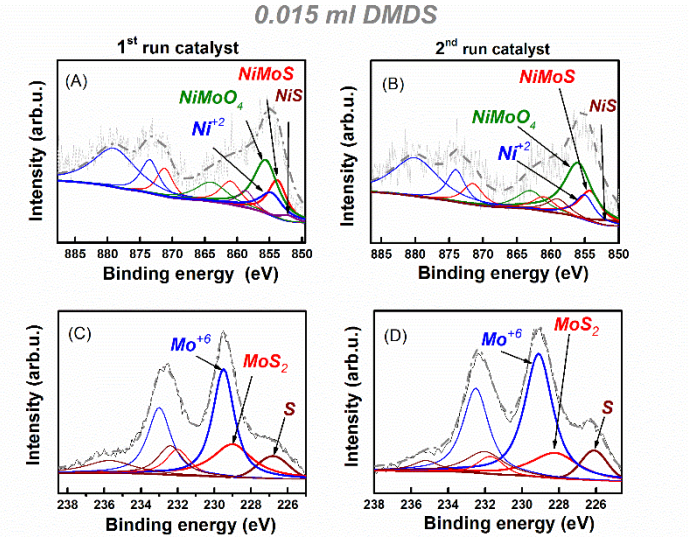

Figure 24. XPS deconvolution of the Ni 2p, Mo 3d and S 2s for: (A) Ni of first run catalyst (B) Ni of second run catalysts (C) Mo of first run catalyst (D) Mo of second run catalysts. Catalysts were maintained with 0.015 mL DMDS.

The Ni 2p (Ni $2p_{1/2}$, Ni $2p_{3/2}$, and shake-up satellites), and Mo 3d/S 2s (Mo $3d_{3/2}$, $Mo3d_{5/2}$, S 2s and shake-up satellite) core level spectrums were deconvoluted by fitting a Gaussian-Lorentzian function. Also, the detected active sulfided NiMoS and MoS_2 phases were all estimated based on the measured area of the corresponding deconvoluted peaks (Table 3).

Table 3. The active sulfide metal content of sulfided $NiMo/Al_2O_3$ recovered from 1st and 2nd HDO runs following different DMDS treatment.

Active sulfided phases	1st run catalyst			2nd run catalyst
	0.3 mL DMDS	0.03 mL DMDS	0.015 mL DMDS	0.015 mL DMDS
NiMoS	75%	49%	45%	42%
MoS_2	80%	42%	31%	29%

The XPS results of 1st run catalysts clearly indicates that the fractions of both NiMoS and MoS_2 phases decreased when the concentration of the sulfiding agent (DMDS) decreased. The results in Table 3 shows that a 95% decrease in the amount of added DMDS (from 0.3 mL to 0.015 mL) results in approximately 42% and 63% decrease in the content of NiMoS and MoS_2 phases, respectively. The same trend was also observed from the 2nd run catalysts (partially shown in Figure 24). Moreover, comparing the XPS results between the unused catalyst (Figure 16) and 1st run catalyst, it can be seen that the lower concentrations of DMDS (0.03 mL and 0.015 mL) were not sufficient to maintain the sulfidation state of the catalysts. Moreover, with higher concentrations of DMDS (0.3 mL and 0.03 mL), the results showed that the fractions of both active metal phases (NiMoS and MoS_2) detected from the 1st and 2nd runs catalysts were almost identical. And, with lowest DMDS concentration (0.015 mL), the fraction of active phases only slightly decreased (Figure 24 and Table 3). Therefore, it can clearly be concluded that concentration of DMDS has a significant impact on preservation of the active metal sulfide phases of the sulfided HDO catalyst.

4.5.3 Carbon deposition of 1st run and 2nd run $NiMo/Al_2O_3$ catalysts

The carbon content of the recoverd catalysts from the 1st and 2nd runs HDO experiments were measured by temperature programmed oxidation (TPO). During the TPO experiments, the evolving CO and CO_2 peaks were monitored, then the carbon contents of the samples were measured based on the peak areas of CO and CO_2. For the purpose of easier verification, the CO and CO_2 concentrations were added together, and they are shown in the form of CO_x. Also, during the TPO, water is expected to be formed due to oxidation of the deposited hydrocarbon species. Therefore, the water concentration signals were monitored and the amount of produced water was measured from the water peak areas. Figures 25 and 26 presents the CO_x and H_2O concentration peaks during the TPO experiments.

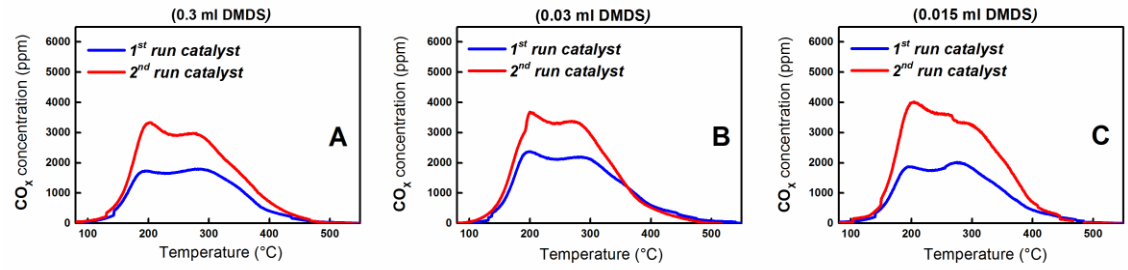

Figure 25. Concentration profile of the CO_x during the TPO of the first run and second runs catalysts in 21% O_2/Ar. The sulfidity of catalysts were maintained with: 0.3 mL DMDS (A), 0.03 mL DMDS (B) and 0.015 mL DMDS (C).

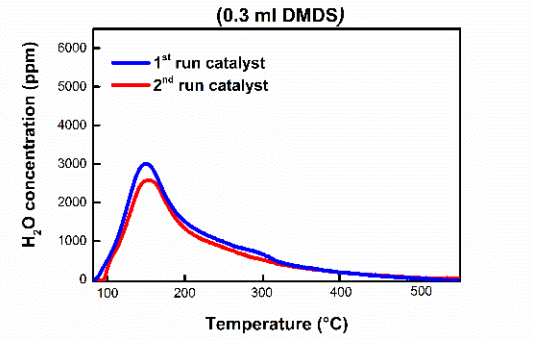

Figure 26. Concentration profile of the H_2O during the TPO of the first run and second runs catalysts maintained with 0.3 mL DMDS, in 21% O_2/Ar.

For all concentrations of DMDS (0.3, 0.03 and 0.015 mL), the CO_x peaks from both 1st and 2nd run catalysts were all in forms of double peaks, evolved in the same temperature range between 180 °C to 300 °C (Figure 25). The measured carbon contents of the 1st run catalysts, measured based on the peak areas of CO and CO_2, were almost the same (~ 8.6 wt%) and no correlation between the DMDS concentration and amount of carbon deposition was found.

As previously mentioned, carbon deposition often occurs by degradation of reactant/product which leads to the blockage of the active sites of catalysts and pores of the catalyst supports. Also, the XPS results in section (4.5.2) indicated that the sulfidity of catalysts were almost preserved when the same amount of DMDS was added to the catalysts. Therefore, for each DMDS concentration, the observed drop in the activity of the 2nd run catalysts compared to 1st runs (Figure 21), can be related to the loss in number of active sites of the 1st run catalysts due to carbon deposition. On the other hand, unlike the 1st run catalysts, the carbon contents of the catalysts recovered from the 2nd HDO runs increased when the concentration of DMDS decresed. The carbon deposition measurements showed that when the amount of added DMDS decreased by 95% (from 0.3 mL to 0.015 mL), the carbon content of the catalysts increased by almost 30%. Moreover, the XPS results from the section (4.5.2) showed that the same decrease in the amount of added DMDS results in a decrease of nearly 42% and 63% of NiMoS and MoS2 metal sulfide active phases, respectively. Thus, the drop in the activity of the 2nd run catalysts can be relate to both carbon deposition and loss in sulfidity.

Furthermore, for each catalyst, a C/H mass ration was calculated from the water and CO_x peaks (Figure 25 and Figure 26). The calculated C/H ratios for the 1st and 2nd catalysts were approximately 6 and 15, respectively. This shows that the coking process on the 2nd run samples is in a more advance stage of coking reactions with more carbonaceous deposits compared to that for the 1st run catalysts.

4.6 HDO of abietic acid

Two HDO reactions of abietic acid were performed. Both reactions were started with abietic acid (2.26 g) mixed with dodecane (solvent, 148 mL), at 320 °C, with the sulfided $NiMo/Al_2O_3$ catalyst (0.5 g), under 54 bar H_2. The first HDO run was stopped after only 1 h of reaction but the second HDO run was continued for 6 h of reaction. These two experiments were performed to obtain detailed information about the intermediates and products formed from HDO of abietic acid. During the course of the 1h HDO experiment,

samples were taken at 10 min intervals, giving a total of six samples. During the longer HDO experiment (6h), initially two samples were taken at shorter intervals of every 30 min, and then samples were taken at longer intervals (60 min). Throughout the analysis, the products with major yields were quantified but other identified products with lower yields (less than 1 mol%) such as naphthalene were not considered. The reproducibility of the results were evaluated from repeated experiments and indicated by the error bars. The results of these two HDO experiments are shown in Figure 27.

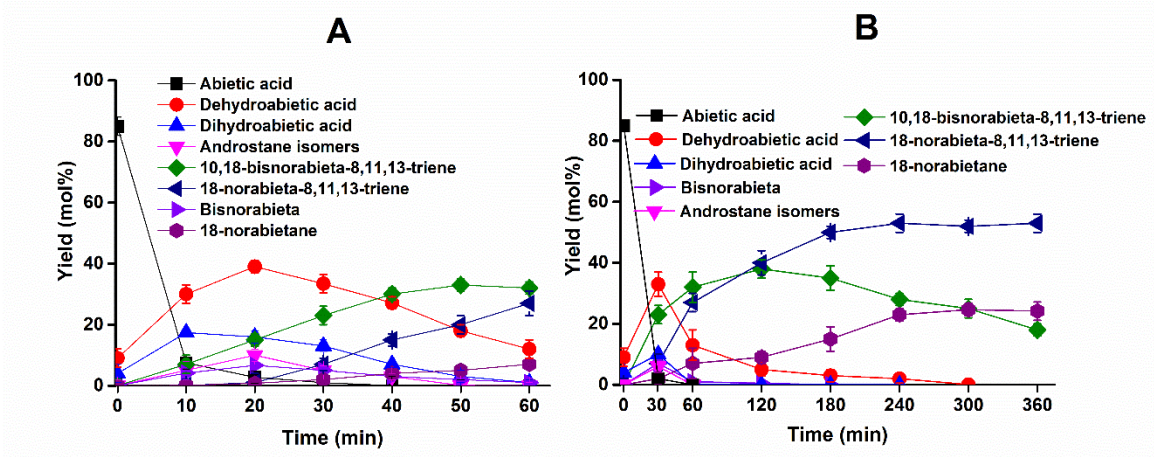

Figure 27. Distribution of the detected reactant and products of a hydrodeoxygenation reaction of abietic acid for 1 h (A), and 6 h (B). Reaction condition: temperature = 320 °C, pressure = 54 bar, catalyst (500 mg), abietic acid (2.26 g), dodecane (solvent, 148 mL (111 g)), DMDS (0.1 mL) and stirring rate = 1000 rpm.

The abietic acid start feed contained impurities such as dehydroabietic acid (9 wt%) and dihydroabietic acid (2 wt%) and pimaric acid (4 wt%). As a result, their yields at time zero are equal to these values (Figure 27). The results in Figure 27A show that the concentration of abietic acid decreased sharply during less than 10 min, with a high initial reaction rate to a small yield of 7.1% and then was almost fully converted after a reaction time of 40 min. The same result (fast depletion of abietic acid) was also observed during the first 30 min of the longer HDO experiment (Figure 27B). Previously, Wang et al. reported that at high temperature (250-290 °C) and in presence of a catalyst, abietic acid with its reactive conjugated double bonds can easily lose hydrogen and then rearrange to form a disproportionated rosin acid such as dehydroabietic acid and dihydroabietic acid [78]. The observed fast increase in the yields of dehydroabietic acid and dihydroabietic acid during the initial stage of HDO reactions is evidence of the fast disproportionation of abietic acid. The disproportionation is also reported to involve HYD, dehydrogenation and isomerization reaction pathways [189, 190].

However, after an initial increase, the yields of dehydroabietic acid and dihydroabietic acid decreased and after 1 h of reaction time they reached 17 mol% and 0.1 mol%, respectively. The yields of deoxygenated tri-ring components such as 18-norabieta-8, 11, 13-triene, 10, 18-bisnorabieta-8, 11, 13-triene and 18-norabietane however increased and, after 1h of HDO reaction, reached 32%, 27% and 8%, respectively. 18-norabieta-8, 11, 13-triene is probably produced via DO, and also cracking of the isopropyl group of the dehydroabietic acid. 10, 18-bisnorabieta-8, 11, 13-triene could also be produced via DCO_x

of dehydroabietic acid. The DCO_x and HYD of dihydroabietic acid and HYD of 10, 18-bisnorabieta-8, 11, 13-triene could produce 18-norabietane [191].

A very similar trend was also observed during the initial stage (less than 60 min) of the longer (6 h) experiment (Figure 27B), as the initial rapid conversion of abietic acid was followed by quick production of 18-norabieta-8, 11, 13-triene and the 10, 18-bisnorabieta-8, 11, 13-triene. Similarly, the disproportionated dehydroabietic acid and dihydroabietic acid were detected as the main intermediate products during the initial stage. However, after 60 min of reaction, the yields of dehydroabietic and dihydroabietic acid decreased and after 300 min of reaction, finally they were both fully converted. Also, after 120 min of reaction, the yield of 10, 18-bisnorabieta-8, 11, 13-triene decreased and eventually after 6 h of reaction reached 18% with a slow average reaction rate of 19 mmol g^{-1} h^{-1}. The yields of 18-norabieta-8, 11, 13-triene and 18-norabietane, both increased, and finally reached 53% and 25%, respectively. After 6 h of HDO reaction, all oxygenates (reactants and products) related to the abietic acid feed were fully converted to deoxygenated unsaturated and saturated hydrocarbons. Based on these results, a reaction mechanism for the HDO of abietic acid is suggested and presented in Figure 28.

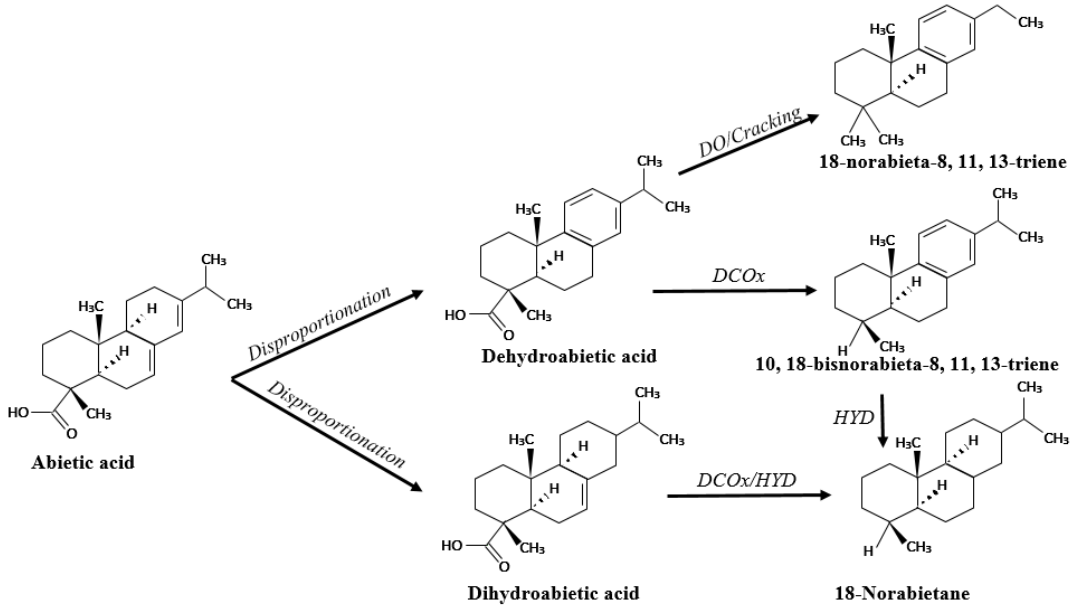

Figure 28. Proposed reaction mechanism for the HDO of abietic acid. Deoxygenation (DO), Decarbonylation/Decarboxylation (DCO_x) and Hydrogenation (HYD).

4.6.1 Effect of abietic acid on HDO of oleic acid

The effect of the abietic acid concentration on the deoxygenation rate of oleic acid was investigated in two sets of HDO experiments. In both sets, the HDO experiments were performed with 10 wt% feed, including varying ratios of abietic acid and oleic acid, in 90 wt% dodecane (solvent), at 320 °C. The first set of HDO experiments (1^{st} run), were performed with 0.5 g of freshly sulfided $NiMo/Al_2O_3$ catalyst but the second set (2^{nd} run) was performed with the recovered $NiMo/Al_2O_3$ catalyst from the 1^{st} run. For a complete stoichiometric hydrodeoxygenation of each mole of oleic acid and abietic acid, 4 moles and 5 moles of H_2 is required, respectively. Thus, depending on the quantity of added abietic

acid (0 wt%, 0.5 wt%, 1 wt% and 1.5 wt%), reactions were started with pressures of 54 bar, 55 bar, 55.5 bar and 56 bar of H_2, respectively. The fatty acid oxygenate conversion results of both HDO (1st and 2nd) experiments are shown in Figure 29 and the rosin acid oxygenate conversion results of the 1st HDO experiments are presented in Figure 30. The reported fatty acid (FA) oxygenate conversion is defined as the ratio of the number of moles of converted FA (oleic acid and stearic acid) to the initial number of moles of the oleic acid. The reported rosin acid (RA) oxygenate conversion is defined as the ratio of the number of moles of converted RA (abietic acid, dehydroabietic acid and dihydroabietic acid) to the initial number of moles of the abietic acid.

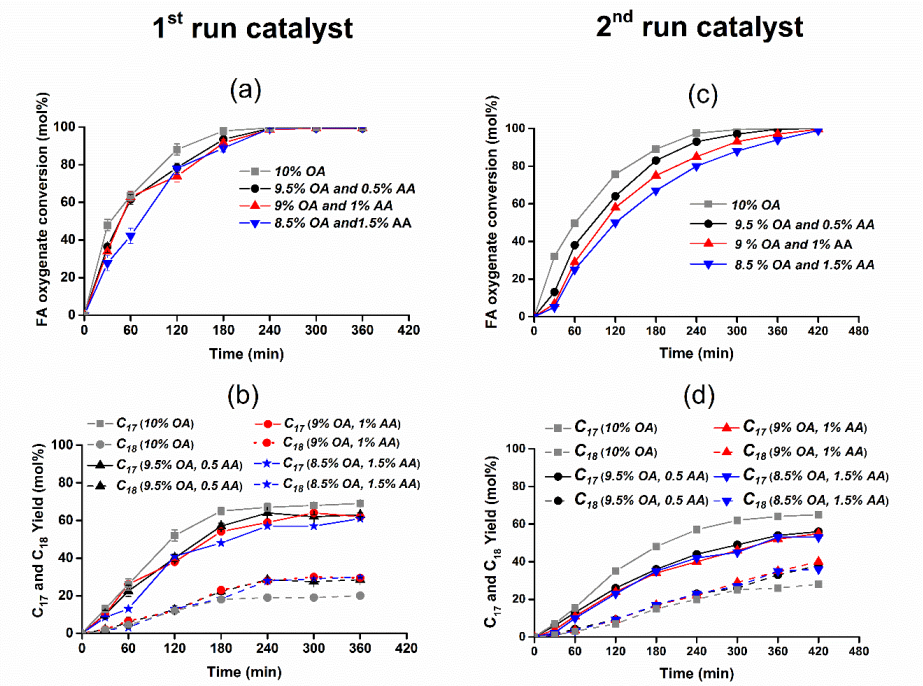

Figure 29. Effect of the abietic acid (AA) concentration on: (a) fatty acid (FA) oxygenate conversion rate of oleic acid (OA) portion of feed with 1st run catalysts, (b) yields of heptadecane (C_{17}) and octadecane (C_{18}) with 1st run catalysts, (c) fatty acid (FA) oxygenate conversion rate of oleic acid (OA) portion of feed with 2nd run catalysts, (d) yields of heptadecane (C_{17}) and octadecane (C_{18}) with 2nd run catalysts. Experiments were performed at 320 °C, with 500 mg freshly sulfided catalysts, maintained by DMDS (0.1 mL) under pressures 54 -56 bar H_2.

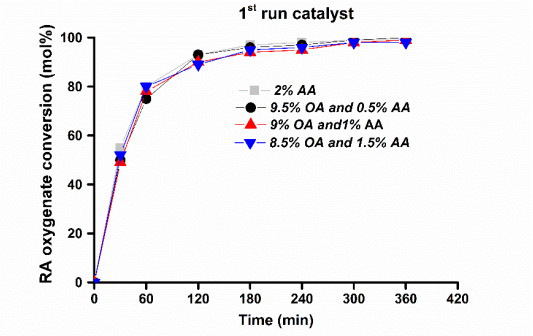

Figure 30. Effect of the oleic acid (OA) concentration on abietic acid (AA) oxygenate conversion rate with 1st run catalysts. Experiments were performed at 320 °C, with 500 mg freshly sulfided catalysts, maintained by DMDS (0.1 mL) under pressures 54 -56 bar H_2.

For both 1st and 2nd HDO runs, the oleic acid portion of feed was initially converted to stearic acid via the rapid saturation of its double bond (-C=C-) and then, stearic acid was eventually converted to straight chain heptadecane (C_{17}) and octadecane (C_{18}), as in good agreement with our previous study and other reports [140, 187, 192]. The abietic acid portion of feed (Figure 30, only shown for 1st runs) was also initially converted to dehydroabietic acid and dihydroabietic acid and then at the end of the HDO reactions (both 1st and 2nd runs), deoxygenated tri-ring hydrocarbons were produced. Therefore, after 6 h of HDO reactions, all oxygenates (reactants and products) related to oleic acid as well as abietic acid portions of the feeds were completely converted.

For the 1st run catalysts (Figure 29a), a complete FA oxygenate conversion was reached after 3 h when oxygenate feed contained only oleic acid. However, addition of abietic acid delayed the complete FA oxygenate conversion for almost one hour, so the complete FA oxygenate conversions were reached only after 4h. Also, a similar trend was observed for the 2nd HDO runs (Figure 29c), as the addition of abietic acid to the feed decreased the FA oxygenate conversion, most notably, the initial stage (first 30 min) of the FA oxygenate conversion. Moreover, addition of abietic acid clearly decreased the C_{17} selectivity and increased the C_{18} selectivity of the catalysts, thus DO is favored over DCO_x (Figure 29 b and d). However, for both 1st and 2nd HDO experiments, the RA oxygenate conversion rate (Figure 30, only shown for 1st runs) was almost unaffected by addition of oleic acid to the feeds.

The apparent initial inhibition in the deoxygenation rate of FA (Figure 29a and c) may partly be due to the rapid disproportionation of abietic acid due to its stronger adsorption on sites compared to oleic acid. Alternatively, the inhibition may be partly due to the fact that abietic acid is bulkier than oleic acid and thus it may sterically hinder adsorption on more neighboring sites and in this way hinder reaction of the fatty acids. It has been reported that strong adsorption of large polyaromatics such as phenanthrene on the active phase of a $NiMo/Al_2O_3$ catalyst can completely or partially cover the active phase of the catalysts and consequently inhibit its activity [193]. Another possible explanation for the decreased FA deoxygenation rate would be the amount of the carbon deposition (coking) on the catalysts that can partially block their active sites. Moreover, the proportionate decrease in start concentration of oleic acid may also have influenced the FA oxygenate conversion rate. If the reaction is first order with respect to FA concentration, then the rate of increase of conversion would be independent of the starting concentration. However, for a reaction order greater than one, a lower start concentration would also reduce the rate of increase of conversion and if reaction order is lesser than one then the opposite effect would be expected.

To evaluate this hypothesis, the effect of the oleic acid start concentration on the rate of FA oxygenate conversion was assessed and the results are shown in Figure 31. These experiments were started with different concentrations of oleic acid (10 wt%, 8 wt% and 6 wt%) in dodecane (solvent), at 320 °C, with freshly sulfided $NiMo/Al_2O_3$ catalyst (500 mg). A near identical rate of increase of FA oxygenate conversion was observed for these HDO experiments. Also, based on the experimental data obtained from time zero to

360 min and using regression analysis, a first order reaction rate constant (k) was estimated as 0.0191 min^{-1}. Then, the value of the estimated reaction rate constant was used to predict a first order conversion which is also presented in Figure 31. For the studied range of oleic acid concentrations, a comparison between the experimental conversions and the predicted first order conversion shows that the rate of reaction of FA is very nearly first order. The order of oleic acid conversion is also reported to be first order elsewhere [187].

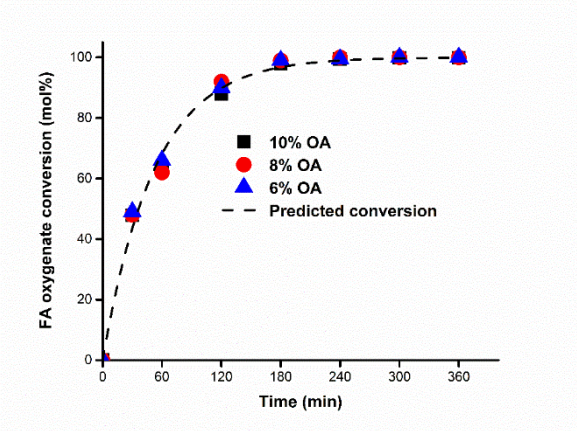

Figure 31. Effect of the start concentration of oleic acid (OA) on rate of change of oxygenate conversion. Experiments were performed at 320 °C, with freshly sulfided catalysts (500 mg), maintained by DMDS (0.1 mL) under H_2 pressure of 54 bar. The dotted line is corresponding the predicated first order conversion.

In order to further validate the observed inhibition due to the addition of abietic acid, two additional HDO experiments with a higher catalyst/feed weight ratio were performed. In these experiments, a catalyst to feed weight ratio of 0.06, at 320 °C and under a constant hydrogen pressure of 60 bar was used. The new results (see Paper III) also clearly confirmed the inhibition of abietic acid on the HDO of the oleic acid. Therefore, the observed initial inhibition of the deoxygenation rate of FA, shown in Figure 29, is related to the addition of abietic acid.

4.6.2 Characterization of spent sulfided NiMo/Al_2O_3 catalysts

The carbon and sulfur contents of the recovered catalysts from both sets of HDO were measured by TPO studies and elemental microanalysis. Also, the textural properties such as specific surface area, pore volume and pore size were measured by using N_2-physisorption. Table 4 presents the carbon and sulfur contents as well as the textural properties of the spent NiMoS catalysts recovered from the 1st run of HDO experiments. The carbon content of the spent catalyst from the 1st HDO run that was started with 2% abietic acid is nearly 1.75 times higher than the spent catalyst from the reaction which started under similar condition but with 10% oleic acid only. Moreover, when the percentage of abietic in the feed for the mixed feed experiments increased from 0.5% to 1.5%, the carbon deposition increased by nearly 21%. Furthermore, the measured textural properties of the spent catalysts indicate that addition of abietic acid to the oleic acid feed slightly reduced the specific BET surface area, pore volume and average pore size due to carbon deposition.

Figure 32 presents the TPO measurements of the NiMoS catalyst recovered from the 2nd HDO run. Detailed quantifications of the carbon contents of the 2nd run catalysts are presented in Paper III. Compared to the first run catalysts (Table 4), the measured carbon deposition of the 2nd run catalysts (Figure 32) was on average nearly 30% higher. Also, the carbon content of the 2nd run catalysts increased with an increase in the start concentration of abietic acid. After running two sets of HDO experiments, it may therefore be concluded that higher concentrations of abietic acid resulted in a larger portion of deposited carbon. However, the variation in abietic start concentration did not significantly affect the sulfidity of samples. This is probably due to the fact that the same amount of DMDS was used in all experiments, also the amount of DMDS used was in excess to what is required for a complete sulfidation of both nickel and molybdenum phases.

Table 4. Carbon and sulfur content of recovered NiMoS/Al_2O_3 samples following the first runs of HDO experiments.

Feed composition	C (wt%)	S (wt%)	C/H (mass ratio)	BET surface area (m^2/g)	Pore volume (cm^3/g)	Average pore size (Å)
Feed 1 [a]	0.7 (TPO [b]), 0.8 (EM [c])	9.4 (EM [c])	11.7 (TPO [b])	133.4	0.27	67.1
Feed 2 [a]	1.1 (TPO [b]), 1.3 (EM [c])	9.1 (EM [c])	12.5 (TPO [b])	131.1	0.26	65.4
Feed 3 [a]	1.2 (TPO [b]), 1.3 (EM [c])	9.5 (EM [c])	13.6 (TPO [b])	130.8	026	64.9
Feed 4 [a]	1.4 (TPO [b]), 1.4 (EM [c])	9.6 (EM [c])	14 (TPO [b])	128.2	0.25	61.2
Feed 5 [a]	1.2 (TPO [b]), 1.4 (EM [c])	9.4 (EM [c])	12.2 (TPO [b])	-	-	-

[a] Feed 1 (10 wt% Oleic acid), Feed 2 (9.5 wt% Oleic acid and 0.5 wt% Abietic acid), Feed 3 (9 wt% Oleic acid and 1 wt% Abietic acid), Feed 4 (8.5 wt% Oleic acid and 1.5 wt% Abietic acid), Feed 5 (2 wt% Abietic acid). [b] TPO (Temperature programmed oxidation). [c] EM (Elemental Microanalysis Ltd. UK).

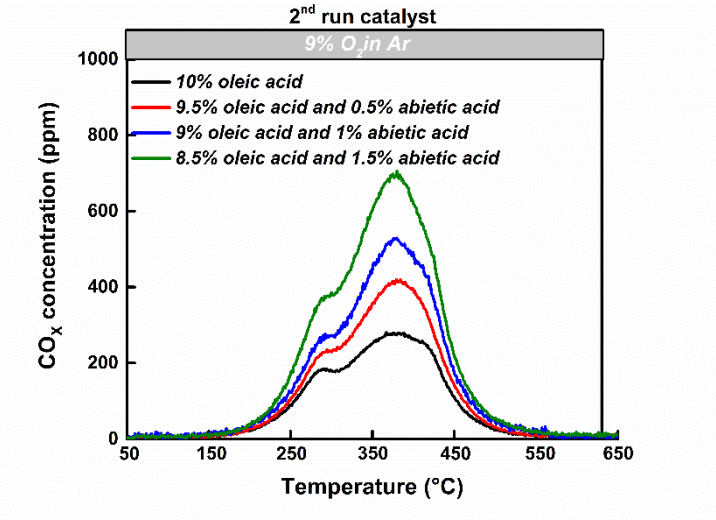

Figure 32. Concentration profiles of CO_x during the TPO of the recovered catalysts (from the second HDO experiments) in 9% O_2 in Ar.

Additionally, the evolved CO_x profile for both 1st (not shown here) and 2nd (Figure 32) HDO runs seems to be composed of two convoluted peaks at ~ 290 ºC and at ~ 365 ºC. The difference in the oxidation temperature may indicate that the deposited carbon on the samples was comprised of at least two different carbonaceous structures. From the water signals, the C/H mass ratios of all spent catalysts (1st and 2nd runs) were calculated and the C/H mass ratios of 1st run catalysts are presented in Table 4. It can be noted that the calculated C/H mass ratios are higher than the structure based C/H mass ratios of oleic acid (6.35), abietic acid (8) and their intermediates and products. Thus, the reactants, intermediates and products were largely removed during the catalyst recovery step (washing and filtration) and the argon treatment performed before the TPO measurements.

The deconvolution of the CO_x and the corresponding water profile (see Paper III) showed that the low temperature regions had a lower C/H mass ratio compared to the higher temperature regions. The fraction of the detected carbon deposits with lower temperature of oxidation and lower C/H mass ratio result from species in an early stage of the coke formation reactions (adsorption and dehydrogenation). However, the carbon portions with higher temperature of oxidation and larger C/H mass ratio should result from species from a more advanced stage of coking reactions, such as polymerization and cyclization of hydrogen deficient fragments. In addition, nearly 40% of the deposited carbon of the 1st run sample from the experiment started with 10% oleic acid had a C/H mass ratio of 8, evolving at lower temperature (290 ºC) and 60% had a higher C/H mass ratio of 14.7, at higher temperature (365 ºC). In other words, approximately only half of the deposited carbon reached the more advanced stage of coke formation. On the other hand, for other samples from the experiments started with abietic acid in their feed, on average 75% of the deposited carbon had higher C/H mass ratios of ~ 15 at the higher temperature (365 ºC). Thus, nearly 75% of the deposited carbon on these samples with abietic acid reached the more advanced stage of the coking reaction. In conclusion, compared to oleic acid feed, abietic acid seems to produce different types of coke precursors with greater quantities that advance more readily to form coke with a higher temperature stability.

4.7 Effect of iron poison on HDO of oleic acid

The effect of iron concentration on the activity and selectivity of sulfided $NiMo/Al_2O_3$ and Mo/Al_2O_3 catalysts during HDO of oleic acid was studied. As mentioned earlier, iron was added as an iron oleate complex. The activity results for HDO of the Ni promoted Mo/Al_2O_3 are presented in Figure 33 but the activity results of unpromoted sulfided Mo/Al_2O_3 can be accessed from Paper IV. The oleic acid HDO experiments were started under 60 bar of total pressure at 325 °C, over 1 g of sulfided $NiMo/Al_2O_3$ catalysts for 330 min. In all experiments, 0.1 mL of DMDS was added to 150 mL of a feed containing 15 wt% oleic acid, 85 wt% dodecane and different quantities of iron oleate (0 wt. ppm to 8400 wt. ppm based on the total weight of the feed (acid and solvent)). The reported ppm concentrations of iron are calculated based on the percentage of iron in the added iron oleate (nearly 24%, done by ICP-SFMS). A part from the experiment with 2000 ppm iron (the highest Fe concentration), the molar balances of liquid products from the rest of HDO

experiments were over 90% on average. The molar balance for intermediate samples of the experiment with 2000 ppm iron were generally poor, so only results for the sample collected at the end of the experiment (after 330 minutes), directly collected from the reactor, then analyzed and are shown here.

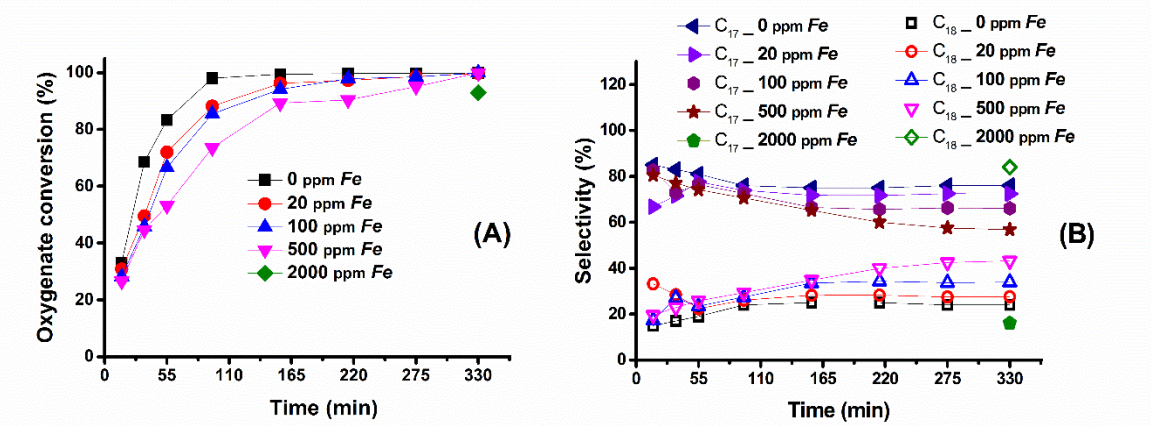

Figure 33. Effect of poison concentration (Fe) on: (A) oxygenate conversion and (B) selectivity for C_{17} (heptadecane) and C_{18} (octadecane) during HDO of oleic acid over sulfided $NiMo/Al_2O_3$ catalyst.

The overall oxygenate conversion rate of the HDO experiment that was started without the iron poison (0 ppm Fe, Figure 33A) was the highest observed rate (32 $mmolg^{-1}h^{-1}$), nearly 4 times higher than the observed average rates (~ 8.6 $mmolg^{-1}h^{-1}$) of other experiments that started with iron poison. Clearly, addition of iron has inhibited the oxygenate conversion rate of oleic acid. Moreover, the selectivity results presented in Figure 33B shows that the increase in the amount of iron poison has resulted in significant changes in the selectivities towards heptadecane (C_{17}) and octadecane (C_{18}). When, the added concentration of iron poison increased from 0 ppm to 500 ppm, the selectivity towards C_{17} decreased from 76 mol% to 57 mol%, while the selectivity towards C_{18} increased from 24 mol% to 43 mol%. Also, compared to HDO experiment with no added poison (0 ppm Fe), when the highest concentration of iron was used (2000 ppm Fe, green points), the selectivity towards C_{17} decreased by nearly 79% and the selectivity towards C_{18} increased from 24 mol% to 83 mol%. Unlike the $NiMo/Al_2O_3$ catalyst, the Mo/Al_2O_3 catalyst (not shown here) was more selective towards C_{18}. However, similar to $NiMo/Al_2O_3$ catalyst, the overall oxygenate rate of the Mo/Al_2O_3 catalyst decreased when iron oleate was added to the feed. Also, addition iron oleate, decreased the C_{18} selectivity and increased the C_{17} selectivity of the Mo/Al_2O_3 catalyst. Moreover, no correlation between the iron concentration and amount of carbon deposition on the samples was found. In conclusion, addition of iron decreased the HDO activity of the promoted and unpromoted Mo/Al_2O_3 catalysts, and also changed their selectivity towards the major products.

4.7.1 Effect of iron poison on deactivation of NiMo catalyst

The effect of addition of iron on the morphology of the active phases of sulfided NiMo catalysts were studied by using transmission electron microscopy (TEM) technique coupled with XEDS elemental mapping (Figure 34). A high-angle annular dark-field scanning transmission electron microscopy (HAADF-STEM) micrograph, showing a nanostructure of MoS_2 clusters in the spent sulfided NiMo catalyst, is presented in Figure

34A. To determine the elemental concentration gradients and distributions of Ni, Mo, Fe and S, a specific area which is depicted as a yellow box (198x198 pixels) was chosen to be scanned and analyzed by XEDS elemental mapping. The concentration gradients of Ni, Mo, Fe and S are shown in Figure 34(B-E). Figure 34B shows that the nickel is mainly concentrated in form of two particles with sizes of nearly 25 nm and 17 nm, whereas Mo and to some extent S, are uniformly distributed on the probed area of the sample (Figure 34D and E).

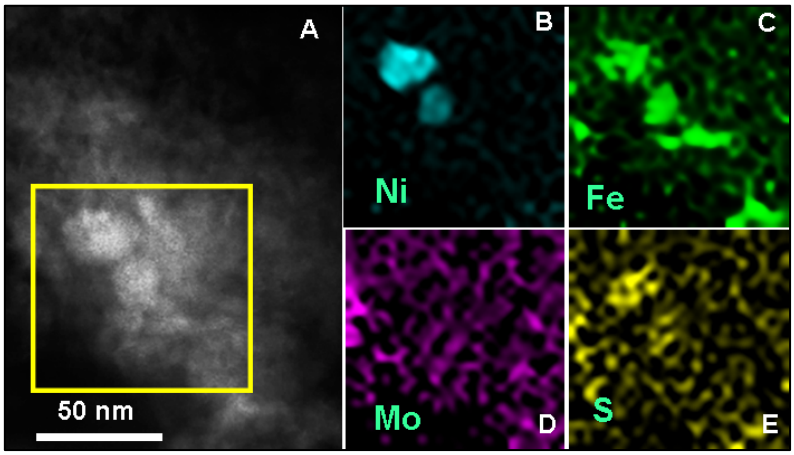

Figure 34. HAADF-STEM imaging and EDX mapping of catalyst recovered after 330 mins of HDO (NiMo_500 Fe) experiment exhibiting (A) coverage of MoS_2 clusters; sub images present elemental distribution of (B) nickel (C) iron (D) molybdenum and (E) sulfur.

Iron species are deposited on the catalysts due to the deoxygenation of the oleate ligands. However, Figure 34C shows that the distribution of Fe is mainly concentrated around Ni particles, even though scattered signals for Fe are also detected in other areas. These results may indicate that iron has possibly reacted with Ni species and produce a new bimetallic sulfide phase (e.g. $Fe_xNi_yS_z$) which has a different chemical structure compared to active NiMoS phase. In other words, iron seems to be interfering with the promoting effect of Ni which caused the observed decrease in DCO_x selectivity of the $NiMo/Al_2O_3$ catalyst (Figure 33B). On the other hand, iron may partially act as a promoter on the unpromoted Mo/Al_2O_3 catalyst to increase the DCO_x selectivity.

4.8 Hydroconversion of rosin acid

Hydroconversion experiments of rosin acid over alumina, USY-zeolite and mixed alumina/USY-zeolite supported NiMoS catalysts were performed. In these experiments, a RA feed containing abietic acid (85 wt%), dehydroabietic acid (9 wt%), pimaric acid (4 wt%) and dihydroabietic acid (2 wt%) were used. The reactor setup and experimental conditions for these experiments are described in sections 3.3.2 and 3.3.8.

4.8.1 Catalyst activity measurements

Figure 35 presents the product mole distributions during a hydroconversion of abietic acid over a sulfided NiMo catalyst supported on alumina/USY-zeolite with a 50/50 weight ratio. Hydroconversion of abietic acid resulted in a large number of different products, where in total 32 components were identified by GC-MS analysis (Paper V, Figure 6). However, the distributions of 19 major products were quantified and they are

presented in Figure 36. The reported product mole distributions are calculated based on the number of moles of a product divided by the total moles of the identified reactant and products at each sampling point, excluding dodecane. On average, 60 wt% of the carbon of the RA feed was recovered in the liquid samples based on the identified and quantified major products. In the gas sample, products such as CO, CO_2, CH_4, C_2H_6 and C_3H_8 were detected. To simplify the presentation of the results, different major reactants and products were grouped by the number of their carbon rings.

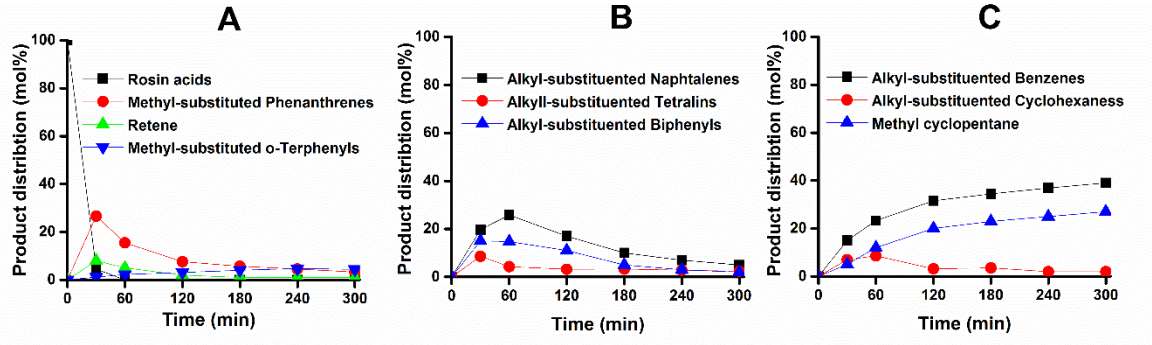

Figure 35. Distributions of the detected reactant and products using sulfided NiMo catalyst supported on alumina/USY-zeolite with a 50/50 weight ratio: tri-ring structures (A), di-ring structures (B) and mono-ring structures (C). RA feed contain abietic acid, dehydroabietic acid, pimaric acid and dihydroabietic acid. For more details see Paper V.

Figure 35A shows tri-ring reactant and product distributions during the hydroconversion reaction. A complete oxygenate conversion for the oxygenated RA components such as abietic acid, dehydroabietic acid, pimaric acid and dihydroabietic acid was achieved during the reaction time less than 60 min. Moreover, during the initial stage of reaction (first 30 min reaction), the concentrations of retene and the methyl-substituted phenanthrene components (containing mono, di and tri-methyl phenanthrene) increased to 8 mol% and 27 mol%, respectively. The methyl-substituted phenanthrenes and retene are possibly formed via HDO (including DCO_x and DO routes) of the carboxylic groups of rosin acids on the metal and metal sulfide sites, as well as dehydrogenation of the rings and cracking of the alkyl groups on the Brønsted acid sites [149, 194, 195]. Then, after 30 min of reaction, the concentrations of retene and the methyl-substituted phenanthrenes gradually decreased and finally after 5 h of reaction, small values of nearly 1 mol% and 5 mol%, respectively were reached. The concentration of the methyl substituted o-terphenyl components however steadily increased and finally reached 6 mol%. A possible ring-opening (RO) reaction of the middle ring of the methyl-substituted phenanthrenes on the Brønsted acid sites could also produce the alkyl-substituted biphenyls [196].

The distributions of the di-ring products are presented in Figure 35B. The concentrations of the di-ring hydrocarbons, including methyl-substituted naphthalene, tetralin and biphenyl components initially (first 30 min) increased and then gradually decreased. The alkyl-substituted naphthalenes are most likely formed via the HDO reaction on the metal and metal sulfide sites, as well as the RO and dehydrogenation reactions of rosin acids on the Brønsted acid site [194]. Then, alkyl-substituted naphthalenes are most likely converted to the alkyl-substituted tetralins via a possible HYD reaction on the metal

and Brønsted acid sites [197, 198]. Afterward, the alkyl-substituted tetralins can be converted into dimethyl indan via HYD and isomerization reactions on the Brønsted acid sites [198].

Figure 35C presents the distributions of the mono-ring products. The concentrations of the methyl-substituted benzenes and methyl cyclopentane always increased and finally reached 40.1 mol% and 29 mol%, respectively. However, the concentrations of the methyl-substituted cyclohexanes initially increased and then gradually decreased to a small value of 2 mol%. The alkyl-substituted benzenes may have been formed via the cracking of both dimethyl indan and alkyl-substituted biphenyl intermediate components on Brønsted acid sites [199]. Also, a ring-saturation (RS) and cracking reactions of the alkyl-substituted benzenes can result in formation of the methyl-substituted cyclohexane and methyl cyclopentane products [198, 200].

Finally, it should be noted that amongst the final products, some branched alkanes such as dimethyl pentane and dimethyl hexane were identified. The detected branched alkanes can be formed from either the RO reaction of cycloalkane methyl or cracking of the dodecane (solvent) [199, 201]. However, extra hydroconversion experiments that were performed, using only dodecane as the feed over supported NiMo catalysts, indicated that most of dimethyl pentane was formed from the dodecane feed. Also, it was found that the cracking of dodecane was even slightly higher when rosin acid was not included in the feed. It has been reported that the apparent extra cracking of dodecane may be due to the fact that compared to dodecane, rosin acids are more nucleophilic towards the active acid and metal sites and as a result, they can inhibit cracking of dodecane [199]. As a result, it is very difficult to quantify how much of the detected branched alkanes were produced from rosin acids, and thus their distributions were not considered in this thesis. Based on the above discussion of likely reactions, a reaction scheme for the HDO of abietic acid is suggested and presented in Figure 36.

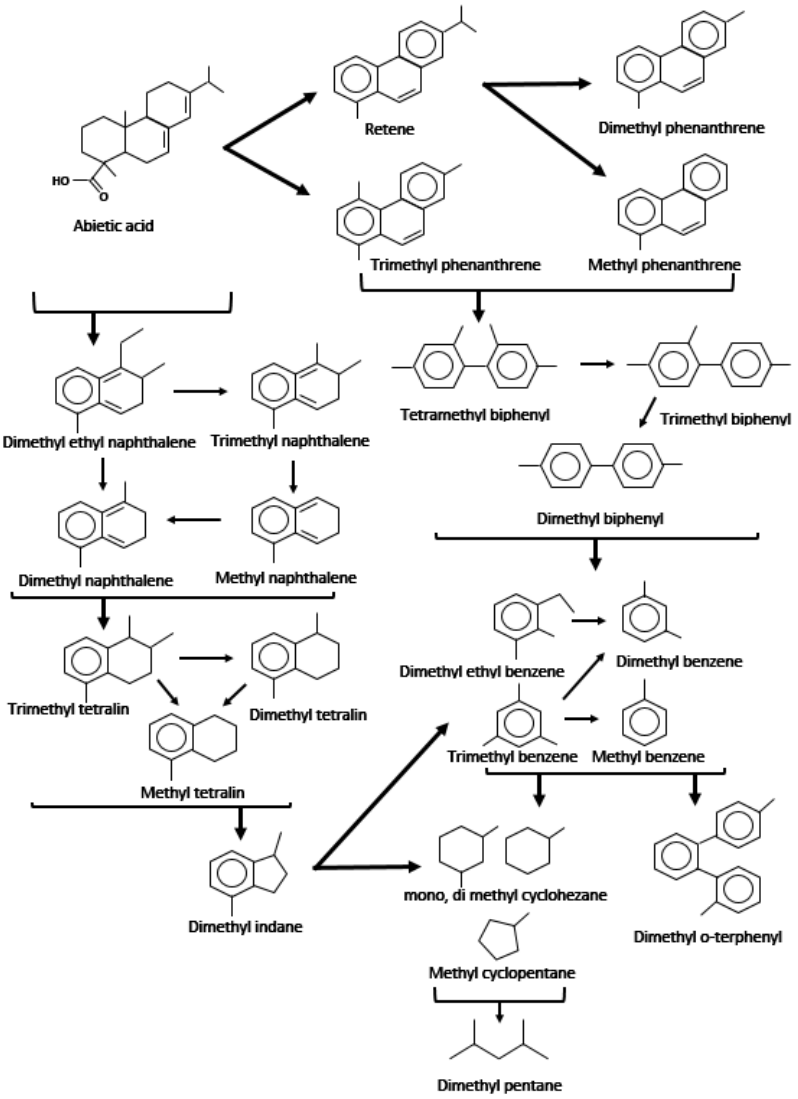

Figure 36. Proposed reaction scheme for the formation of single ring structures and branched alkanes from the hydroconversion of rosin acids.

4.8.2 Catalyst selectivity measurements

Figure 37 presents the changes in the product selectivity over sulfided NiMo catalysts with different supports. The results shown in Figure 37A reveal that the highest selectivity towards the mono-ring structures and the lowest selectivity towards the tri-ring structures was achieved over the NiMo catalyst supported only on USY-zeolite. However, the results in Figure 37A and B shows that a significant decrease in the USY-zeolite content of the support i.e. from 100 wt% to 50 wt% only caused a moderate reduction in the selectivities for the mono-ring products. Whereas, the largest reduction in selectivity for the mono-ring products and increase for the tri-ring products occurred when the USY-zeolite content of the support was reduced from 25 wt% to 0 wt% (Figure 37C and D). Thus, only a small increase in the USY-zeolite content of the support (to 25 wt%) significantly promoted the RO reaction route, but further increases in the USY-zeolite content resulted only in moderate selectivity changes.

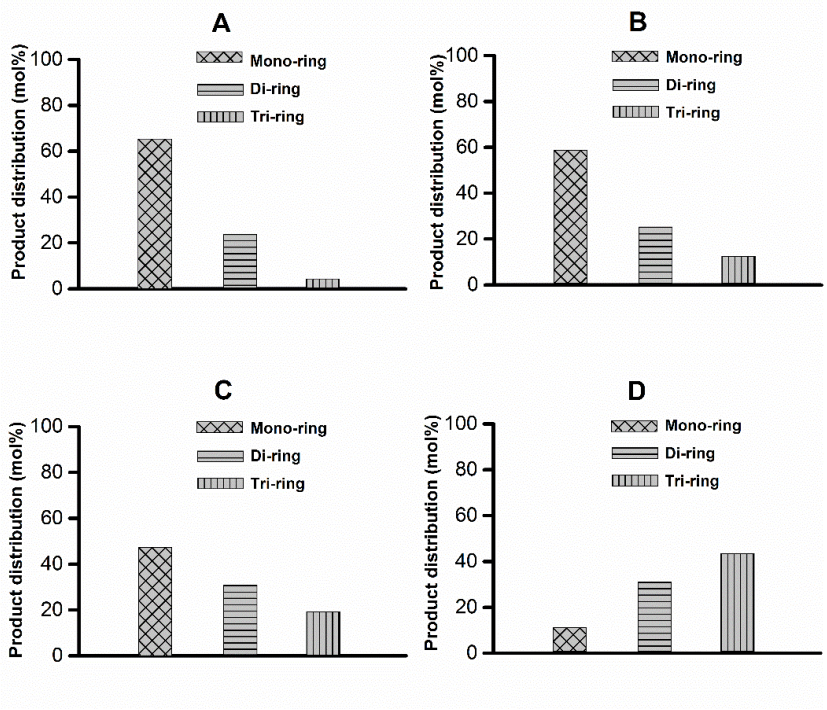

Figure 37. Change of product selectivity over NiMo sulfided catalysts with varying support compositions. Sulfided NiMo catalyst supported on USY-zeolite only (A), 50 wt% alumina and 50 wt% USY-zeolite (B), 75 wt% alumina and 25 wt% USY-zeolite (C) and on alumina only (D).

4.8.3 Catalyst characterization

The supported NiMoS catalysts were characterized using ICP-SFMS, N_2-physysoption, ethylamine-TPD, SEM, STEM and TPO. However, only the results from ethylamine-TPD, STEM and TPO characterizations are presented in this summary and the rest are presented in Paper V. Figure 38 presents the ethylamine-TPD results for the fresh and nonsulfided catalysts which are summarized in Table 5.

It is widely accepted that the Brønsted acid sites are created due to the proton (H^+) donations to satisfy the Al tetrahedron when the Al^{+3} ions substitute the Si^{+4} ions in the alumina-silica frameworks of e.g zeolites [202]. Various TPD studies indicated that using appropriate molecule probes such as alkylamines can be an effective method to measure and distinguish between Brønsted acid and Lewis acid site densities of solids [203-205]. According to the Hofmann elimination, a molecule probe such as ethylamine decomposes over Brønsted acid sites and produces ethylene and ammonia molecules [206]. On the other hand, desorption of the intact Ethylamine molecule can indicate the number of Lewis acid sites [207]. Therefore, the number of Lewis and Brønsted acid site densities of the samples were calculated from the ethylamine and ethylene desorption signals, respectively.

Figure 38A shows that the ethylamine desorption peaks from all samples appeared in the same temperature region between 100 °C to 220 °C with near similar shapes. Also, the corresponding results in Table 5 reveal that the alumina supported NiMo sample contains the highest number of Lewis acid sites whereas the USY-zeolite only supported catalyst contains the lowest number of Lewis acid sites. Furthermore, the number of Lewis acid sites decreased slightly when the weight fraction of USY-zeolite of the support increased. On the other hand, the ethylene desorption peaks (Figure 38B),

corresponding to the Brønsted acid sites, appeared in a relatively higher temperature range between 300 °C to 480 °C and were significantly larger compared to the ethylamine peaks. Calculations of the Brønsted acid site densities shows that the alumina supported NiMo catalyst contained the lowest number of Brønsted acid sites while the number of Brønsted acid sites increased proportionately to the USY-zeolite content of the support (Table 5).

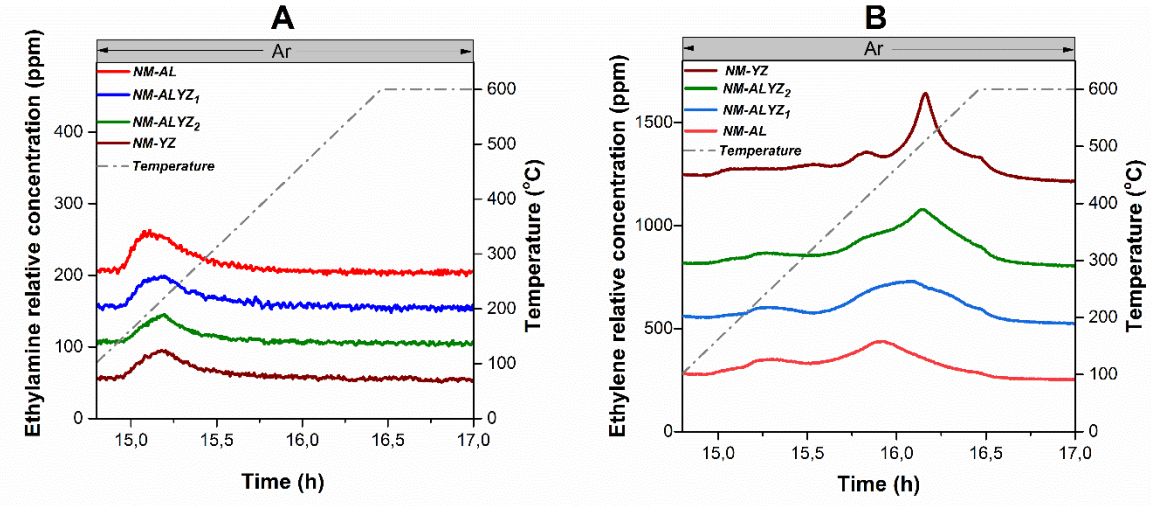

Figure 38. Relative desorption concentration profiles of ethylamine (A) and ethylene (B) during the ethylamine-TPD of NiMo catalysts supported on USY-zeolite only (NM-YZ), 50 wt% alumina and 50 wt% USY-zeolite (NM-AlYZ$_2$), 75 wt% alumina and 25 wt% USY-zeolite (NM-AlYZ$_1$) and alumina only (NM-AL).

Table 5. Concentration of the Lewis and Brønsted acid sites and quantities of desorbed probe molecules for the supported NiMo catalysts from ethylamine-TPD.

Sample	$C_2H_5NH_2$ (μmol)	Lewis acid site density (μmol g^{-1})	C_2H_4 (μmol)	Brønsted acid site density (μmol g^{-1})
NM-YZ[a]	0.6	22.2	12.1	401.4
NM-ALYZ$_2$[a]	0.63	25.3	9.9	369.9
NM-ALYZ$_1$[a]	0.66	25.6	7.8	311.6
NM-AL[a]	0.9	30.1	6.6	257.5

Several studies have indicated that the increase in the concentration of Brønsted acid sites of supported catalysts results in higher rates of cracking, isomerization, RS and RO reactions [195, 198, 208]. Therefore, the observed higher selectivity towards production of the mono-ring components with catalysts containing higher amount of USY-zeolite (Figure 37) can partially be due to their higher concentrations of Brønsted acid sites.

A selection of STEM micrographs of the sulfided NiMo supported on USY-zeolite, alumina/USY-zeolite and alumina supports are presented in Figure 39. Based on the STEM results, the average particle size for the NiMo phases were estimated. The average particle size for the NiMo phases supported on USY-zeolite only, alumina/USY-zeolite with 50% weight ratio and alumina only were estimated to be 18.5 nm (22 particles counted), 21 nm (15 particles counted) and 31 nm (10 particles counted), respectively. The results from the STEM characterization shows that the supported NiMo samples that

contained a larger portion of USY-zeolite in their support had a smaller average NiMo particle size and thus improved dispersions. Therefore, improvements in the dispersion of the metal NiMo phases on the USY-zeolite containing catalysts, may also be considered as a significant factor contributing to the increase in selectivity of the RO and cracking reactions in Figure 37.

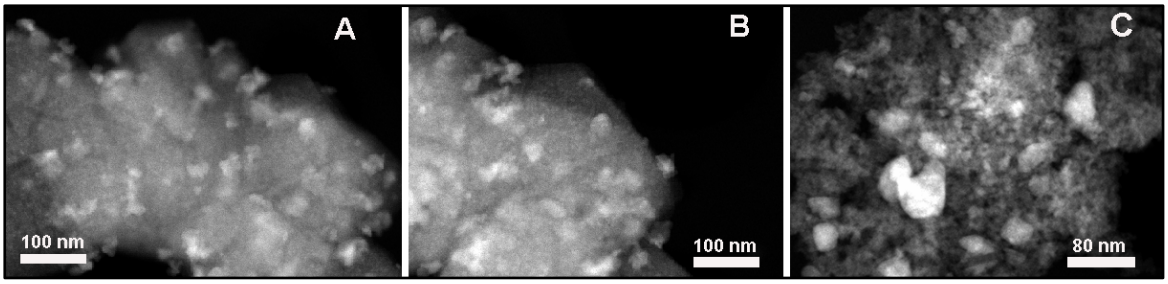

Figure 39. STEM micrographs of (A) NiMoS supported on USY-zeolite only, (B) NiMoS supported on alumina/USY-zeolite with 50% ratio and (C) NiMoS supported on alumina only.

The carbon content of the catalysts recovered from the rosin acid hydroconversion reactions were quantified by TPO. Detailed quantification of the carbon contents are presented in Paper V. The correlations between the USY-zeolite, the carbon contents and the selectivity of mono-ring structures of the supported NiMo catalysts is shown in Figure 40.

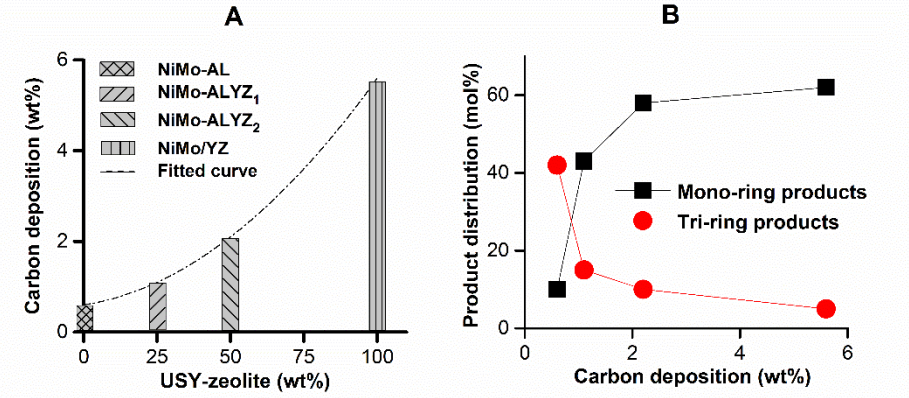

Figure 40. Carbon content versus the USY-zeolite contents (A) and Variation of the mono and tri-ring products versus the carbon deposition of the NiMo catalysts (B). NiMo catalysts supported on USY-zeolite only (NM-YZ), 50 wt% alumina and 50 wt% USY-zeolite (NM-AlYZ$_2$), 75 wt% alumina and 25 wt% USY-zeolite (NM-AlYZ$_1$) and alumina only (NM-AL).

Figure 40A shows that the carbon content increased nearly exponentially with the USY-zeolite content of the catalysts. Figure 40B shows that the largest variations in the carbon deposition occurred when only moderate selectivity changes towards both mono and tri-ring products occurred. Whereas, significant variations in selectivities only resulted in moderate carbon deposition variations. In other words, a significant decrease in the USY-zeolite content of the support caused a substantial reduction in the carbon deposition and only moderate changes in selectivities. Based on these results, it seems that the NiMo catalyst supported on alumina/USY-zeolite with 50% weight ratio is the most promising catalyst for the hydroconversion of rosin acids of the examined materials.

5 Concluding remarks

Hydrotreatment of renewable feedstocks over alumina and zeolite supported sulfided NiMo and CoMo catalysts is recognized as one of the most efficient and promising processes for producing high quality renewable diesel fuels. However, loss in activity and changes in selectivity of hydrotreating catalysts are very complex processes and they have raised major concerns from economic and technological perspectives. The objective of this thesis was to deepen the understanding of how different catalyst preparations and process parameters affect the activity and selectivity of the hydrotreating catalysts.

Alumina supported Ni, Co and Mo containing catalysts were synthesized via an impregnation method. The effect of different synthesizing and pretreatment parameters on the hydrogen uptake capacity and dispersion of metal phases of the catalysts were investigated. The results showed that the pH of the impregnating solutions is an important parameter that can significantly impact the size and dispersion of metal phases of catalysts. For the metal precursors used in this thesis, an optimum range for the pH was proposed that results in a considerable improvement for the catalyst dispersion. Also, it was shown that that performing a pre-calcination in air can have very detrimental effects on the vital catalyst properties such as reducibility, dispersion and hydrogen uptake capacity. For instance, a non-calcined Ni/Al_2O_3 sample was found to have a much higher hydrogen uptake capacity compared to the calcined Ni/Al_2O_3 samples. The detrimental effect of calcination was related to promotion of high metal-support interactions that resulted in formation of heteropolymetal compounds and complex species such as $CoAl_2O_4$, $NiAl_2O_4$, $Al_2(MoO_4)_3$ and $CoMoO_4$ which are generally very stable and difficult to reduce. Therefore, when operating with nonsulfided HDO catalysts, it would be very beneficial to avoid the calcination step but instead, directly reduce the catalysts in a hydrogen containing atmosphere.

Moreover, the activity of sulfided $NiMo/Al_2O_3$ and Mo/Al_2O_3 catalysts used for the HDO reaction of oleic acid and abietic acid was studied. The HDO reactions of oleic acid were mainly proceeded through DCO_x and DO reaction routes from which heptadecane and octadecane were produced, respectively. The sulfided $NiMo/Al_2O_3$ catalyst was more selective towards heptadecane whereas sulfided Mo/Al_2O_3 catalyst was more selective towards octadecane. The HDO reactions of abietic acid were initially proceeded through disproportionation route when dehydroabietic and dihydroabietic acid

were produced and then the final deoxygenated products (tri-cycles) were produced mainly through DCO_x, HYD and dehydration routes.

Additionally, the effect of DMDS concentrations on the activity of the sulfided NiMo catalysts was investigated. For the studied concentrations of DMDS, the activity results showed that higher concentration of DMDS generally improved the oxygenate conversion rate of the NiMo catalyst. Also, higher concentration of DMDS notably increased the production of heptadecane, but the production of octadecane was almost unaffected by using different concentrations of DMDS. In other words, higher concentrations of DMDS promoted DCO_x route and obstructed DO route. The XPS results showed that the active phases such as NiMoS and MoS_2 of the NiMo catalyst were better maintained when higher concentrations of DMDS were used. The TPO results showed that higher concentration of DMDS decreased the contents of more carbonaceous deposits on spent catalysts. The results in this thesis also shows that addition of abietic acid to an oleic acid feed inhibits the oxygenate conversion of oleic acid. The observed inhibition was related to fast disproportionation of more strongly adsorbed abietic acid as well as possibly steric hindrance associated to adsorption of rosin acids. Also, the results revealed that compared to oleic acid, abietic acid produced different types of coke precursors with greater quantities that advanced more readily to more carbonaceous coke with higher temperature stability.

Furthermore, the deactivation of HDO catalysts due to iron poisoning is revealed in this thesis. The oxygen conversion rates of both NiMo and Mo catalysts decreased when an iron poison was added to the oxygenate feed. Also, addition of the iron poison affected the selectivities of both catalysts. The reason for the apparent inhibition of NiMo catalyst was revealed to be due to the disturbance on the promotional effect of Ni atoms which was caused by iron.

Finally, sulfided NiMo catalysts supported on alumina, USY-zeolite and mixed alumina/USY-zeolite were used to investigate the deoxygenation and ring opening reactions of tri-ring structured rosin acids. The increase in the number of Brønsted acid sites as well as improvement in the dispersion of the metal NiMo phases of the catalysts containing more USY-zeolite in their supports, resulted in the increase in selectivity of the RO and cracking reactions. However, the extensive Brønsted acidity of the Y-zeolite modified NiMo catalyst resulted in formation of the tetra-ring structures (pyrene) via undesirable dealkylation and bimolecular reactions. As a final point, this thesis shows that the Brønsted acidity of the support could be optimized by the USY-zeolite content of the catalyst to achieve a satisfactory level of deoxygenation, RO and cracking of the rosin acid while avoiding excessive coke formation.

In future study, using other characterization methods such as NMR, for characterization of the liquid samples, and optimized soxhlet technique for further identification of the deposited carbon on spent catalysts should be considered. Moreover, further improvement of the NiMo containing hydroconverting catalysts with higher catalytic activity performance at lower temperatures with low quality feeds such as rosin acids is interesting to be investigated. Furthermore, as relatively fast catalyst deactivation

via coking can frequently occur during the hydrotreating processes, for a reasonably expensive catalyst, a regeneration (decoking) process on a regular basis may be required. Therefore, it is very interesting to examine and optimize different regeneration methods.

As well, hydrotreating of the emerging new types of bio oils such as lignin and algae oils is very interesting and could be important areas in the future.

Acknowledgements

This work is financially supported by Formas in collaboration with Preem AB (Contract: 239-2012-1584 and 239-2014-164) and was performed at the Competence Centre for Catalysis (KCK) which is hosted by Chalmers University of Technology. The financial support from the Swedish Energy Agency and the KCK member companies AB Volvo, ECAPS AB, Haldor Topsøe A/S, Scania CV AB, Volvo Car Corporation AB and Wärtsilä Finland Oy is also immensely acknowledged.

I would also like to thank:

Professor Louise Olsson, my main supervisor and examiner, for giving me such a great opportunity to start my PhD studies, also for her inspirational supervision, appreciated expertise and her trust in my work.

Professor Derek Creaser, my co-supervisor, for his patience, invaluable discussions, his enjoyable supervision and motivating recommendations.

Dr. Stefanie Tamm my previous co-supervisor, also Stefan Nyström and Eva Lind Grennfelt from Preem AB for their vital contributions in my research.

Professor Bengt Andersson, Professor Claes Niklasson, Professor Anders Rasmuson, Professor Magnus Skoglundh, Professor Henrik Grönbeck, Professor Hanna Härelind, Associate Professor Per-Anders Carlsson, Associate Professor Anders Hellman, Associate Professor Jonas Sjöblom and Associate Professor Henrik Ström for their valuable advice and discussions.

My wonderful parents for their endless love, support and encouragement. My amazing wife Nina for her belief in me to start and continue my studies. Without your incredible patience and support, it would not have been possible to finalize my study. To my bundle of joy and pride, my precious son Darius, the reason that I wake up every morning to see him smile.

All my past and present friends and colleques at Chalmers University of Technology for creating such unforgettable joyful moments over the past five years.

In addition, I would like to acknowledge the help from Dr. Stefan Gustafsson and Dr. Lunjie Zeng from the division of applied physics of Chalmers University of Technology with the SEM and TEM analysis. Also, immense thank to Mattias Zetterberg for his kind assistance during the lab work and purchasing chemicals.

References

(1) Naik, S. N.; Goud, V. V.; Rout, P. K.; Dalai, A. K. Production of first and second generation biofuels: A comprehensive review. *Renew. Sust. Energ. Rew.* **2010,** *14*, 578.

(2) Nehring, R. Traversing the mountaintop: world fossil fuel production to 2050. *Philos T R Soc B* **2009,** *364*, 3067.

(3) International Energy Outlook 2017. https://www.eia.gov/outlooks/ieo/pdf/0484(2017).pdf.

(4) Cox, P. M.; Betts, R. A.; Jones, C. D.; Spall, S. A.; Totterdell, I. J. Acceleration of global warming due to carbon-cycle feedbacks in a coupled climate model (vol 408, pg 184, 2000). *Nature* **2000,** *408*, 750.

(5) Kamm, B.; Gruber, P. R.; Kamm, M., Biorefineries – Industrial Processes and Products. In *Ullmann's Encyclopedia of Industrial Chemistry*, Eds.; Wiley-VCH Verlag GmbH & Co. KGaA: 2000.

(6) Chakraborty, S.; Aggarwal, V.; Mukherjee, D.; Andras, K. Biomass to biofuel: a review on production technology. *Asia-Pacific Journal of Chemical Engineering* **2012,** *7*, S254.

(7) Brennan, L.; Owende, P. Biofuels from microalgae—A review of technologies for production, processing, and extractions of biofuels and co-products. *Renew. Sust. Energ. Rew.* **2010,** *14*, 557.

(8) Berndes, G.; Hoogwijk, M.; van den Broek, R. The contribution of biomass in the future global energy supply: a review of 17 studies. *Biomass Bioenerg* **2003,** *25*, 1.

(9) McKendry, P. Energy production from biomass (part 1): overview of biomass. *Bioresource Technol* **2002,** *83*, 37.

(10) Balat, M.; Balat, H. Recent trends in global production and utilization of bio-ethanol fuel. *Appl Energ* **2009,** *86*, 2273.

(11) Wilkie, A. C.; Riedesel, K. J.; Owens, J. M. Stillage characterization and anaerobic treatment of ethanol stillage from conventional and cellulosic feedstocks. *Biomass Bioenerg* **2000,** *19*, 63.

(12) Mojović, L.; Nikolić, S.; Rakin, M.; Vukasinović, M. Production of bioethanol from corn meal hydrolyzates. *Fuel.* **2006,** *85*, 1750.

(13) Fukuda, H.; Kondo, A.; Noda, H. Biodiesel Fuel Production by Transesterification of Oils. *J. Biosci. Bioeng.* **2001,** *92*, 405.

(14) Demirbas, A. Biodiesel Fuels from Vegetable Oils via Catalytic and Non-catalytic Supercritical Alcohol Transesterifications and Other Methods: A Survey. *Energ Convers. Manage.* **2003,** *44*, 2093.

(15) Srivastava, A.; Prasad, R. Triglycerides-based diesel fuels. *Renew Sust Energ Rev* **2000,** *4*, 111.

(16) Bournay, L.; Casanave, D.; Delfort, B.; Hillion, G.; Chodorge, J. A. New heterogeneous process for biodiesel production: A way to improve the quality and the value of the crude glycerin produced by biodiesel plants. *Catal. Today* **2005,** *106*, 190.

(17) Donnis, B.; Egeberg, R. G.; Blom, P.; Knudsen, K. G. Hydroprocessing of Bio-Oils and Oxygenates to Hydrocarbons. Understanding the Reaction Routes. *Top. Catal.* **2009,** *52*, 229.

(18) Demirbas, A. Biomass resource facilities and biomass conversion processing for fuels and chemicals. *Energ Convers. Manage.* **2001,** *42*, 1357.

(19) Danuthai, T.; Sooknoi, T.; Jongpatiwut, S.; Rirksomboon, T.; Osuwan, S.; Resasco, D. E. Effect of extra-framework cesium on the deoxygenation of methylester over CsNaX zeolites. *Appl. Catal., A* **2011,** *409*, 74.

(20) Ayodele, O. B.; Farouk, H. U.; Mohammed, J.; Uemura, Y.; Daud, W. M. A. W. Hydrodeoxygenation of Oleic Acid into N- and Iso-Paraffin Biofuel Using Zeolite Supported Fiuoro-Oxalate Modified Molybdenum Catalyst: Kinetics Study. *J. Taiwan Inst. Chem. Eng.* **2015,** *50*, 142.

(21) Reimann, W. A.; Siggelkow, B. A. Cold Flow Treatment: FAME, HVO & Diesel Blends. http://www.biodieselmagazine.com/articles/9400/cold-flow-treatment-fame-hvo-diesel-blends (accessed October 2013).
(22) Hamada, H.; Kato, H.; Ito, N.; Takase, Y.; Nanbu, H.; Mishima, S.; Sakaki, H.; Sato, K. Effects of Polyglycerol Esters of Fatty Acids and Ethylene-Vinyl Acetate Co-polymer on Crystallization Behavior of Biodiesel. *Eur. J. Lipid Sci. Technol.* **2010,** *112*, 1323.
(23) Fuel Regulations. https://www.dieselnet.com/standards/fuels.php#eu.
(24) Demirbas, A. Production of biodiesel from tall oil. *Energ Source Part A* **2008,** *30*, 1896.
(25) Aro, T.; Fatehi, P. Tall oil production from black liquor: Challenges and opportunities. *Separation and Purification Technology* **2017,** *175*, 469.
(26) Niemi, S.; Vauhkonen, V.; Mannonen, S.; Ovaska, T.; Nilsson, O.; Sirviö, K.; Heikkilä, S.; Kiijärvi, J. Effects of wood-based renewable diesel fuel blends on the performance and emissions of a non-road diesel engine. *Fuel* **2016,** *186*, 1.
(27) Johansson, A. By- product recoverey and valorization in the Kraft industry-a review of current trends in the recovery and use of turpentine and tall oil derivatives. *Biomass* **1982,** *2*, 103.
(28) Anthonykutty, J. M.; Van Geem, K. M.; De Bruycker, R.; Linnekoski, J.; Laitinen, A.; Rasanen, J.; Harlin, A.; Lehtonen, J. Value Added Hydrocarbons from Distilled Tall Oil via Hydrotreating over a Commercial NiMo Catalyst. *Ind. Eng. Chem. Res.* **2013,** *52*, 10114.
(29) Anthonykutty, J. M.; Linnekoski, J.; Harlin, A.; Laitinen, A.; Lehtonen, J. Catalytic upgrading of crude tall oil into a paraffin-rich liquid. *Biomass Convers. Biorefinery* **2015,** *5*, 149.
(30) Do, P. T.; Chiappero, M.; Lobban, L. L.; Resasco, D. E. Catalytic Deoxygenation of Methyl-Octanoate and Methyl-Stearate on Pt/Al2O3. *Catal. Lett.* **2009,** *130*, 9.
(31) Snare, M.; Kubickova, I.; Maki-Arvela, P.; Eranen, K.; Murzin, D. Y. Heterogeneous Catalytic Deoxygenation of Stearic Acid for Production of Biodiesel. *Ind. Eng. Chem. Res.* **2006,** *45*, 5708.
(32) *International Energy Outlook 2016; US Department of Energy*; May 2016, May 2016; pp 1.
(33) Sotelo-Boyas, R.; Liu, Y. Y.; Minowa, T. Renewable Diesel Production From the Hydrotreating of Rapeseed Oil with Pt/Zeolite and NiMo/Al_2O_3 Catalysts. *Ind. Eng. Chem. Res.* **2011,** *50*, 2791.
(34) Furimsky, E. Catalytic Hydrodeoxygenation. *Appl. Catal., A* **2000,** *199*, 147.
(35) Massoth, F. E.; Politzer, P.; Concha, M. C.; Murray, J. S.; Jakowski, J.; Simons, J. Catalytic hydrodeoxygenation of methyl-substituted phenols: Correlations of kinetic parameters with molecular properties. *J. Phys. Chem. B* **2006,** *110*, 14283.
(36) Zuo, H.; Liu, Q.; Wang, T.; Ma, L.; Zhang, Q.; Zhang, Q. Hydrodeoxygenation of Methyl Palmitate over Supported Ni Catalysts for Diesel-like Fuel Production. *Energ Fuels* **2012,** *26*, 3747.
(37) Yang, Y.; Wang, Q.; Zhang, X.; Wang, L.; Li, G. Hydrotreating of C18 fatty acids to hydrocarbons on sulphided NiW/SiO2–Al2O3. *Fuel Process. Technol.* **2013,** *116*, 165.
(38) Sabatier, P., *" Catalysis in organic chemistry"*. Van Nostrand:New York, 1922.
(39) Girgis, M. J.; Gates, B. C. REACTIVITIES, REACTION NETWORKS, AND KINETICS IN HIGH-PRESSURE CATALYTIC HYDROPROCESSING. *Ind. Eng. Chem. Res.* **1991,** *30*, 2021.
(40) Elliott, D. C. Historical developments in hydroprocessing bio-oils. *Energ. Fuel.* **2007,** *21*, 1792.
(41) Oyama, S. T. Novel catalysts for advanced hydroprocessing: transition metal phosphides. *J. Catal.* **2003,** *216*, 343.
(42) Knudsen, K. G.; Cooper, B. H.; Topsoe, H. Catalyst and process technologies for ultra low sulfur diesel. *Appl. Catal., A* **1999,** *189*, 205.
(43) Furimsky, E.; Massoth, F. E. Deactivation of hydroprocessing catalysts. *Catal. Today* **1999,** *52*, 381.
(44) Fogler, H. S., *External Diffusion Effects on Heterogeneous Reactions, In: Elements of Chemical Reaction Engineering*. Prentice-Hall Inc:New Jersey, 2006; p pp:757.

(45) Thomas, J. M. T., W.J., *Principles and Practice of Heterogeneous Catalysis*. VCH:New York, 1997.
(46) Dudukovic, M. P.; Larachi, F.; Mills, P. L. Multiphase reactors - revisited. *Chemical Engineering Science* **1999,** *54*, 1975.
(47) Mortensen, P. M.; Grunwaldt, J. D.; Jensen, P. A.; Knudsen, K. G.; Jensen, A. D. A review of catalytic upgrading of bio-oil to engine fuels. *Appl. Catal., A* **2011,** *407*, 1.
(48) Demirbas, A. Competitive liquid biofuels from biomass. *Appl Energ* **2011,** *88*, 17.
(49) Zhang, S. P.; Yan, Y. J.; Ren, J. W.; Li, T. C. Study of hydrodeoxygenation of bio-oil from the fast pyrolysis of biomass. *Energy Sources* **2003,** *25*, 57.
(50) Wang, Y.; He, T.; Liu, K.; Wu, J.; Fang, Y. From biomass to advanced bio-fuel by catalytic pyrolysis/hydro-processing: Hydrodeoxygenation of bio-oil derived from biomass catalytic pyrolysis. *Bioresource Technol* **2012,** *108*, 280.
(51) Senol, O. I.; Viljava, T. R.; Krause, A. O. I. Hydrodeoxygenation of Methyl Esters on Sulfided NiMo/gamma-Al2O3 and CoMo/gamma-Al2O3 Catalysts. *Catal. Today* **2005,** *100*, 331.
(52) Huber, G. W.; O'Connor, P.; Corma, A. Processing Biomass in Conventional Oil Refineries: Production of High Quality Diesel by Hydrotreating Vegetable Oils in Heavy Vacuum Oil Mixtures. *Appl. Catal., A* **2007,** *329*, 120.
(53) Kubickova, I.; Kubicka, D. Utilization of Triglycerides and Related Feedstocks for Production of Clean Hydrocarbon Fuels and Petrochemicals: A Review. *Waste and Biomass Valorization* **2010,** *1*, 293.
(54) Baladincz, P.; Hancsok, J. Fuel from waste animal fats. *Chem Eng J* **2015,** *282*, 152.
(55) Adjaye, J. D.; Bakhshi, N. N. PRODUCTION OF HYDROCARBONS BY CATALYTIC UPGRADING OF A FAST PYROLYSIS BIO-OIL .1. CONVERSION OVER VARIOUS CATALYSTS. *Fuel Process. Technol.* **1995,** *45*, 161.
(56) Wildschut, J.; Mahfud, F. H.; Venderbosch, R. H.; Heeres, H. J. Hydrotreatment of Fast Pyrolysis Oil Using Heterogeneous Noble-Metal Catalysts. *Ind. Eng. Chem. Res.* **2009,** *48*, 10324.
(57) Miao, C.; Marin-Flores, O.; Davidson, S. D.; Li, T. T.; Dong, T.; Gao, D. F.; Wang, Y.; Garcia-Perez, M.; Chen, S. L. Hydrothermal Catalytic Deoxygenation of Palmitic Acid over Nickel Catalyst. *Fuel* **2016,** *166*, 302.
(58) Senol, O. I.; Ryymin, E. M.; Viljava, T. R.; Krause, A. O. I. Reactions of Methyl Heptanoate Hydrodeoxygenation on Sulphided Catalysts. *J. Mol. Catal. A: Chem.* **2007,** *268*, 1.
(59) de Miguel Mercader, F.; Groeneveld, M. J.; Kersten, S. R. A.; Way, N. W. J.; Schaverien, C. J.; Hogendoorn, J. A. Production of advanced biofuels: Co-processing of upgraded pyrolysis oil in standard refinery units. *Applied Catalysis B: Environmental* **2010,** *96*, 57.
(60) Egeberg, R. G.; Michaelsen, N. H.; Skyum, L. Novel hydrotreating technology for production of green diesel 2011, p. http://www.topsoe.com/business_areas/refining/~/media/PDF%20files/Refining/novel_hydrotreating_technology_for_production_of_green_diesel.ashx.
(61) Dupont, C.; Lemeur, R.; Daudin, A.; Raybaud, P. Hydrodeoxygenation pathways catalyzed by MoS2 and NiMoS active phases: A DFT study. *J. Catal.* **2011,** *279*, 276.
(62) Bui, V. N.; Laurenti, D.; Delichère, P.; Geantet, C. Hydrodeoxygenation of guaiacol: Part II: Support effect for CoMoS catalysts on HDO activity and selectivity. *Appl. Catal., B* **2011,** *101*, 246.
(63) Lofstedt, J.; Dahlstrand, C.; Orebom, A.; Meuzelaar, G.; Sawadjoon, S.; Galkin, M. V.; Agback, P.; Wimby, M.; Corresa, E.; Mathieu, Y.; Sauvanaud, L.; Eriksson, S.; Corma, A.; Samec, J. S. M. Green Diesel from Kraft Lignin in Three Steps. *ChemSusChem* **2016,** *9*, 1392.
(64) Chon, S.; Allen, D. T. Catalytic hydroprocessing of chlorophenols. *AIChE Journal* **1991,** *37*, 1730.
(65) Odebunmi, E. O.; Ollis, D. F. Catalytic hydrodeoxygenation: I. Conversions of o-, p-, and m-cresols. *J. Catal.* **1983,** *80*, 56.
(66) Kubicka, D.; Horacek, J. Deactivation of HDS Catalysts in Deoxygenation of Vegetable Oils. *Appl. Catal., A* **2011,** *394*, 9.

(67) Deliy, I. V.; Vlasova, E. N.; Nuzhdin, A. L.; Gerasimov, E. Y.; Bukhtiyarova, G. A. Hydrodeoxygenation of methyl palmitate over sulfided Mo/Al2O3, CoMo/Al2O3 and NiMo/Al2O3 catalysts. *Rsc Adv* **2014,** *4*, 2242.
(68) Cavani, F. A., S. Basile, F. Gandini, A, *Chemicals and fuels from bio-based building blocks* 1ed.; Wiley-VCH Verlag GmBH & Company KGaA:Germany, 2016; Vol. 2, p 744.
(69) Sahoo, S. K.; Ray, S. S.; Singh, I. D. Structural Characterization of Coke on Spent Hydroprocessing Catalysts Used for Processing of Vacuum Gas Oils. *Appl. Catal., A* **2004,** *278*, 83.
(70) Wang, Y.; Lin, H. F.; Zheng, Y. Hydrotreatment of Lignocellulosic Biomass Derived Oil Using a Sulfided NiMo/gamma-Al2O3 Catalyst. *Catal. Sci. Technol.* **2014,** *4*, 109.
(71) Daudin, A. B., L. Chapus, T. Method of converting effluents of renewable origin into fuel of excellent quality by using a molybdenum-based catalyst. US8546626B2, 2013.
(72) Venderbosch, R. H.; Ardiyanti, A. R.; Wildschut, J.; Oasmaa, A.; Heeres, H. J. Stabilization of biomass-derived pyrolysis oils. *Journal of Chemical Technology & Biotechnology* **2010,** *85*, 674.
(73) Anthonykutty, J. M. Hydrotreating of tall oils on a sulfided NiMo catalyst for the production of basechemicals in steam crackers. School of Chemical Technology, Aalto University, Finland, 2015.
(74) Norlin, L.-H., Tall Oil. In *Ullmann's Encyclopedia of Industrial Chemistry*, Eds.; Wiley-VCH Verlag GmbH & Co. KGaA: 2000.
(75) Foran, C. D. Tall oil soap recovery. http://www.tappi.org/content/events/08kros/manuscripts/3-7.pdf.
(76) Fuenzalida, D. M. A.; Markovits, R. A.; Leiva, H. R.; Markovits, S. E., High efficiency method for obtaining an unsaponifiable fraction from black-liquor soaps or crude tall oil. Google Patents: 1999.
(77) Weidner, E. *ANALYSIS OF THE EUROPEAN CRUDE TALL OIL INDUSTRY – ENVIRONMENTAL IMPACT, SOCIOECONOMIC*

VALUE & DOWNSTREAM POTENTIAL; 2016.
(78) Wang, L. L.; Chen, X. P.; Liang, J. Z.; Chen, Y. Y.; Pu, X. D.; Tong, Z. F. Kinetics of the catalytic isomerization and disproportionation of rosin over carbon-supported palladium. *Chem Eng J* **2009,** *152*, 242.
(79) Anthonykutty, J. M.; Linnekoski, J.; Harlin, A.; Lehtonen, J. Hydrotreating reactions of tall oils over commercial NiMo catalyst. *Energy Science & Engineering* **2015,** *3*, 286.
(80) Magee, T. V.; Zinkel, D. F. Composition of American distilled tall oil. *J Am Oil Chem Soc* **1992,** *69*, 321.
(81) Cashman, S. A.; Moran, K. M.; Gaglione, A. G. Greenhouse Gas and Energy Life Cycle Assessment of Pine Chemicals Derived from Crude Tall Oil and Their Substitutes. *J. Ind. Ecol.* **2016,** *20*, 1108.
(82) Demirbas, A. Methylation of wood fatty and resin acids for production of biodiesel. *Fuel* **2011,** *90*, 2273.
(83) Lee, S. Y.; Hubbe, M. A.; Saka, S. PROSPECTS FOR BIODIESEL AS A BYPRODUCT OF WOOD PULPING - A REVIEW. *Bioresources* **2006,** *1*, 150.
(84) Peng, B.; Zhao, C.; Kasakov, S.; Foraita, S.; Lercher, J. A. Manipulating catalytic pathways: Deoxygenation of palmitic acid on multifunctional catalysts. *Chemistry - A European Journal* **2013,** *19*, 4732.
(85) Peng, B.; Yao, Y.; Zhao, C.; Lercher, J. A. Towards quantitative conversion of microalgae oil to diesel-range alkanes with bifunctional catalysts. *Angewandte Chemie - International Edition* **2012,** *51*, 2072.
(86) Li, K. L.; Wang, R. J.; Chen, J. X. Hydrodeoxygenation of Anisole over Silica-Supported Ni_2P, MoP, and NiMoP Catalysts. *Energ Fuels* **2011,** *25*, 854.
(87) Andersson, J. R. B., M, *Catalysis sience and technology*. Springer-Verlag Berlin Heidelberg:1996; Vol. 11, p 325.

(88) Kordulis, C.; Bourikas, K.; Gousi, M.; Kordouli, E.; Lycourghiotis, A. Development of nickel based catalysts for the transformation of natural triglycerides and related compounds into green diesel: a critical review. *Applied Catalysis B: Environmental* **2016,** *181*, 156.
(89) Mortensen, P. M.; Grunwaldt, J. D.; Jensen, P. A.; Jensen, A. D. Screening of Catalysts for Hydrodeoxygenation of Phenol as a Model Compound for Bio-oil. *Acs Catal* **2013,** *3*, 1774.
(90) Shetty, M.; Murugappan, K.; Green, W. H.; Roman-Leshkov, Y. Structural Properties and Reactivity Trends of Molybdenum Oxide Catalysts Supported on Zirconia for the Hydrodeoxygenation of Anisole. *Acs Sustainable Chemistry & Engineering* **2017,** *5*, 5293.
(91) Centeno, A.; Laurent, E.; Delmon, B. Influence of the Support of CoMo Sulfide Catalysts and of the Addition of Potassium and Platinum on the Catalytic Performances for the Hydrodeoxygenation of Carbonyl, Carboxyl, and Guaiacol-Type Molecules. *J. Catal.* **1995,** *154*, 288.
(92) Breysse, M.; Afanasiev, P.; Geantet, C.; Vrinat, M. Overview of support effects in hydrotreating catalysts. *Catal. Today* **2003,** *86*, 5.
(93) Kumar, C. R.; Anand, N.; Kloekhorst, A.; Cannilla, C.; Bonura, G.; Frusteri, F.; Barta, K.; Heeres, H. J. Solvent free depolymerization of Kraft lignin to alkyl-phenolics using supported NiMo and CoMo catalysts. *Green Chem* **2015,** *17*, 4921.
(94) Rodriguez, J. C.; Romeo, E.; Fierro, J. L. G.; Santamaria, J.; Monzon, A. Deactivation by Coking and Poisoning of Spinel-Type Ni Catalysts. *Catal. Today* **1997,** *37*, 255.
(95) Morgan, T.; Santillan-Jimenez, E.; Harman-Ware, A. E.; Ji, Y. Y.; Grubb, D.; Crocker, M. Catalytic deoxygenation of triglycerides to hydrocarbons over supported nickel catalysts. *Chem Eng J* **2012,** *189*, 346.
(96) Pan, Z.; Wang, R.; Chen, J. Deoxygenation of methyl laurate as a model compound on Ni-Zn alloy and intermetallic compound catalysts: Geometric and electronic effects of oxophilic Zn. *Appl. Catal., B.*
(97) Topsoe, H.; Egeberg, R. G.; Knudsen, K. G. Future Challenges of Hydrotreating Catalyst Technology. *Prepr. - Am. Chem. Soc., Div. Energy Fuels* **2004,** *49*, 568.
(98) Breysse, M.; Portefaix, J. L.; Vrinat, M. Support effects on hydrotreating catalysts. *Catal. Today* **1991,** *10*, 489.
(99) Rocha, A. S.; Faro, A. C.; Oliviero, L.; Lélias, M. A.; Travert, A.; van Gestel, J.; Maugé, F. Effect of the electronic properties of Mo sulfide phase on the hydrotreating activity of catalysts supported on Al2O3, Nb2O5 and Nb2O5/Al2O3. *Catal. Lett.* **2006,** *111*, 27.
(100) Gosselink, R. W.; Hollak, S. A. W.; Chang, S. W.; van Haveren, J.; de Jong, K. P.; Bitter, J. H.; van Es, D. S. Reaction Pathways for the Deoxygenation of Vegetable Oils and Related Model Compounds. *ChemSusChem* **2013,** *6*, 1576.
(101) Laurenti, D.; Phung-Ngoc, B.; Roukoss, C.; Devers, E.; Marchand, K.; Massin, L.; Lemaitre, L.; Legens, C.; Quoineaud, A.-A.; Vrinat, M. Intrinsic potential of alumina-supported CoMo catalysts in HDS: Comparison between γc, γT, and δ-alumina. *J. Catal.* **2013,** *297*, 165.
(102) Luck, F. A REVIEW OF SUPPORT EFFECTS ON THE ACTIVITY AND SELECTIVITY OF HYDROTREATING CATALYSTS. *Bull. Soc. Chim. Belg.* **1991,** *100*, 781.
(103) Ratnasamy, P.; Sivasanker, S. STRUCTURAL CHEMISTRY OF CO-MO-ALUMINA CATALYSTS. *Catal Rev* **1980,** *22*, 401.
(104) Bartholomew, C. H.; Farrauto, R. J. Chemistry of nickel-alumina catalysts. *J. Catal.* **1976,** *45*, 41.
(105) Bridgwater, A. V. CATALYSIS IN THERMAL BIOMASS CONVERSION. *Appl. Catal., A* **1994,** *116*, 5.
(106) Elliott, D. C.; Hu, J.; Hart, T. R.; Neuenschwander, G. G., Palladium catalyzed hydrogenation of bio-oils and organic compounds. Google Patents: 2011.
(107) Vissers, J. P. R.; Scheffer, B.; de Beer, V. H. J.; Moulijn, J. A.; Prins, R. Effect of the support on the structure of Mo-based hydrodesulfurization catalysts: Activated carbon versus alumina. *J. Catal.* **1987,** *105*, 277.
(108) Gutierrez, A.; Kaila, R. K.; Honkela, M. L.; Slioor, R.; Krause, A. O. I. Hydrodeoxygenation of guaiacol on noble metal catalysts. *Catal. Today* **2009,** *147*, 239.

(109) Chuah, G. K.; Liu, S. H.; Jaenicke, S.; Li, J. High surface area zirconia by digestion of zirconium propoxide at different pH. *Microporous Mesoporous Mater.* **2000,** *39*, 381.
(110) Klicpera, T.; Zdražil, M. Preparation of High-Activity MgO-Supported Co–Mo and Ni–Mo Sulfide Hydrodesulfurization Catalysts. *J. Catal.* **2002,** *206*, 314.
(111) Narani, A.; Chowdari, R. K.; Cannilla, C.; Bonura, G.; Frusteri, F.; Heeres, H. J.; Barta, K. Efficient catalytic hydrotreatment of Kraft lignin to alkylphenolics using supported NiW and NiMo catalysts in supercritical methanol. *Green Chem* **2015,** *17*, 5046.
(112) Lee, S.-U.; Lee, Y.-J.; Kim, J.-R.; Jeong, S.-Y. Rational synthesis of silylated Beta zeolites and selective ring opening of 1-methylnaphthalene over the NiW-supported catalysts. *Appl. Catal., B* **2017,** *219*, 1.
(113) Blanchard, J.; Breysse, M.; Fajerwerg, K.; Louis, C.; Hedoire, C. E.; Sampieri, A.; Zeng, S.; Perot, G.; Nie, H.; Li, D., Acidic zeolites and Al-SBA-45 as supports for sulfide phases: application to hydrotreating reactions. In *Molecular Sieves: From Basic Research to Industrial Applications, Pts a and B*, Cejka, J.; Zilkova, N.; Nachtigall, P., Eds.; 2005; Vol. 158, pp 1517.
(114) Fu, W.; Zhang, L.; Wu, D.; Xiang, M.; Zhuo, Q.; Huang, K.; Tao, Z.; Tang, T. Mesoporous zeolite-supported metal sulfide catalysts with high activities in the deep hydrogenation of phenanthrene. *J. Catal.* **2015,** *330*, 423.
(115) Vissers, J. P. R.; Mercx, F. P. M.; Bouwens, S. M. A. M.; de Beer, V. H. J.; Prins, R. Carbon-covered alumina as a support for sulfide catalysts. *J. Catal.* **1988,** *114*, 291.
(116) Brown, S. M.; Wallace, D. N., Process for preparing phosphated alumina extrudates. Google Patents: 1976.
(117) Kemp, R. A.; Adams, C. T. Hydrogel-derived catalysts. Laboratory results on nickel-molybdenum and cobalt-molybdenum hydrotreating catalysts. *Appl. Catal., A* **1996,** *134*, 299.
(118) Eijsbouts, S.; Mayo, S. W.; Fujita, K. Unsupported transition metal sulfide catalysts: From fundamentals to industrial application. *Appl. Catal. A: Gen.* **2007,** *322*, 58.
(119) Moene, R.; Tijsen, E. P. A. M.; Makkee, M.; Moulijn, J. A. Synthesis and thermal stability of Ni, Cu, Co, and Mo catalysts based on high surface area silicon carbide. *Appl. Catal. A: Gen.* **1999,** *184*, 127.
(120) Bezemer, G. L.; Radstake, P. B.; Koot, V.; van Dillen, A. J.; Geus, J. W.; de Jong, K. P. Preparation of Fischer–Tropsch cobalt catalysts supported on carbon nanofibers and silica using homogeneous deposition-precipitation. *J. Catal.* **2006,** *237*, 291.
(121) Chmielarz, L.; Rutkowska, M.; Kustrowski, P.; Drozdek, M.; Piwowarska, Z.; Dudek, B.; Dziembaj, R.; Michalik, M. An influence of thermal treatment conditions of hydrotalcite-like materials on their catalytic activity in the process of N2O decomposition. *J. Therm. Anal. Calorim.* **2011,** *105*, 161.
(122) van Dillen, A. J.; Terorde, R.; Lensveld, D. J.; Geus, J. W.; de Jong, K. P. Synthesis of supported catalysts by impregnation and drying using aqueous chelated metal complexes. *J. Catal.* **2003,** *216*, 257.
(123) Anderson, J. R., *Structure of Metallic Catalysts*. Academic Press:London, New York, San Francisco, 1975.
(124) Roy, B.; Martinez, U.; Loganathan, K.; Datye, A. K.; Leclerc, C. A. Effect of preparation methods on the performance of Ni/Al2O3 catalysts for aqueous-phase reforming of ethanol: Part I-catalytic activity. *Int J Hydrogen Energ* **2012,** *37*, 8143.
(125) Brunelle, J. P. Preparation of catalysts by metallic complex adsorption on mineral oxides *Pure Appl Chem* **1978,** *50*, 1211.
(126) Zdrazil, M. MgO-supported Mo, CoMo and NiMo sulfide hydrotreating catalysts. *Catal. Today* **2003,** *86*, 151.
(127) Ferdous, D.; Dalai, A. K.; Adjaye, J. A series of NiMo/A1(2)O(3) catalysts containing boron and phosphorus Part I. Synthesis and characterization. *Appl. Catal., A* **2004,** *260*, 137.
(128) Guevara-Lara, A.; Bacaud, R.; Vrinat, M. Highly Active NiMo/TiO_2-Al_2O_3 Catalysts: Influence of the Preparation and the Activation Conditions on the Catalytic Activity. *Appl. Catal., A* **2007,** *328*, 99.

(129) Ojagh, H.; Creaser, D.; Tamm, S.; Hu, C. Q.; Olsson, L. Effect of Thermal Treatment on Hydrogen Uptake and Characteristics of Ni-, Co-, and Mo-Containing Catalysts. *Ind. Eng. Chem. Res.* **2015,** *54*, 11511.
(130) Liotta, L. F.; Pantaleo, G.; Macaluso, A.; Di Carlo, G.; Deganello, G. CoO_x catalysts supported on alumina and alumina-baria: influence of the support on the cobalt species and their activity in NO reduction by C_3H_6 in lean conditions. *Appl. Catal., A* **2003,** *245*, 167.
(131) Shaheen, W. M.; Abd El Maksod, I. H. Thermal solid–solid interactions and physicochemical properties of Co3O4/MoO3 system treated with Al2O3. *J Alloy Compd* **2009,** *475*, 874.
(132) Nava, R.; Pawelec, B.; Castaño, P.; Álvarez-Galván, M. C.; Loricera, C. V.; Fierro, J. L. G. Upgrading of bio-liquids on different mesoporous silica-supported CoMo catalysts. *Appl. Catal., B* **2009,** *92*, 154.
(133) Wivel, C.; Candia, R.; Clausen, B. S.; Mørup, S.; Topsøe, H. On the catalytic significance of a Co□Mo□S phase in Co□MoAl2O3 hydrodesulfurization catalysts: Combined in situ Mössbauer emission spectroscopy and activity studies. *J. Catal.* **1981,** *68*, 453.
(134) Grilc, M.; Likozar, B.; Levec, J. Hydrodeoxygenation and hydrocracking of solvolysed lignocellulosic biomass by oxide, reduced and sulphide form of NiMo, Ni, Mo and Pd catalysts. *Appl. Catal., B* **2014,** *150*, 275.
(135) Wang, X. Q.; Ozkan, U. S. Characterization of active sites over reduced Ni-Mo/Al2O3 catalysts for hydrogenation of linear aldehydes. *J. Phys. Chem. B* **2005,** *109*, 1882.
(136) Liu, J.; Fan, K.; Tian, W.; Liu, C.; Rong, L. Hydroprocessing of Jatropha oil over NiMoCe/Al2O3 catalyst. *Int J Hydrogen Energ* **2012,** *37*, 17731.
(137) Lestari, S.; Maki-Arvela, P.; Beltramini, J.; Lu, G. Q. M.; Murzin, D. Y. Transforming Triglycerides and Fatty Acids into Biofuels. *ChemSusChem* **2009,** *2*, 1109.
(138) Kubička, D. Future refining Catalysis - Introduction of biomass feedstocks. *Collect Czech Chem C* **2008,** *73*, 1015.
(139) Cesano, F.; Bertarione, S.; Piovano, A.; Agostini, G.; Rahman, M. M.; Groppo, E.; Bonino, F.; Scarano, D.; Lamberti, C.; Bordiga, S.; Montanari, L.; Bonoldi, L.; Millini, R.; Zecchina, A. Model oxide supported MoS2 HDS catalysts: structure and surface properties. *Catal. Sci. Technol.* **2011,** *1*, 123.
(140) Ojagh, H.; Creaser, D.; Tamm, S.; Arora, P.; Nyström, S.; Lind Grennfelt, E.; Olsson, L. Effect of Dimethyl Disulfide on Activity of NiMo Based Catalysts Used in Hydrodeoxygenation of Oleic Acid. *Ind. Eng. Chem. Res.* **2017,** *56*, 5547.
(141) Candia, R.; Clausen, B. S.; Topsøe, H. The origin of catalytic synergy in unsupported CoMo HDS catalysts. *J. Catal.* **1982,** *77*, 564.
(142) Marchand, K.; Legens, C.; Guillaume, D.; Raybaud, P. A Rational Comparison of the Optimal Promoter Edge Decoration of HDT NiMoS vs CoMoS Catalysts. *Oil Gas Sci. Technol.-Rev. IFP* **2009,** *64*, 719.
(143) Guichard, B.; Roy-Auberger, M.; Devers, E.; Pichon, C.; Legens, C.; Lecour, P. Influence of the Promoter's Nature (Nickel or Cobalt) on the Active Phases 'Ni(Co)MoS' Modifications During Deactivation in HDS of Diesel Fuel. *Catal. Today* **2010,** *149*, 3.
(144) Topsøe, H.; Clausen, B. S.; Candia, R.; Wivel, C.; Mørup, S. In situ Mössbauer emission spectroscopy studies of unsupported and supported sulfided Co□Mo hydrodesulfurization catalysts: Evidence for and nature of a Co□Mo□S phase. *J. Catal.* **1981,** *68*, 433.
(145) Paul, J.-F.; Cristol, S.; Payen, E. Computational studies of (mixed) sulfide hydrotreating catalysts. *Catal. Today.* **2008,** *130*, 139.
(146) Travert, A.; Dujardin, C.; Mauge, F.; Veilly, E.; Cristol, S.; Paul, J. F.; Payen, E. CO adsorption on CoMo and NiMo sulfide catalysts: A combined IR and DFT. *J. Phys. Chem. B* **2006,** *110*, 1261.
(147) Van Doorn, J.; Moulijn, J. A.; Djéga-Mariadassou, G. High-resolution Electron Microscopy of Spent Ni-Mo/Al203 Hydrotreating Catalysts. *Appl. Catal.* **1990,** *63*, 77.
(148) Topsøe, H.; Clausen, B. S.; Massoth, F. E., Hydrotreating Catalysis. In *Catalysis: Science and Technology*, Anderson, J. R.; Boudart, M., Eds.; Springer Berlin Heidelberg: Berlin, Heidelberg. 1996; pp 1.

(149) Romero, Y.; Richard, F.; Brunet, S. Hydrodeoxygenation of 2-ethylphenol as a model compound of bio-crude over sulfided Mo-based catalysts: Promoting effect and reaction mechanism. *Appl. Catal., B* **2010,** *98*, 213.
(150) Sun, M.; Nelson, A. E.; Adjaye, J. Adsorption and dissociation of H2 and H2S on MoS2 and NiMoS catalysts. *Catal. Today* **2005,** *105*, 36.
(151) Bunch, A.; Zhang, L. P.; Karakas, G.; Ozkan, U. S. Reaction network of indole hydrodenitrogenation over NiMoS/gamma-Al2O3 catalysts. *Appl. Catal., A* **2000,** *190*, 51.
(152) Harris, S.; Chianelli, R. R. Catalysis by transition metal sulfides: A theoretical and experimental study of the relation between the synergic systems and the binary transition metal sulfides. *J. Catal.* **1986,** *98*, 17.
(153) Topsoe, N. Y.; Topsoe, H. FTIR STUDIES OF MO/AL2O3-BASED CATALYSTS .2. EVIDENCE FOR THE PRESENCE OF SH-GROUPS AND THEIR ROLE IN ACIDITY AND ACTIVITY. *J. Catal.* **1993,** *139*, 641.
(154) Ryymin, E.-M.; Honkela, M. L.; Viljava, T.-R.; Krause, A. O. I. Competitive reactions and mechanisms in the simultaneous HDO of phenol and methyl heptanoate over sulphided NiMo/γ-Al2O3. *Appl. Catal., A* **2010,** *389*, 114.
(155) Topsoe, N. Y.; Topsoe, H. FTIR Studies of Mo/Al2O3-Based Catalysts. *J. Catal.* **1993,** *139*, 641.
(156) Ryymin, E.-M.; Honkela, M. L.; Viljava, T.-R.; Krause, A. O. I. Insight to sulfur species in the hydrodeoxygenation of aliphatic esters over sulfided NiMo/γ-Al2O3 catalyst. *Appl. Catal., A* **2009,** *358*, 42.
(157) Badawi, M.; Cristol, S.; Paul, J.-F.; Payen, E. DFT study of furan adsorption over stable molybdenum sulfide catalyst under HDO conditions. *Comptes Rendus Chimie* **2009,** *12*, 754.
(158) Yoshimura, Y.; Sato, T.; Shimada, H.; Matsubayashi, N.; Nishijima, A. INFLUENCES OF OXYGEN-CONTAINING SUBSTANCES ON DEACTIVATION OF SULFIDED MOLYBDATE CATALYSTS. *Appl. Catal.* **1991,** *73*, 55.
(159) Besenbacher, F.; Brorson, M.; Clausen, B. S.; Helveg, S.; Hinnemann, B.; Kibsgaard, J.; Lauritsen, J.; Moses, P. G.; Norskov, J. K.; Topsoe, H. Recent STM, DFT and HAADF-STEM studies of sulfide-based hydrotreating catalysts: Insight into mechanistic, structural and particle size effects. *Catal. Today* **2008,** *130*, 86.
(160) Bartholomew, C. H. Mechanisms of Catalyst Deactivation. *Appl. Catal., A* **2001,** *212*, 17.
(161) Forzatti, P.; Lietti, L. Catalyst deactivation. *Catal. Today.* **1999,** *52*, 165.
(162) Moulijn, J. A.; van Diepen, A. E.; Kapteijn, F. Catalyst deactivation: is it predictable?: What to do? *Appl. Catal. A: Gen.* **2001,** *212*, 3.
(163) Tsakoumis, N. E.; Rønning, M.; Borg, Ø.; Rytter, E.; Holmen, A. Deactivation of cobalt based Fischer–Tropsch catalysts: A review. *Catal. Today.* **2010,** *154*, 162.
(164) Laurent, E.; Delmon, B. Influence of water in the deactivation of a sulfided NiMoγ-Al2O3 catalyst during hydrodeoxygenation. *J. Catal.* **1994,** *146*, 281.
(165) Mortensen, P. M.; Gardini, D.; Damsgaard, C. D.; Grunwaldt, J. D.; Jensen, P. A.; Wagner, J. B.; Jensen, A. D. Deactivation of Ni-MoS2 by Bio-Oil Impurities During Hydrodeoxygenation of Phenol and Octanol. *Appl. Catal., A* **2016,** *523*, 159.
(166) Ledoux, M. J.; Hantzer, S. Hydrotreatment catalyst poisoning by vanadium and nickel porphyrin: ESR and NMR. *Catal. Today* **1990,** *7*, 479.
(167) Kim, C. S.; Massoth, F. E.; Furimsky, E. Structure and catalytic activity of regenerated spent hydrotreating catalysts. *Fuel Process. Technol.* **1992,** *32*, 39.
(168) Knuuttila, P.; Nousiainen, J.; RISSANEN, A., Process and apparatus for producing hydrocarbons from feed-stocks comprising tall oil and terpene-compounds. Google Patents: 2016.
(169) Ouni, T.; Sippola, V.; Lindqvist, P., Use of renewable oil in hydrotreatment process. Google Patents: 2015.
(170) Fonseca, A.; Zeuthen, P.; Nagy, J. B. 13C n.m.r. quantitative analysis of catalyst carbon deposits. *Fuel.* **1996,** *75*, 1363.
(171) Marafi, M.; Stanislaus, A. Effect of initial coking on hydrotreating catalyst functionalities and properties. *Appl. Catal., A* **1997,** *159*, 259.

(172) Hollak, S. A. W.; de Jong, K. P.; van Es, D. S. Catalytic Deoxygenation of Fatty Acids: Elucidation of the Inhibition Process. *ChemCatChem* **2014,** *6*, 2648.
(173) Wolf, E. E.; Alfani, F. Catalysts Deactivation by Coking. *Catal. Rev.: Sci. Eng.* **1982,** *24*, 329.
(174) Netzel, D. A.; Miknis, F. P.; Mitzel, J. M.; Zhang, T.; Jacobs, P. D.; Haynes Jr, H. W. Carbon-13 solid-state n.m.r. investigation of coke deposits on spent catalysts used in coal liquefaction. *Fuel.* **1996,** *75*, 1397.
(175) Menon, P. G. Coke on catalysts-harmful, harmless, invisible and beneficial types. *J Mol Catal* **1990,** *59*, 207.
(176) Wrammerfors, Å. Catalyst deactivation by coke " a study of the carbonaceous layer on a used hydrogenation catalyst". Chalmers University of Technology, Gothenburg, 1993.
(177) Senol, O. I.; Viljava, T. R.; Krause, A. O. I. Effect of Sulfiding Agents on the Hydrodeoxygenation of Aliphatic Esters on Sulfided Catalysts. *Appl. Catal., A* **2007,** *326*, 236.
(178) Laurent, E.; Delmon, B. Study of the hydrodeoxygenation of carbonyl, carboxylic and guaiacyl groups over sulfided CoMo/γ-Al2O3 and NiMo/γ-Al2O3 catalyst. II. Influence of water, ammonia and hydrogen sulfide. *Applied Catalysis A, General* **1994,** *109*, 97.
(179) Chorkendorff, I., Niemantsverdriet, J. W., *Concept of Modern Catalysis and Kinetics*. WILEY-VCH Verlag GmbH & Co. Weinheim:Federal Republic of Germany, 2003; p 452.
(180) Wagner, C. D.; Gale, L. H.; Raymond, R. H. 2-DIMENSIONAL CHEMICAL-STATE PLOTS - STANDARDIZED DATA SET FOR USE IN IDENTIFYING CHEMICAL-STATES BY X-RAY PHOTOELECTRON-SPECTROSCOPY. *Anal Chem* **1979,** *51*, 466.
(181) Lee, Y. J.; Jun, K. W.; Park, J. Y.; Potdar, H. S.; Chikate, R. C. A simple chemical route for the synthesis of gamma-Fe2O3 nano-particles dispersed in organic solvents via an iron-hydroxy oleate precursor. *Journal of Industrial and Engineering Chemistry* **2008,** *14*, 38.
(182) Tsigdinos, G. A., Heteropoly compounds of molybdenum and tungsten. In *Topics in Current Chemistry: Aspects of Molybdenum and Related Chemistry*, Eds.; Springer Berlin Heidelberg: Berlin, Heidelberg. 1978; pp 1.
(183) Moulder, J. F., William, F. S., Sobel, P. E.,Bomber, K. D., Hand Book of X-Ray Photoelectron Spectroscopy. Chastian, J., Eds.; Perkin-Elmer Corporation :Minnesota. 1992; pp 222.
(184) Szarvas, T.; Eller, Z.; Kasza, T.; Ollar, T.; Tetenyi, P.; Hancsok, J. Radioisotopic investigation of the oleic acid-1-C-14 HDO reaction pathways on sulfided Mo/P/Al2O3 and NiW/Al2O3 catalysts. *Appl. Catal., B* **2015,** *165*, 245.
(185) Monnier, J.; Sulimma, H.; Dalai, A.; Caravaggio, G. Hydrodeoxygenation of Oleic Acid and Canola Oil over Alumina-Supported Metal Nitrides. *Appl. Catal., A* **2010,** *382*, 176.
(186) Immer, J. G.; Kelly, M. J.; Lamb, H. H. Catalytic Reaction Pathways in Liquid-Phase Deoxygenation of C18 Free Fatty Acids. *Appl. Catal., A* **2010,** *375*, 134.
(187) Coumans, A. E.; Hensen, E. J. M. A Model Compound (Methyl Oleate, Oleic Acid, Triolein) Study of Triglycerides Hydrodeoxygenation over Alumina-Supported NiMo Sulfide. *Appl. Catal., B* **2017,** *201*, 290.
(188) Senol, O. I.; Ryymin, E. M.; Viljava, T. R.; Krause, A. O. I. Effect of hydrogen sulphide on the hydrodeoxygenation of aromatic and aliphatic oxygenates on sulphided catalysts. *J. Mol. Catal. A: Chem.* **2007,** *277*, 107.
(189) Huang, Y. Y.; Wang, L. L.; Chen, X. P.; Wei, X. J.; Liang, J. Z.; Li, W. Intrinsic kinetics study of rosin hydrogenation on a nickel catalyst supported on spent equilibrium catalyst. *Rsc Adv* **2017,** *7*, 25780.
(190) Wang, L.; Chen, X.; Sun, W.; Liang, J.; Xu, X.; Tong, Z. Kinetic model for the catalytic disproportionation of pine oleoresin over Pd/C catalyst. *Industrial Crops and Products* **2013,** *49*, 1.
(191) Kulikov, A. B.; Onishchenko, M. I.; Maksimov, A. L.; Lysenko, S. V.; Karakhanov, E. A. Hydroconversion of rosin acids in the presence of Pt-containing Al–HMS mesoporous aluminosilicate. *Petroleum Chemistry* **2016,** *56*, 717.

(192) Arend, M.; Nonnen, T.; Hoelderich, W. F.; Fischer, J.; Groos, J. Catalytic Deoxygenation of Oleic Acid in Continuous Gas Flow for the Production of Diesel-Like Hydrocarbons. *Appl. Catal., A* **2011,** *399*, 198.
(193) Dejonghe, S.; Hubaut, R.; Descourieres, T.; Grimblot, J. Influence of the competitive adsorption of polyaromatic and vanadylprophyrin molecules on the deactivation of Ni-MoS2-Al2O3 catalyst. *Appl. Catal.* **1990,** *61*, L9.
(194) Dutta, R. P.; Schobert, H. H. HYDROGENATION-DEHYDROGENATION REACTIONS OF ROSIN. *Abstr. Pap. Am. Chem. S.* **1993,** *206*, 55.
(195) Du, H.; Fairbridge, C.; Yang, H.; Ring, Z. The chemistry of selective ring-opening catalysts. *Appl. Catal., A* **2005,** *294*, 1.
(196) Lemberton, J.-L.; Guisnet, M. Phenanthrene hydroconversion as a potential test reaction for the hydrogenating and cracking properties of coal hydroliquefaction catalysts. *Appl. Catal.* **1984,** *13*, 181.
(197) Ardakani, S. J.; Smith, K. J. A comparative study of ring opening of naphthalene, tetralin and decalin over Mo2C/HY and Pd/HY catalysts. *Appl. Catal., A* **2011,** *403*, 36.
(198) Arribas, M. A.; Martínez, A. The influence of zeolite acidity for the coupled hydrogenation and ring opening of 1-methylnaphthalene on Pt/USY catalysts. *Appl. Catal., A* **2002,** *230*, 203.
(199) Park, J. I.; Lee, J. K.; Miyawaki, J.; Kim, Y. K.; Yoon, S. H.; Mochida, I. Hydro-conversion of 1-methyl naphthalene into (alkyl)benzenes over alumina-coated USY zeolite-supported NiMoS catalysts. *Fuel* **2011,** *90*, 182.
(200) Echeandia, S.; Pawelec, B.; Barrio, V. L.; Arias, P. L.; Cambra, J. F.; Loricera, C. V.; Fierro, J. L. G. Enhancement of phenol hydrodeoxygenation over Pd catalysts supported on mixed HY zeolite and Al2O3. An approach to O-removal from bio-oils. *Fuel* **2014,** *117*, 1061.
(201) Santana, R. C.; Do, P. T.; Santikunaporn, M.; Alvarez, W. E.; Taylor, J. D.; Sughrue, E. L.; Resasco, D. E. Evaluation of different reaction strategies for the improvement of cetane number in diesel fuels. *Fuel* **2006,** *85*, 643.
(202) Gorte, R. J. What do we know about the acidity of solid acids? *Catal. Lett.* **1999,** *62*, 1.
(203) Abdelrahman, O. A.; Vinter, K. P.; Ren, L. M.; Xu, D. D.; Gorte, R. J.; Tsapatsis, M.; Dauenhauer, P. J. Simple quantification of zeolite acid site density by reactive gas chromatography. *Catal. Sci. Technol.* **2017,** *7*, 3831.
(204) Oyama, S. T.; Wang, X. Q.; Radhakrishnan, R., Adsorption of ethylamine on silica-supported nickel phosphide. In *Science and Technology in Catalysis 2002*, Anpo, M.; Onaka, M.; Yamashita, H., Eds.; 2003; Vol. 145, pp 347.
(205) Kresnawahjuesa, O.; Gorte, R. J.; de Oliveira, D.; Lau, L. Y. A simple, inexpensive, and reliable method for measuring Bronsted-acid site densities in solid acids. *Catal. Lett.* **2002,** *82*, 155.
(206) Hofmann, A. W. Beiträge zur Kenntniss der flüchtigen organischen Basen. *Ann. Chem. Pharm.* **1851,** *78*.
(207) Ingelsten, H. H.; Skoglundh, M.; Fridell, E. Influence of the support acidity of Pt/aluminum-silicate catalysts on the continuous reduction of NO under lean conditions. *Appl. Catal., B* **2003,** *41*, 287.
(208) Loricera, C. V.; Castano, P.; Infantes-Molina, A.; Hita, I.; Gutierrez, A.; Arandes, J. M.; Fierro, J. L. G.; Pawelec, B. Designing supported ZnNi catalysts for the removal of oxygen from bio-liquids and aromatics from diesel. *Green Chem* **2012,** *14*, 2759.